BIOMECHANICS OF TIBIA TRAY AUGMENTATION IN TOTAL KNEE ARTHROPLASTY

BIOMECHANICS OF TIBIA TRAY AUGMENTATION IN TOTAL KNEE ARTHROPLASTY

By

QIANG YIN, B.SC (Mechanical Engineering)

East China Jiaotong University, China

A Thesis

Submitted to the School of Graduate Studies

in Partial Fulfillment of the Requirements

for the Degree

Master of Applied Science

McMaster University

MASTER OF APPLIED SCIENCE (2006) McMaster University

(Mechanical Engineering) Hamilton, Ontario

TITLE: Biomechanics of Tibia Tray Augmentation
In Total Knee Arthroplasty

AUTHOR: Qiang Yin, B.SC (Mechanical Engineering)
East China Jiaotong University, China

SUPERVISOR: Dr. Samir Ziada
Dr. Ata Hashemi
Department of Mechanical Engineering
McMaster University

MUNBER OF PAGES: xvii, 156

Abstract

In total knee arthroplasty with bone defect of the tibia, it was believed that with older designs of tibial tray, both block and stem augments must be used with the tibial tray to improve the knee stability. Obviously, the extended stem causes more difficulties to the surgery as well as more suffering to the patients. Getting rid of the extended stem and still maintaining enough stability is therefore very desirable. The newest tray design, Deltafit Keel tray, which provides much more contact with the human bone structure, may provide enough stability without the extra long stem. The objective in this project is to answer the questions – Is the stem augmentation definitely required alongside the block implant for the cases of bone defect in TKA (Total Knee Arthroplasty) when using the Deltafit Keel tibial tray design? In other words, does the configuration of Deltafit Keel tray with a block provide enough stability in the cases of bone defect? In order to give a reliable answer, three configurations have been studied by conducting both experiments and FEA simulation. The three cases are Deltafit Keel tibial tray only (case 1- no bone defect defect), tray with block augment (case 2- with bone defect assumed) and tray with block and extended stem (case 3- with bone defect assumed). In this study, three commercially available composite bones with isotropic material properties are utilized. For each configuration, the bones are clamped in a testing apparatus and

3000 N static compressive load is imposed on the top surface of the tibia tray at central, medial and lateral locations. In experiment, the strains and displacements at strategically selected locations were measured by strain rosettes (strain gages) and DVRT (Differential Variable Reluctance Transducer) displacement transducers, respectively. In order to simulate the three cases, FE model is established by employing several advanced software including CATIA, True Grid Mesh generator and Abaqus. In order to compare with the experimental results, nine cases (three implant configurations with three different loading positions for each) have been simulated using Abaqus/Standard 6.4. In addition to the nine-case studies, the influence of load offsetting is also investigated by shifting the nodal load along medial-lateral and anterior-posterior directions. It is found that load shifting one node in either direction does not cause significant change in either strain or displacement. Furthermore, FE results of adjacent elements are checked as well and no sudden changes are observed. Since the discrepancy of the output from adjacent elements is negligible, an average value of the elements can be used to represent the output in a small region to compare the experimental strain measured by strain rosettes.

Both the experimental data and FEA simulation results lead to the conclusion that comparable stability can be achieved with the configuration of Deltafit Keel tibial tray and a block as compared to the case of Deltafit Keel tray only without bone defect. Moderate improvement of stability, but with significant stress shielding, is found when the extended stem is implanted. For the amount of bone defect and the bone material properties used in this study, the Deltafit Keel tray with a block is the

best choice because it is able to provide adequate stability and avoid excessive stress shielding. The loss of a substantial amount of bone to implant an extended stem to trade for the excessive stability may not be worthwhile. Besides, stress shielding is a potential problem which may exist if the extended stem is used.

Acknowledgements

Study at McMaster University is an excellent learning experience. It has been highly appreciated to have the opportunity to concentrate on the interesting and challenging research project –Biomechanics of Stem Tibia Tray Augmentation in Total Knee Arthroplasty. There are many people to be thanked.

First of all, I would like to express my deepest appreciation and thanks to my supervisors, Dr. Samir Ziada and Dr. Ata Hashemi, for their continuous guidance, constructive discussions and suggestions, critical reviews of my work and support throughout this research.

I want to take the chance to thank Dr. Don Metzger for his suggestions and guidance. I would also like to give many thanks to Dr. Anthony Adili and Dr. Sanjay Dixit for providing all the artificial implants and preparing the experimental tibia bones. Special thanks to Warren Reynolds and Mike Burger for their help and consultation in geometric modeling and meshing. It has been highly appreciated to have the opportunity to share their enriched experience.

Finally, I would like to especially thank my dear wife, Li Ning and my dear children Weiyi and Joyce for their support, patience and encouragement during this work. A big special thank to my dear parents who have always supported me.

Contents

List of Illustrations

List of Tables

Chapter 1

Introduction

Total joint replacement has become a widely accepted treatment for many destructive joint diseases including osteoarthritis, rheumatoid arthritis, osteonecrosis and very severe pathologic fractures. Of total joint replacements, the two most commonly and successfully replaced joints are the knee and the hip. Sir John Charnely, a British orthopaedic surgeon who was knighted for his development of joint replacements, developed the fundamental principles of the artificial hip and designed a hip in the mid and late 1960's that still sees widespread use today. Frank Gunston developed one of the first artificial knee joints in 1969. Since then, joint replacement surgery has become one of the most successful orthopaedic treatments. The number of hip replacements done in the world per year is between 500,000 and 1 million. The total number of knee replacements done in the world per year is less, but probably still numbers between 250,000 and 500,000.

1.1 Motivation

The investigation of this project deals with the topic of TKA (total knee arthroplasty), which is the surgical procedure of the complete replacement of the damaged components of a natural human knee with synthetic implants. This procedure is even more complicated with the presence of bone defect. Commonly, the medical opinion is held that when bone defect occurs, both a block and a stem augmentation must accompany the tibial tray for stability. However, this belief is based on older tibial tray designs, not the newest Deltafit Keel design. Obviously, the extended stem causes more difficulties to the surgery as well as more suffering to the patients. If the Deltafit Keel tibial tray design can be used with only the block augment in TKA and achieve enough stability, this would have significant implications to the surgery procedure itself in terms of cost and time reductions, as well as to the patient in terms of decreased recovery time and post operative complications.

In order to answer the question of whether the stem augmentation is definitely required alongside the block implant for the cases of bone defect in TKA when using the Deltafit Keel tibial tray design, experimental investigation are necessary for the following cases:

Case 1: Deltafit Keel tibial tray only (no bone defect defect).

Case 2: Deltafit Keel tibial tray with block augment (with bone defect defect).

Case 3: Deltafit Keel tibial tray with block and extended stem augments (with bone defect defect).

Preliminary tests were conducted on three human cadaveric tibiae [1] and the experimental results were twofold. First, a negligible change in stability was found between the case of a keel tray only and a keel tray with block augmentation. Second, a moderate increase in stability was found between the case of a keel tray with block augment and a keel tray with both block and stem augments. These results inferred that when bone defects were present, sufficient stability may be achieved with the Deltafit Keel tray design with a block augment only. Although the addition of the stem was found to provide added stability, the amount of this increase might not prove helpful to the patient in the long run. Negative side-effects brought on by the stem augment might outweigh this moderate increase in stability.

In general, the results from the preliminary tests mentioned above are based on a limited number of measurements. More reliable conclusions can be achieved by performing additional experiments and modeling of the above cases by means of FEA. Therefore, this research basically includes four parts, i.e., experiments, 3D geometric modeling, finite element simulation and comparison of results.

1.2 Research objectives

The research objective of this study is: from the strain-stress point of view, investigate whether in case of tibial defects, the Deltafit Keel tray design is sufficient in term of stability with just a block augment, as opposed to both block and stem augments by means of experimental and FEA studies.

In order to give a reliable answer, the following investigations need to be carried out:

- Geometric modeling of artificial knee components (Deltafit Keel tibial tray, block and stem), the tibial bone with and without bone defect, and the model assembly.
- Experimentally testing the three cases mentioned previously in terms of strain and deformation under certain loads.
- Finite element simulation of the three cases.
- Comparing the simulation predictions with the experimental results and drawing the conclusions.

Chapter 2

Literature Review

2.1 Human knee

As we know, human knees are the largest joints in our body. They support our body and give the flexibility that we need for a variety of activities. Natural human knee is very complex as shown in Figure 2.1 [2]. It consists of **thigh bone/femur**, **shin bone/tibia** and **knee cap/patella**. The lower end of the thigh bone/femur rotates on the upper end of the shin bone/tibia, and the knee cap/patella slides in a groove on the end of the femur. Each bone end is covered with a layer of smooth shiny **cartilage** that cushions and protects while allowing near frictionless movement. Cartilage contains no nerve endings or blood supply but receives nutrients from the fluid contained within the joint. Surrounding the knee structure is the synovial lining, which produces this moisturizing lubricant. If damaged, the cartilage is not capable of repairing itself [3].

There are four major tough fibers, called ligaments, linking the bones of the knee joint and holding them in place, adding stability and elasticity for movement and also preventing unwanted movement. They are medial collateral ligament, lateral collateral

ligament, anterior cruciate ligament and posterior cruciate ligament. Muscles and tendons also play an important role in keeping the knee joint stable and mobile.

The portion of the knee joint which will be modeled in this project is the tibia. There are two types of bone within the tibia with different material properties. The **cortical bone** comprises the hard outer shell and bears most of the load while the **cancellous bone** occupies the center of the bone and serves as a transport of blood and nutrients to the cortical bone. The cancellous bone is softer, less dense and less organized in formation than the cortical bone, therefore, the strength of the bone decreases exponentially with respect to the distance from the cortex to the center.

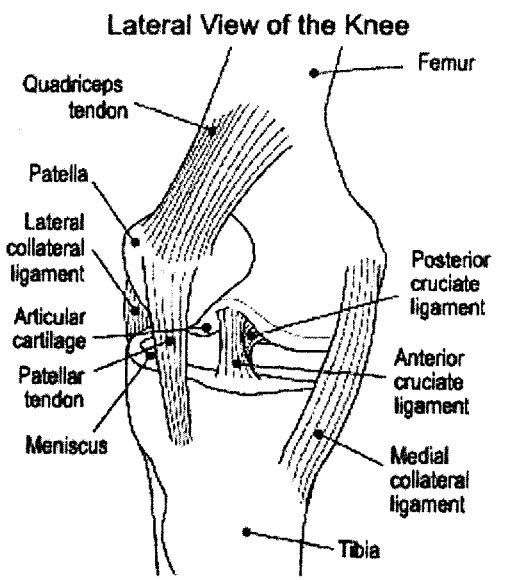

Figure 2.1 Structure of human knee [2]

2.2 Human knee problems

Knee problems can be classified into two general types, i.e., mechanical and inflammatory. Mechanical knee problems result from injury, for instance, a direct blow or sudden movements that strain the knee beyond its normal range of movement. Trauma-related arthritis results when the joint is injured and it causes joint damage, pain and loss of mobility [3]. Inflammatory problems, such as osteoarthritis in the knee, result from wear and tear on knee parts. Inflammatory knee problems that occur in certain rheumatic diseases, such as rheumatoid arthritis and systemic lupus erythematosus, can damage the knee [2]. Osteoarthritis is a disease that involves the breakdown of tissues that allow joints to move smoothly. For example, the layers of cartilage and synovium become damaged and wear away, leaving the underlying bones unprotected from wearing against each other. It usually occurs in people over 60. Rheumatoid arthritis is a systemic disease because it may attack any or all joints in the body. It affects women more often than men and can strike young and old alike. With rheumatoid arthritis, the body's immune system produces a chemical that attacks and destroys the synovial lining covering the joint capsule, the protective cartilage and the joint surface, causing pain, swelling, joint damage, and loss of mobility.

When conservative methods of knee treatment fail to provide adequate relief and the degree of pain, deterioration and loss of movement is severe enough, total knee replacement should be considered.

In summary, the three major knee problems in Total Knee Arthroplasty (TKA) are osteoarthrosis, rheumatoid arthritis and posttraumatic arthrosis.

2.3 Artificial knee

As mentioned in chapter one, the development of the artificial knee has lagged behind that of the hip because the complexity of the knee joint has presented special challenges in the design and insertion of an artificial knee joint. To have general functions, a knee needs to allow the range of movement from zero degree (straight) to 90 degrees at least, with complete stability in all other directions. In order to achieve good results, the artificial knee joint closely follows the contours of the real joint and has been computer-designed to imitate the natural biomechanics of the normal knee. There are many designs of total knee replacement, sometimes named after the type of joint or the surgeons who developed them. Examples are AGC (Anatomic Graduated Components total knee), PCA (Porous-coated Anatomic total knee), Duracon, Insall-Burstein and Miller-Galante.

Generally, there are four major components of a total knee replacement as shown in Figure 2.2:

The femoral component – fits on the lower end of the thigh bone and looks like a large rounded knuckle.

The tibial tray – is a flat plate-like piece and fits on the top of the shin bone.

The plastic spacer – fits between the femoral and tibial components.

The patella button – fixed to the back of the patella/kneecap.

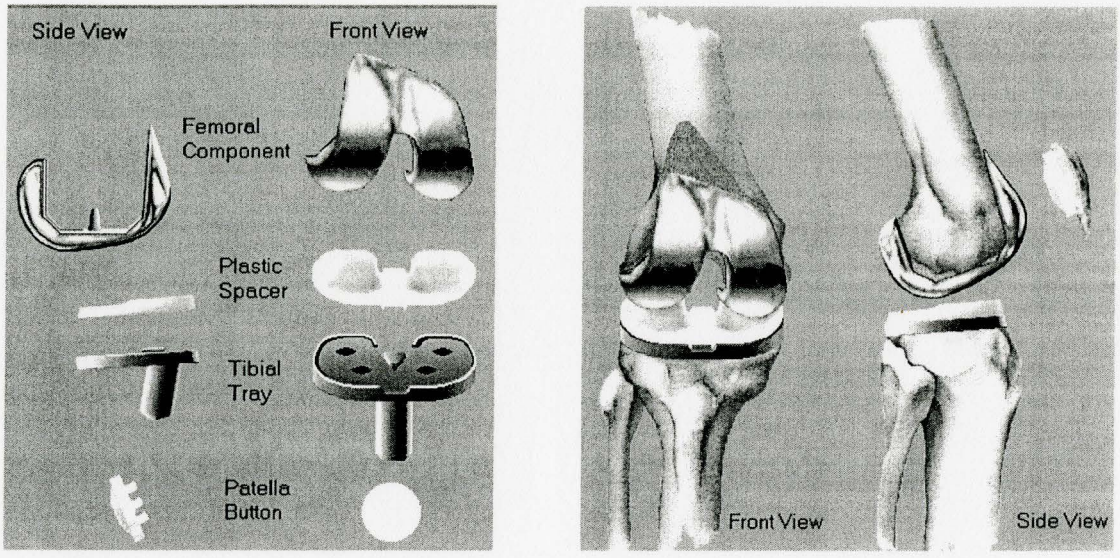

a) Artificial knee components b) Assembled artificial knee

Figure 2.2 Prosthesis [4]

There are two major types of prosthesis, cemented and uncemented. A **cemented prosthesis** is held in place using epoxy type cement that attaches the metal to the bone. An **uncemented prosthesis** has a fine mesh of holes on the surface that allows the bone to grow into the mesh and attaches the prosthesis to the bone.

Regarding to the materials of the prosthesis, the femoral and sometimes the tibial are metal components, made of a steel alloy which has cobalt, chromium and molybdenum in it. The advantage of the alloy is that it does not react with the tissue and fluids in the body to cause problems, and is mechanically very strong. Tibial components can be made of titanium instead which has great strength and is lighter than steel. The plastic components are made of ultra high molecular weight polyethylene (UHMWP) which is very dense, hard and smooth. The combination of metal and plastic gives the

joint very low friction so it moves easily with the body weight on it and wears very slowly.

The factors, which affect a surgeon to choose the type of prosthesis to insert from the variety available, include the surgeon's preferences and the person's age, weight, degree of activity, bone quality and specific knee problems. It is very important to know the success rates of the type of joint prosthesis (artificial joint) used as well as the surgeon's own success rate. Some types of joint replacement have performed much better than others over ten or fifteen years. The results of all reputable joint replacements can usually be found in orthopaedic journals.

Ideal candidates for knee replacement are older and of sedentary lifestyle because they are less likely to stress the joint excessively and cause it to fail. Artificial joints have a finite lifetime and if they have to be revised the operation is much more difficult technically than the initial/primary operation. Normally, the femoral and tibial components of the primary surgery could survive for around 15 years, second surgery lasts 5 years and the third one only survives 2 years. And a knee revision is usually caused by the reasons such as loss of bone stock, component loosing, infection, instability, etc.

2.4 Phenomena in human knee

Some phenomena in human knee affect the quality and the life of artificial joint replacements. For example:

Bone remodeling cycle - Although bone seems as hard as a rock, it is in fact a dynamic organ. Throughout human being's life, old bone is removed and new bone is added. This is bone resorption and bone formation, a process of continuous bone turnover known as bone remodeling. Two main types of cells are responsible for bone renewal: the **osteoblasts** involved in bone formation and the **osteoclasts** involved in bone resorption. During childhood and the beginning of adulthood, bone becomes larger, heavier and denser, bone formation is then more important than bone resorption. The bone mass actually increases until the age of 20~25 where it reaches its maximum value: the peak bone mass (maximum bone density and strength). The higher the peak bone mass is, the lower the risk of osteoporosis is. Bone mass remains stable for a few years (for women, till about 45 years old), during which a perfect equilibrium between bone formation and resorption exists [5]. After a certain range of age, bone resorption outpaces bone formation and bone density begins to decline. Some loss of bone density is normal. Only when the process accelerates osteoporosis, a condition that literally means "porous bones", it becomes a threat [6].

Stress shielding – artificial components remove too much stress from human bones due to their greater stiffness than human bones and lead bones to weaken. This phenomenon is called stress shielding. The bone atrophies where it's unloaded. It's natural for the bone

to take back calcium where it's not needed anymore, and then a reduction in bone mass begins. Atrophy and resorption lead to a loosening and failure of the joint or the bone. Adaptive bone remodeling due to stress shielding has been identified as one of the important causes of the bone resorption [7].

Bone defect – From literature review, the clear definition of bone defect can not be found. However, bone defect can be geometric loss of the bone due to injury or bone mass becomes less due to stress shielding, bone abnormalities such as osteopenia (low bone density), osteoporosis (porous bone), osteomalacia (poor mineralization of bone) and bone atrophies, etc. Bone defect is one of the major problems after TKA. It may be caused mechanically, either by unloading of the bone leading to osteoporosis, or by overloading of the bone leading to bone fractures or bone destruction [8].

Aseptic loosening – Artificial components or implants loosening after replacements.
In aseptic loosening, the interface between implant/cement and bone is overloaded, compressed, resorbed or remodeled so that the implant subsides, tilts and/or rotates. The mechanisms proposed to explain the reason for mechanism behind loosening, include toxic effects on the bone bed, thermal damage during bone cutting, overload due to malalignment or tense soft tissues, failure of initial fixation with micromotion, pressure waves in the fluid of the interface and osteolysis triggered by wear particles from the implant. Aseptic loosening of prosthetic components may eventually lead to pain, instability and loss of function and thus a failure [9]. It has been recognized that bone

tissue has the ability to change its shape and internal architecture according to its loading environment. Krach et al. [10] indicated that due to the insertion of prostheses and/or implants, the stress and strain fields of the bone are dramatically changed and these bone remodeling activities can lead to aseptic loosening of artificial joints. Muratoglu et al. [11] indicated that the major problem in total joint replacements is the wear debris induced peri-prosthetic osteolysis (mostly from UHMWPE components) that leads to aseptic loosening. Yuan et al. [12] investigated wear particle diffusion and tissue differentiation in TKA implant fibrous interfaces and concluded that tissue distortional strain from external forces and interstitial fluid velocity resulting from compression of the fibrous tissue interface play a role in the progression of loosening process.

2.5 Artificial components for the management of tibia bone defects

The tibial tray has many variations of materials and configurations. Figure 2.3 shows some examples of designs. The Deltafit Keel is called new design [13] while the others are called traditional designs. When tibia has peripheral bone defects, various surgical options can be used for handling such defects. There are basically four alternatives available for management of bone defects in total knee arthroplasty [14-17] including:

- Prosthetic augments - using metal wedges, custom made protheses, spacer to fill the defect.

- Autograft - correcting the defect through bone grafting.
- Allograft - using allograft reconstruction of the defect.
- Cement - filling the defect with bone cement or using bone cement reinforced with buttressing screws.

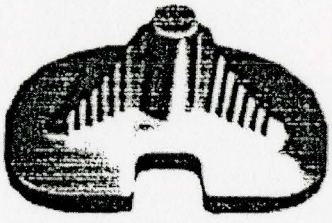

Deltafit keel

Single round post

Rectangular post

Four pegs

Cruciform keel

Figure 2.3 Examples of tibial Tray [1]

Brooks et al. [9] in 1984 demonstrated the ability of metal wedges improving the stability of the tibial bone-impalnt interface, which lead to the development of metal augments in TKA. Figure 2.4 shows the modular augmentation [15].

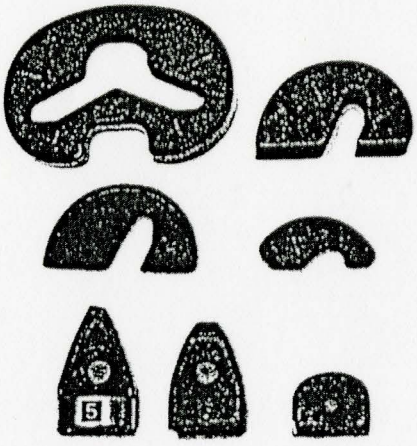

Figure 2.4 Modular augments [15]

There are several important issues involved in the management of bone defects to achieve a successful surgery. They are listed as follows:

- Assess the level of bone defect before the surgery.
- Choose a proper approach among the four alternatives mentioned above.
- Check the available augments in the knee arthroplasty system among a large variety of augment designs/shapes such as hemi-wedges, full wedges and symmetric spacers which are available for the tibial component.
- Choose reliable attachment mechanisms and reliable fixation.
- Ensure the augment can adequately serves the needs of the patient and surgeon. If it does not perfectly fits, a variety of instrumentation techniques are available with regard to adapting the prosthetic augment to the bone defect and/or to adapt the bone defect to the prosthetic augment.

Chen and Krackow [16] indicated that wedge shaped cement structures provided little support against peripheral migration by shearinng force and

stability might be affected by stress concentration at the inner margin of the defect as well. However, converting the slanted defects to ones with horizontal and vertical surfaces would eliminate shearing forces and alleviate marginal stress concentration. Figure 2.5 shows the comparison between the oblique area and the horizontal and vertical surfaces with regard to the stress.

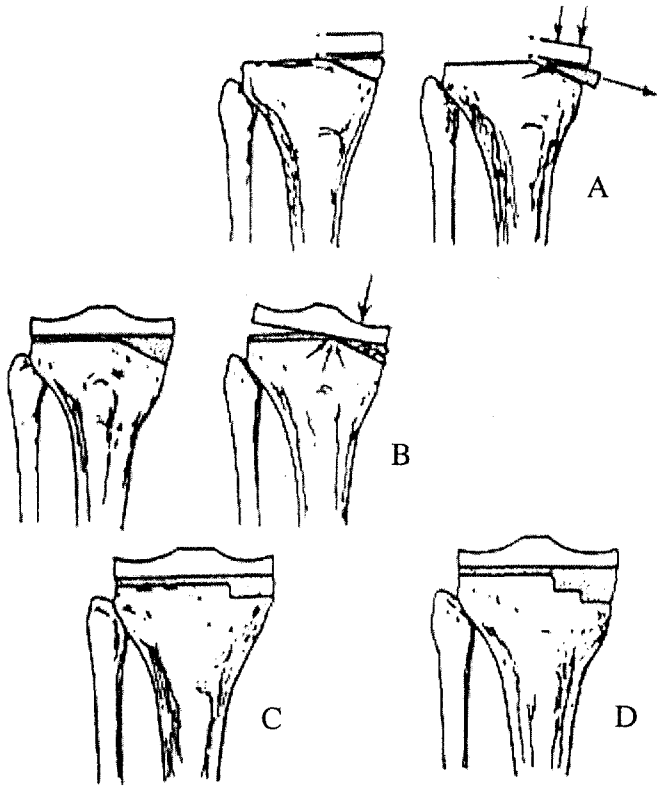

Figure 2.5 Filling or modifying the defects [16]

(A: shear forces acting on the oblique peripheral defect filled with cement may potentially weaken the support of the tibial component overlying the defect. B: Cement on a slanted surface may result in stress concentration at the margin of the defect. C, D: Modifying the surface of these defects will reduce the forces and stress concentration.)

Bone defect size and patients' age are the important factors in choosing the alternatives. Cuckler [14] stated that bone cement can be used conveniently to fill the

defects with size less than 10 mm. If the defect appears to be larger than 10 mm in its largest dimension, augmentation or bone graft should be anticipated. And young patient should be considered for autograft or allograft, in an effort to restore bone stock. Autograft is indicated in primary knee arthroplasties with defects 10 mm or less in size while larger defects may require allograft augmentation.

Generally, the majority of surgeons use stem augments or extensions when prosthetic wedges are necessary to decrease the load at the bone-implant interface at the site of augmentation [9, 14-15, 17-19]. Figure 2.6 shows a long stemmed augment attached to a tibia tray [17]. However, Marcuzzi and Rampley [1] indicated that the standards used to determine the need for a stem augment in the case of a bone defect are based on the traditional designs. In the cases where the stem length is a minimum of 60 mm, some of the load may be directly transferred to the cortical shell. The drawbacks resulted from the stem are definitely not neglectable. First, it increases the risk of experiencing post-operative complications; second, it causes an increase in cost to the procedure, in surgical time and in stress on the patient. Third, it makes the revision of the implant more difficult, with a potential danger of amputation. With all of these in mind, it is still commonly believed that the stem is necessary for stability in the cases of bone defects, also when the Deltafit keel tray is used.

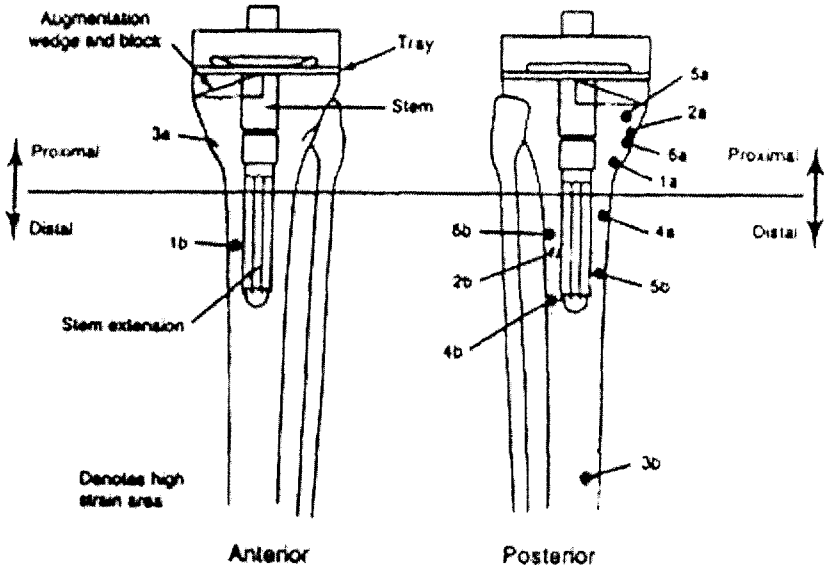

Figure 2.6 Long stem augmentation [17]

Different from the traditional tibial components, Deltafit Keel is designed to reach dense cancellous bone and improve stability [5]. With this new structure, how much influence on the artificial knee performance does the long-stem prosthesis have? And is the long-stem prosthesis definitely required in the cases of bone defects? In order to answer these questions, Marcuzzi and Rampley [1] did an experimental investigation experimentally on the stem issue and they concluded that the extended stem does not show significant effect in terms of strain and displacement. More research is required to give convincable answers to these questions.

2.6 Fixation in TKA

Fixation in TKA has been studied by many researchers. Michael et al. [20] did a detailed review on tibial fixation in revision TKA. In revision TKA, component fixation is a significant challenge due to the loss of bone stock and the presence of bone defects. Research showed that durable long-term fixation relies on the component stability within host bone in revision TKA [21-22]. As described previously, tibial components are often implanted with modular stems to augment the stability of revision TKA. With regard to cement, some contended that the stem should be fully cemented within the tibial canal [23], while some advocated uncemented canal-filling stems [24-25]. The survey of the patients with uncemented stems suggested that extended-length stems enhance component stability and hence implant survival [26-30]. A positive correlation between stem length and implant stability was presented [29-30] but Stern et al. refuted the assertion [31]. Volz et al. [32] showed that the longer stems have significant effect on mitigating motion in softer bone. Michael et al. [20] concluded that the mechanical stability of tibial fixation in revision TKA is signifiantly increased by the addition of a canal-filling stem, even in the presence of poor proximal bone. In all, no general conclusions can be drawn.

Regarding the cement materials, Kenny and Buggy [33] published a very detailed review. Since the first bone cement was deveoped in the 1960s using poly (methyl methacrylate) (PMMA) by Charnley, PMMA still remains the most widely used material for fixation of orthropaedic joint repacements. But nothing is perfect for all different situations. In order to prolong the lifetime of the prosthetic, investigations have been

carried out to develop different types of cements. Kenny and Buggy [33] classified the cements into 10 types, i.e., poly (methyl methacrylate) (PMMA)cements, zinc phosphate cements, zinc polycarboxylate cements, glass polyalkenoate cements, bioglass, apatite/wollastonite glass-ceramics, Synthetic hydroxyapatite, Calcium phosphate cements, resin modified glass ionomer and composites. One of the major problems associated with orthopaedic surgery is the mismatch of stiffness between the bone and metallic/ceramic implant. The amount of stress carried by the bone and the implant is directly related to their stiffness. Since bone is a dynamic material, changing continuously to meet the requirements of its surroundings, prolonged reduction of stress on a bone may result in a phenomenon called stress shielding, leading to increased bone porosity [33]. The criteria for the design of new bone cement are as follows:

- Mechanicl properties of cement matching that of bone to enhance the elimination of stress shielding.
- Quick setting (5-15 minutes) to assist in clinical use and after care of patients.
- In situ setting at body temperature to eliminate the necrosis of the adjacent tissue.
- Bonding to bone and medical grade alloys to eliminate fibrous capsule and thus loosening of the implant.
- Bioactive bone in-growth to enhance both stress transfer and chemical attachment of the implant.
- Radio opaque for subsequent monitoring of implant.

Based on cement, TKA can be classified into cement TKA, cementless TKA and hybrid TKA. Cement TKA techniques have demonstrated high success rates within 10-12 years. Concerns remain regarding the durability of cemented fixation beyond 10-15 years. Due to the major problem of cement TKA, cement debris, cementless TKA was developed. The potential benefits of cementless TKA include durable biologic fixation via bone ingrowth, decreased risk of wear due to cement debris, bone preservation, ease of revision and perhaps decreased operative time. But many cementless TKA designs have demonstrated inferior outcomes when compared with cemented series [34]. Therefore, hybrid TKA was introduced in the late 1980s. It gained the theoretical advantage of durable cementless femoral fixation while avoiding the problems associated with cementless tibial fixation [35]. Generally, with hybrid TKA, the tibial and patellar components are cemented with polymethyl-methacrylate while the femoral components are cementless.

Choosing a proper approach of TKA is based on the host bone quality. For the patients who have poor femoral, tibial and patellar bone quality, a fully cemented TKA should be used. If the patients' femoral and tibial bones have adequate quality, cementless TKA can be applied. Hybrid TKA can be considered for those who have good femoral cancellous bone but poor tibial bone quality [34]. Illgen et al. [34] performed 10 year follow-up investigation on hybrid TKA and concluded that hybrid TKA with the implant designs (PCA-67 and Duracon-45) provided durable fixation with excellent clinical and radiographic performance at 10 years comparable to cemented series. Aseptic loosening and radiographic failure rates were zero percent if patients with metal-backed

patellae were excluded and they indicated that the durability of hybrid fixation beyond 10 years needs further study. Campbell et al. [36] also did a follow-up study on hybrid TKA. They indicated that femoral component fixation in hybrid TKA is unreliable with the component design and thought that hybrid fixation should be abandoned compared to the excellent 10- to 15-year results of cemented condylar knee designs.

2.7 FEA on artificial joints

Finite element modeling and analysis has played a very important role in the fields of designing implants, improving artificial joint replacements, better understanding of biological processes and more realistically revealing the reaction of human body to artificial implants. According to the literature survey by Huiskes and Chao in 1983 [37], FEA was first applied in orthopaedics in 1976 by Berkelmans, et al. [38]. Since then FEA has been proved to be an important tool in orthopaedics biomechanics for many different purposes. Doblare and Garcia [8] summarized the use of FEA in orthopaedics research as follows:

- Design and pre-clinical analysis of implants. Many designs of joint replacement prostheses have been studied using finite element models. Although FEA does not allow accurate quantitative analysis due to anthrophometric differences, comparative analysis can be performed between different implant designs to determine the optimum prothesis design [39-48].

- Obtaining fundamental biomechanical knowledge about musculoskeletal structures, for instance, analysis of bones, cartilage, ligaments, tendons and their relationships [38, 49-53].
- Simulation of different adaptive biological processes to test different constitutive laws for tissue growth, adaptation and degeneration. Computational simulations can be also used to predict tissue behaviour in response to biomechanical factors, wear, implants, etc. [10-12, 52, 54-67].
- Investigation of the effect of implant materials on joint replacements [44, 57, 63, 66, 68]

Most applications of FEA are associated with hip joints and total knee arthroplasty.

2.7.1 FEA on artificial hip joints

According to literature survey, FEA was applied in artificial hip joints prior to TKA. Regarding the artificial hip joints, the problems studied by means of FEA are associated with component shapes, materials, interface, bone adaptation, stress shielding, cemented, non-cemented, etc. The effect of materials on stresses of the various components has been studied [45, 54, 57, and 68]. The assessment of bone adaptation around implants combining with bone remodeling theories has been investigated. The isotropic bone remodeling theory developed in Stanford [69] was used in a 2D FEA to simulate bone adaptation around porous-coated implants of proximal femur and tibia [67] and the predicted bone density distributions around implanted prostheses were consistant with clinical and experimental findings of other investigators. Anistropic bone

remodeling theory was developed by Doblare and Garcia [49] and was applied to analyze the influence of the anisotropy on bone remodeling after a total hip replacement with an Exeter hip prosthesis [56]. They predicted that bone anisotropy changes after replacement, tending to a more isotropic distribution. There are other investigations dealing with THA (Total Hip Arthroplasty), such as load transmission pattern under bonded and unbonded cement-bone interface [70], the dependence of stress shielding on the stiffness of stem [71], etc.

2.7.2 FEA on TKA

From literature survey, the research on TKA by means of FEA can be classified into following aspects:

1. Study the interface between the tibia and femur.

Rakotomanana et al. [60] analysed the load transfer at the tibial bone-implant interface using an elastoplastic description of bone. They analysed three different tibial tray designs: cemented with one central peg, a cemented and uncemented with two short medial and lateral pegs. Cheal et al. [55] developed a 3D finite element model to study the influence of tray size and cement penetration depth. Garg and Walker [72-34] studied the influence of loading mode and other factors on bone stresses beneath the tibial plateau. Later, Tammy, et al. [74] established a finite element model of human knee joint and studied tibial-femoral contact. Chu [73] investigated contact stresses and their distribution on the plastic bearing platform of different artificial knees under different loads and during a walking cycle. Tan et al. [74] developed a FE model to investigate the

performance range of an implanted knee with respect to anterior-posterior (A-P) displacement, internal-external rotation and bearing surface contact stresses as a function of the anterior-posterior force, internal-external rotation torque and axial force acting at the knee.

2. Simulate the effect of artificial components, fixation and material on human bone associated with bone remodeling in TKA.

Nyman et al. [75] studied the effect of stem diameter, cement and interlocking screws on stress shielding in revision TKA by using FE model associated with a bone remodeling algorithm. Simon et al. [63] investigated the influence of the implant material stiffness on stress distribution and micromotion at the interface of bone defect implants and found that the low-stiffness implant was characterized by a more homogeneous stress distribution with stress values in a more physiological range than the stiff implant. Rahman et al. [66] indicated that the advantage of the prostheses made of Titanium alloys or from Cobalt Chromium alloys is their biocompatibility with the human body, however, the disadvantage is the dissimilarity of stiffness between bone and implant, which causes unnatural levels of stresses in adjacent bone leading to bone remodeling and resorption/bone defect and eventually cause loosening of the implant and failure of the join function. They suggested using cellular metal alloys for joint implants to produce higher compressive stresses in adjacent bone. Nyman, et al. [72] developed a FE model to predict bone defect for long stemmed (>60 mm) TKA with four different fixation techniques (cement, press-fit, interlock with bony ingrowth and interlock without bony

ingrowth). They found that interlocking screws caused less bone defect than press-fit fixation and only slightly more bone defect than cement fixation. They suggested porous coating of the interlocking stem for bony ingrowth may be advantageous if it prevents stress shielding associated with distal fixation. Several authors such as Tissakht et al. [61] and Van Lenthe et al. [62] have evaluated stress-shielding in the distal femur due to implantation of a knee prosthesis. More recently, Yuan et al. [12] studied the progression of a loosening process of tibial knee arthroplasty by bone resorption and fibrous tissue interposition, concluding that this effect may equally well be caused by mechanical factors, rather than by wear particles. Barink, et al. [64] proposed a different fixation for femoral component in TKA to preserve the femoral bone stock.

3. Compare the designs of artificial knee joints.

Bell et al. [40] studied the differences in wear between fixed bearing (IB: Insall-Burstain) and mobile bearing knees (MBK) and they found that MBK had greater wear over the IB specimens, which could be attributed to the MBK's higher range of motion. Walker et al [48] proposed a method for designing the tibial guide surface and femoral guide surface and demonstrated that the guide surfaces can be applied to a range of possible knee designs including mobile-bearing types, rotating-platform types and fixed-bearing types [39].

4. Study the performance of TKA.

The knee performance after TKA can be evaluated by knee flexion, knee stability and knee life. According to Chiu et al. [76], a 67 degree of knee flexion is generally needed for the swing phase of the gait, 83 degree to climb stairs, 90 degree to descend stairs and 93 degree to rise from a chair. The minimum flexion of the knee necessary for usual daily living is generally agreed to be 90 degree. A knee-simulating machine was developed by Walker, et al. [48] to evaluate the performance of total knee replacements (TKR) including the kinematics and the wear of TKR.

5. Determine bone properties.

Taylor, et al. [51] utilized FEA and modal analysis to determine orthotropic bone elastic constants.

Chapter 3

Experiments

3.1 Introduction

In order to answer the questions such as how the Deltafit Keel tibial tray affects the stress and strain distribution; if the block causes any potential problems from the stress and strain point of view and whether the extended stem helps to enhance the stability or not, three commercially available composite left tibial bones (Figure 3.1) that have average material properties of human bones were employed for testing. The preparation of the three tibial bones, including cutting bones and installing the implants, was performed by Dr. A. Adili (MD) from McMaster Medical Center. The composite tibia bones (Figure 3.1) were then cut near the middle section. The total length after cutting including the top tray is 266mm. The tibia was then cemented into a ϕ 60 plastic tube with a wall thickness of 4 mm and a height of 109 mm from the bottom side of the tibia. Bone defect was assumed in the medial side, so an augment block was inserted in this area. Cement was applied to bond the implants to the tibia bones (more detailed

information can be found in Appendix A). Figure 3.2 shows the tibia bone with the implant.

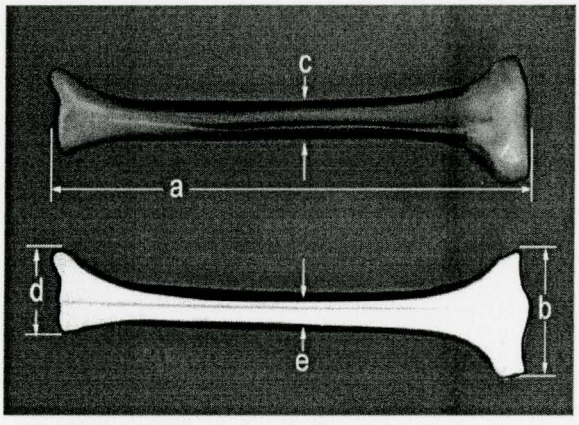

a= 375 mm, b= 74 mm, c= 22 mm, d= 52 mm, e= 9 mm

Figure 3.1 Composite tibia bones

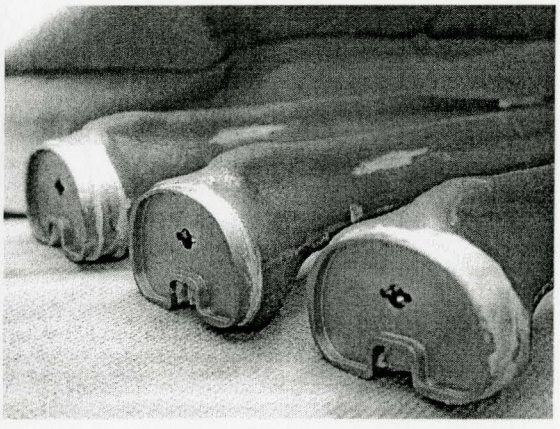

Figure 3.2 Tibia bones with the implant

3.2 Experimental setup

As shown in Figure 3.3, the assembled testing apparatus consists of load applicator, implants, tibia, holding cup, cement, base plate, screws and bolts. The load applicator is threaded directly onto the Instron 4400 Universal material testing machine, which is used as a controlled load source, while the base plate is fastened directly to the table of the Instron machine. The holding cup and the base plates are fixed together with four countersunk bolts. Eight screws were threaded through the holding cup and directly centered and clamped the plastic tube so that tibia bone was in the right position for testing.

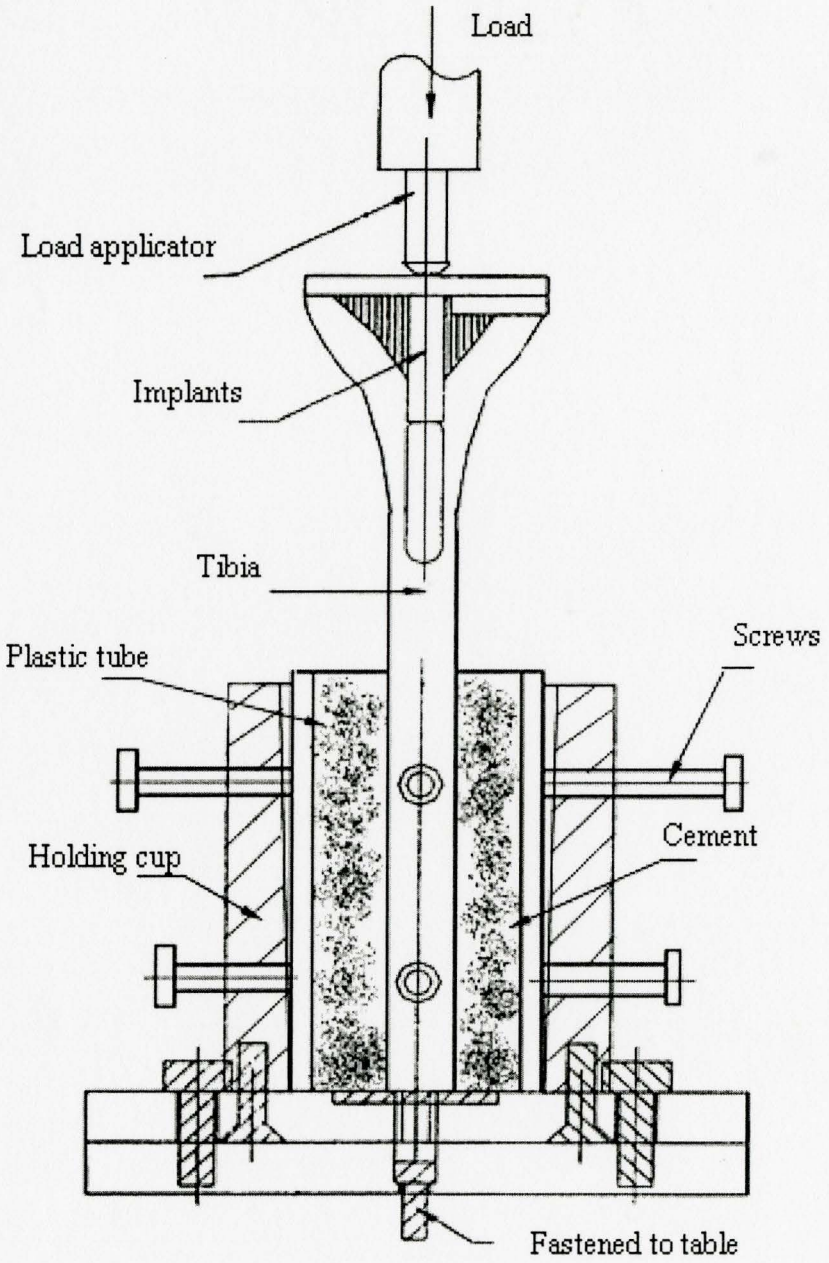

Figure 3.3 Assembled testing apparatus

The equipment employed for the experiment is listed below:

- Testing apparatus (Figure 3.3)
- 3 medium left third-generation composite tibia bones made by Pacific Research Laboratories, INC. item #: 3301 (Fig. 3.1)
- #7 tibial trays, block augment and extend stem manufactured by Stryker Howmedica Osteonics (Fig. 4.1, 4.2)
- Two displacement transducers –DVRTs (Differential Variable Reluctance Transducer) measuring displacements .The DVRTs are Subminiature DVRTs made by MicroStrain Inc., Burlington, VT, USA. The serial numbers are 2352-8 and 2354-8. Their stroke is 8mm and the resolution is 2.0 micron meter.
- 5 strain rosettes (15 strain gauges total) with connecting wires. The strain rosettes are made by Vishay Micro-Measurements Inc., Raleigh, NC, USA. The type of the rosettes is WK-06-060WR-350. The resistance of each rosettes is 350.0$\pm$0.5% OHMs at 24℃.
- 10 channel switch and balance unit made by Vishay Micro-Measurements Inc., Raleigh, NC, USA. The model number is SB-1.
- Portable strain indicator made by The Budd Company Instruments Division. The model number is P-350.
- Power supplies, A/D (Analog to Digital) converter and a PC computer
- Instron 4400 Universal Material Testing Machine

The loading used in this experiment was applied to mimic the loading conditions of human knee and its natural load distribution tendencies. The natural human knee typically bears the most loads when it is in the fully extended position. Therefore, the testing was performed to mimic this load configuration. An axial compressive load of 3000 N (-3~4 times of 75kg, the average body weight of a human being) was applied since this represents the maximum physiological load that the tibia may experience without fracture in day-to-day use. The tibia plateau in the natural knee is not typically symmetrically loaded. During the experiment the tibia was loaded centrally, medially and laterally. Figure 3.4 shows the loading configurations.

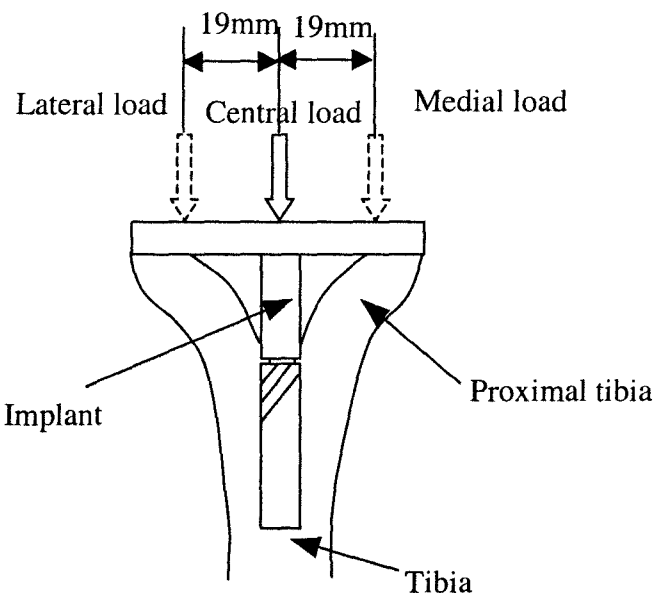

Figure 3.4 Loading configurations

Strain gauges were used to test the strain in bones. 5 strain rosettes (15 gauges in total) were used in each specimen, and were located just under the tibial tray in the following locations: posterior, medial proximal, medial distal, anterior and lateral. Since loading of medial side of the bone is of key interest, 2 strain rosettes were placed at this location, one above the other. Figure 3.5 shows the arrangement of the strain gauges used during the experiment.

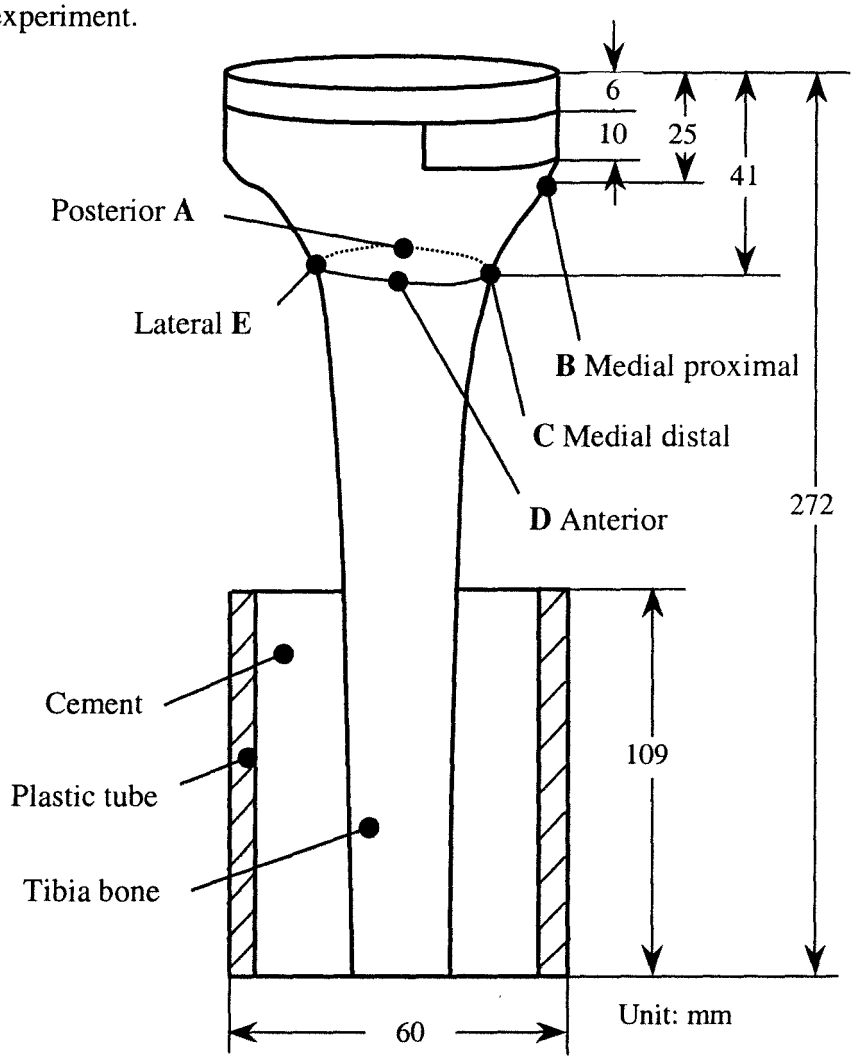

Letters A-E represents strain rosette, each rosette has 3 gauges numbered as follows:
A - 1,2,3; B – 4,5,6; C – 7,8,9; D – 10,11,12; E – 13,14,15

Figure 3.5 Arrangement of strain gauges

The actual experimental device is shown in Figure 3.6. In the cases of central loading, DVRTs were used to measure the displacements at the edges of medial and lateral sides (Figure 3.6 b). The motion of the loading device, which can represent the displacement at the loading region, was measured by a displacement sensor on the Instron 4400 Universal Material Testing Machine. When loading at lateral (Figure 3.6 a), only the displacement at medial edge could be measured by a DVRT because another DVRT couldn't probe at the edge of lateral side due to its conflicting with the loading device. The lateral loading area is marked as lateral* in Figure 3.14. Similarly, under medial loading, the displacement at lateral edge and the loading area marked as medial* in Figure 3.12 were measured as well but not at the central and medial edge.

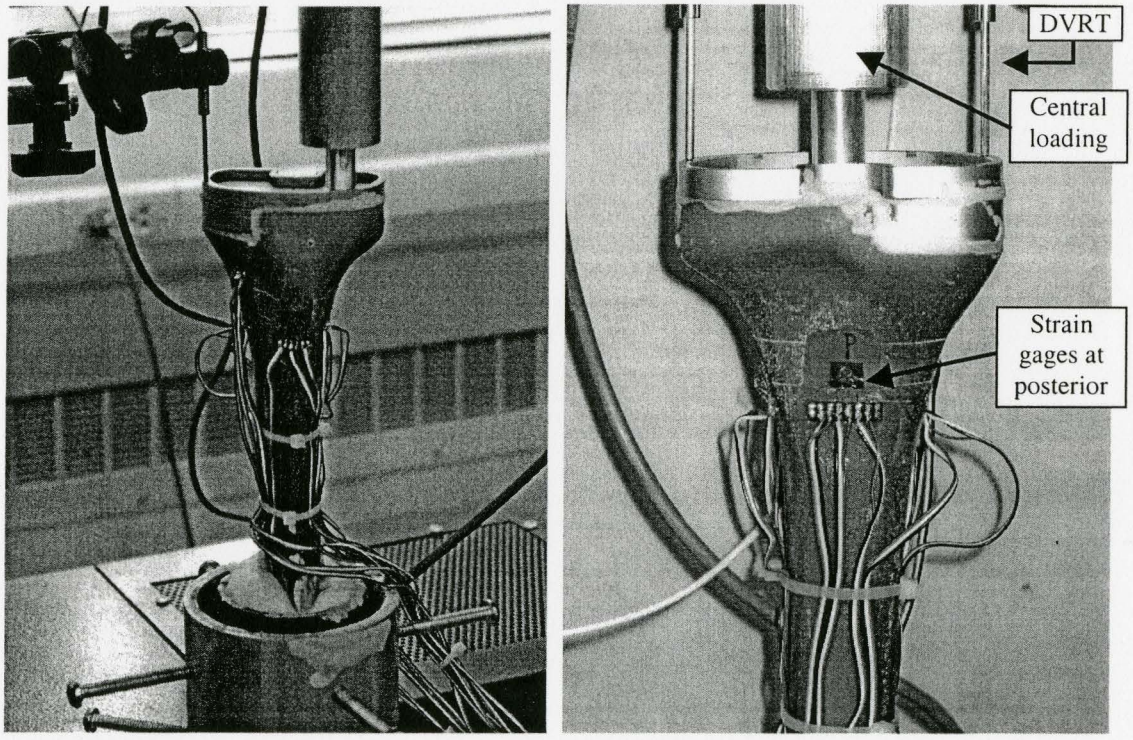

a. Lateral loading b. Central loading

Figure 3.6 Experimental device

3.3 Testing

The testing phase consisted of loading the bone centrally, medially and laterally at 3000 N for each of the following implant cases (shown in Figure 3.7):

1. Deltafit Keel tibial tray only
2. Deltafit Keel tibial tray with block augment
3. Deltafit Keel tibial tray with block and extended stem augments

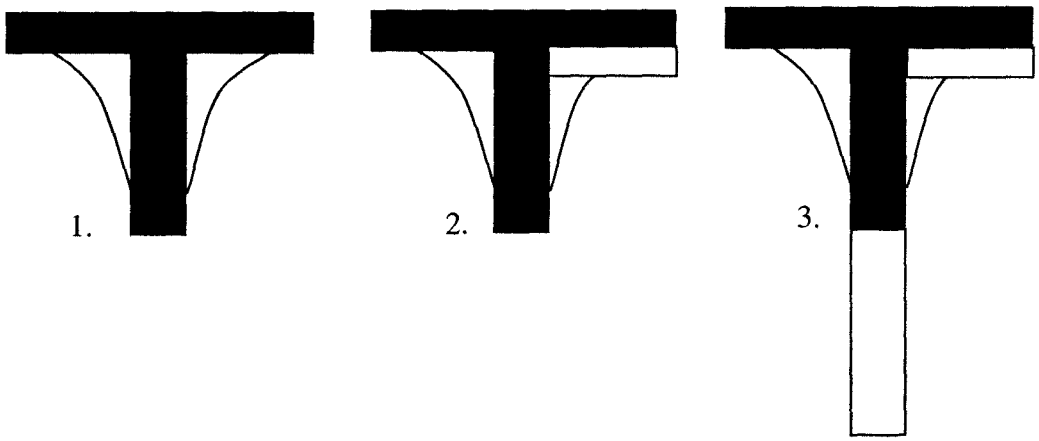

Figure 3.7 Three implant cases tested

For each case, the gauges were zeroed first, after which the bone was gradually loaded up to 3000 N, and then the 15 strain values were recorded. The bone was then gradually unloaded back to 0 N and the strain values were recorded again. Displacement of the DVRTs versus time was recorded on the personal computer for the entire process, as well as load versus time. Since there are three cases under three different loadings and each configuration is repeated 5 times, the total number of tests is 45. Taking the case of tray-block as an example, Table 3.1 and Table 3.2 list the experimental data, the average

and standard deviation. The mean values of the tests for each configuration represent the experimental results. The results show that the standard deviations for all the cases are within a very small range.

Table 3.1 Experimental displacement of medial and lateral loading for tray-block

Medial loading (tray-block)			Lateral loading (tray-block)		
	Lateral	Medial*		Medial	Lateral*
Medial-1	0.3199	-0.7533	Lateral-1	0.1991	-0.6006
Medial-2	0.3071	-0.7279	Lateral-2	0.1957	-0.6515
Medial-3	0.2718	-0.7788	Lateral-3	0.1991	-0.5497
Medial-4	0.2552	-0.7788	Lateral-4	0.1957	-0.6006
Medial-5	0.2578	-0.6770	Lateral-5	0.1914	-0.5752
Mean	0.2823	-0.7431	Mean	0.1962	-0.5955
Standard deviation	0.0249	0.0326	Standard deviation	0.0032	0.0377

Table 3.2 Experimental displacement of central loading for tray-block

Central loading (tray-block)			
	Lateral	Central	Medial
Central-1	-0.2901	-0.3970	-0.2342
Central-2	-0.2739	-0.3970	-0.2342
Central-3	-0.2782	-0.3461	-0.2254
Central-4	-0.2739	-0.3461	-0.2342
Central-5	-0.2739	-0.4000	-0.2298
Mean	-0.2780	-0.3773	-0.2316
Standard deviation	0.0070	0.0284	0.0040

The calibration factors for the DVRT and load cell are as follows:

The sensitivity for the blue DVRT is 0.8507 (mm/volt).

The sensitivity for the red DVRT is 0.8873 (mm/volt).

The sensitivity for load cell is 986.85 (N/volt).

See Appendix B for details.

3.4 Strain calculations

According to the transformation of plane strain, the normal strain in the direction of angle θ in terms of $\varepsilon_x, \varepsilon_y, \gamma_{xy}$ is expressed as follows:

$$\varepsilon(\theta) = \varepsilon_x \cos^2\theta + \varepsilon_y \sin^2\theta + \gamma_{xy} \sin\theta\cos\theta \tag{3.1}$$

Assuming that the arrangement of strain gages used to measure the three normal strains $\varepsilon_1, \varepsilon_2, \varepsilon_3$ is as shown in Figure 3.8, the three normal strains can be represented in terms of $\varepsilon_x, \varepsilon_y, \gamma_{xy}$ as follows:

$$\begin{cases} \varepsilon_1 = \varepsilon_x \cos^2\theta_1 + \varepsilon_y \sin^2\theta_1 + \gamma_{xy} \sin\theta_1 \cos\theta_1 \\ \varepsilon_2 = \varepsilon_x \cos^2\theta_2 + \varepsilon_y \sin^2\theta_2 + \gamma_{xy} \sin\theta_2 \cos\theta_2 \\ \varepsilon_3 = \varepsilon_x \cos^2\theta_3 + \varepsilon_y \sin^2\theta_3 + \gamma_{xy} \sin\theta_3 \cos\theta_3 \end{cases} \tag{3.2}$$

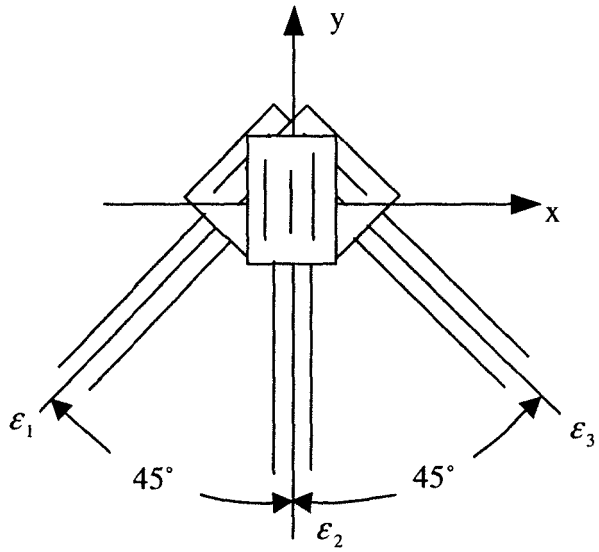

Figure 3.8 Strain gage configuration

The strain rosettes used in our experiment are sets of three strain gauges stacked one on top of another at 45^o to each other (Figure 3.8). Under this configuration, the

three angles corresponding to the three measured normal strains are $\theta_1 = 225^o$, $\theta_2 = 270^o$, $\theta_3 = 315^o$. Based on equation 3.2, the normal and shear strains $\varepsilon_x, \varepsilon_y, \gamma_{xy}$ can be obtained.

The process for solving the principal strains $\varepsilon_a, \varepsilon_b, \varepsilon_c$ is then as follows:

The average strain: $\varepsilon_{avg} = \dfrac{\varepsilon_x + \varepsilon_y}{2}$ (3.3)

The radius of Mohr's circle: $R = \sqrt{\left(\dfrac{\varepsilon_x - \varepsilon_y}{2}\right)^2 + \left(\dfrac{\gamma_{xy}}{2}\right)^2}$ (3.4)

The principal angle: $\tan 2\theta_p = \dfrac{\gamma_{xy}}{\varepsilon_x - \varepsilon_y}$ (3.5)

The principal strains: $\begin{cases} \varepsilon_a = \varepsilon_{avg} - R \\ \varepsilon_b = \varepsilon_{avg} + R \\ \varepsilon_c = -\dfrac{\nu}{1-\nu}(\varepsilon_a + \varepsilon_b) \end{cases}$ (3.6)

where ν is Poisson's ratio, in our case $\nu = 0.3$

The effective strain: $\varepsilon_e = \dfrac{\sqrt{2}}{3}\sqrt{(\varepsilon_a - \varepsilon_b)^2 + (\varepsilon_b - \varepsilon_c)^2 + (\varepsilon_c - \varepsilon_a)^2}$ (3.7)

3.5 Experimental results and discussions

The effective strains and vertical displacements of the measured locations for three cases under central loading, medial loading and lateral loading are shown from Figure 3.9 to Figure 3.14. The following features can be observed from the experimental results:

In the case of central loading (Figure 3.9), a slight change is noted in effective strain between the first case of tray only and the second case of tray with block augment, while the effective strain decreases significantly at all the measured locations in the third case with the addition of the stem. Posterior and lateral side have larger effective strains than the other locations in case one and case two while almost evenly distributed effective strain at all the measured sites is observed in the third case. In terms of vertical displacement (Figure 3.10), both the second case and the third case show a slight decrease as compared to the first case.

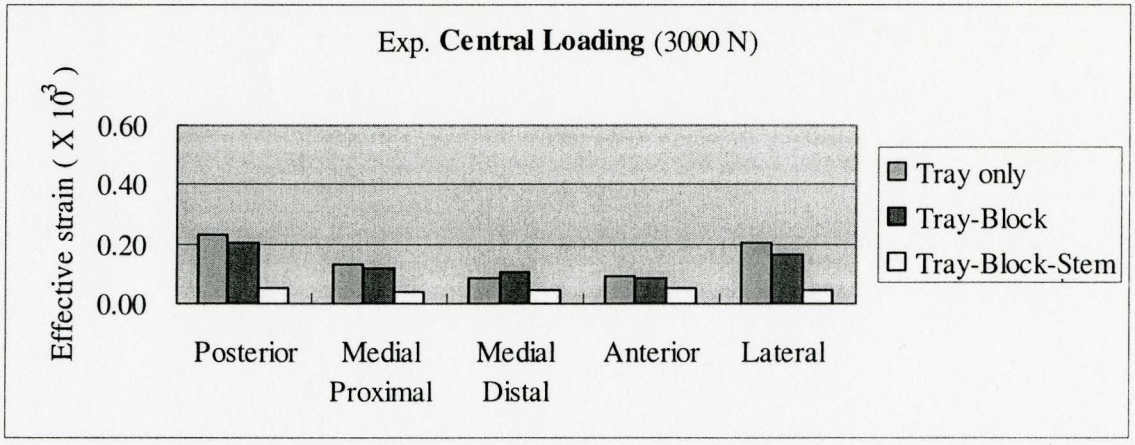

Figure 3.9 Effective strains of three cases under **central loading**

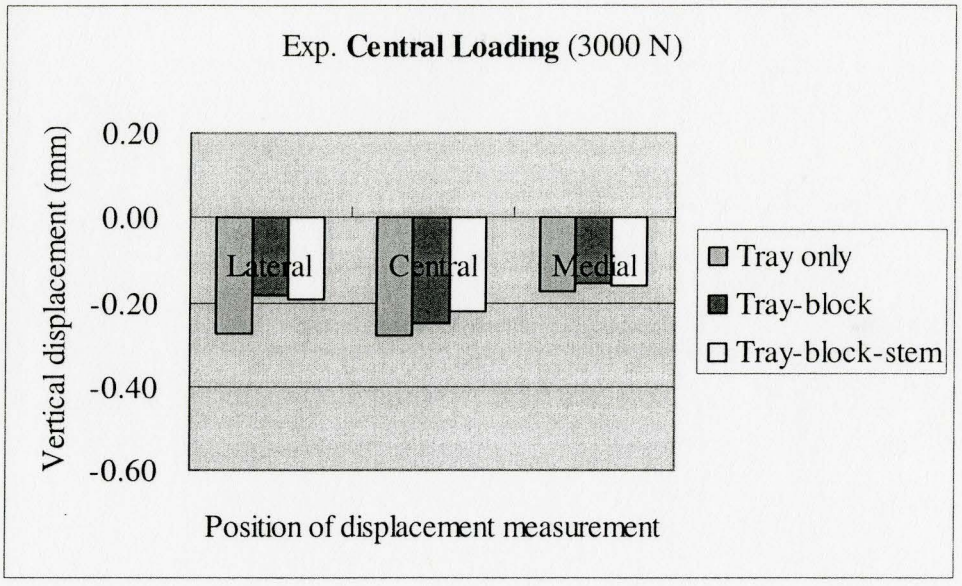

Figure 3.10 Vertical displacement of three cases under **central loading**

In the case of medial loading (Figure 3.11 and Figure 3.12), the results in effective strain somehow confirm the findings in the test of central loading. From the first case to the second case, a slight decrease is noted in effective strain at the location of distal medial, a noticeable drop can be seen at proximal medial, lateral side and posterior and a slight increase at anterior. The displacement change is negligible from the first case to the second case at both lateral and medial measured sites. However, in the last case with the inclusion of the stem, a significant drop in effective strain is noted at the medial side and again more evenly distributed strain can be observed as compared to the other two cases. Larger effective strain and vertical displacement occur in medial side than the other measured locations. Moreover, the results show a tipping effect in displacement as the lateral side actually displaces in the opposite direction to the load application.

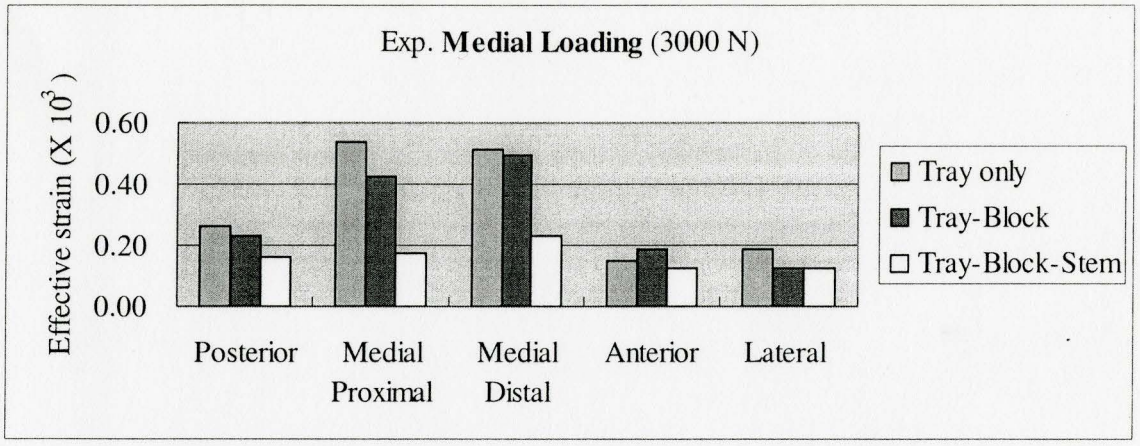

Figure 3.11 effective strains of three cases under **medial loading**

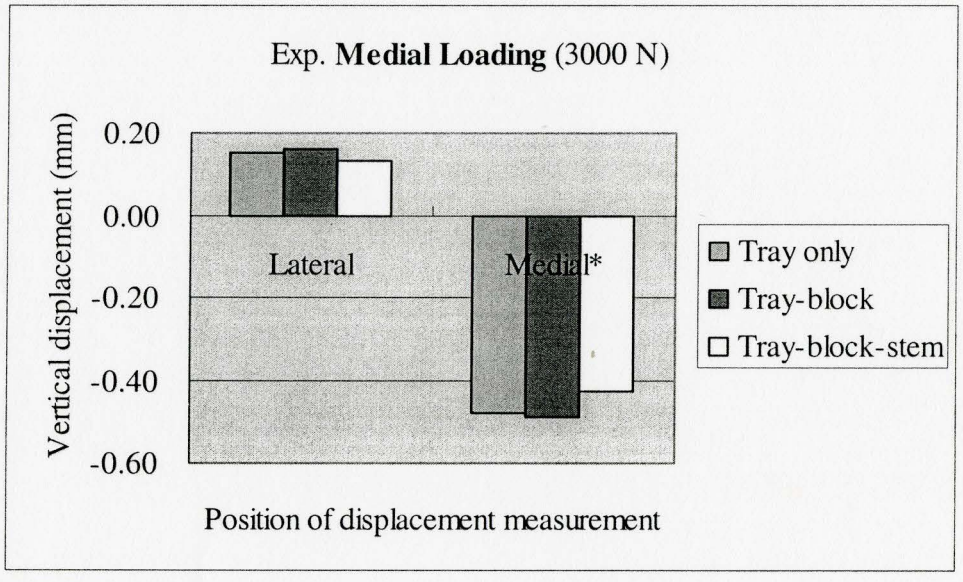

Figure 3.12 Vertical displacements of three cases under **medial loading**

In the case of lateral loading (Figure 3.13 and Figure 3.14), similar phenomena are observed. A negligible change is presented in effective strain between the first case and the second case at almost all the measured locations while a significant decrease as compared to case one and case two and more evenly distributed strain at all the measure locations are noted in the third case. Lateral side and posterior have larger strain than the

other measured locations. Again a tipping effect in displacement is found as the medial side actually displaces in the opposite direction to the direction of loading.

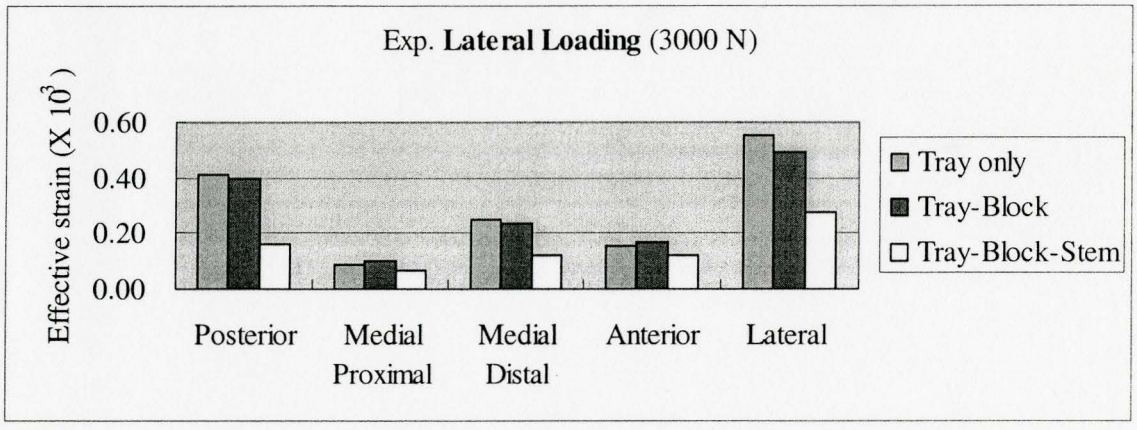

Figure 3.13 effective strains of three cases under lateral loading

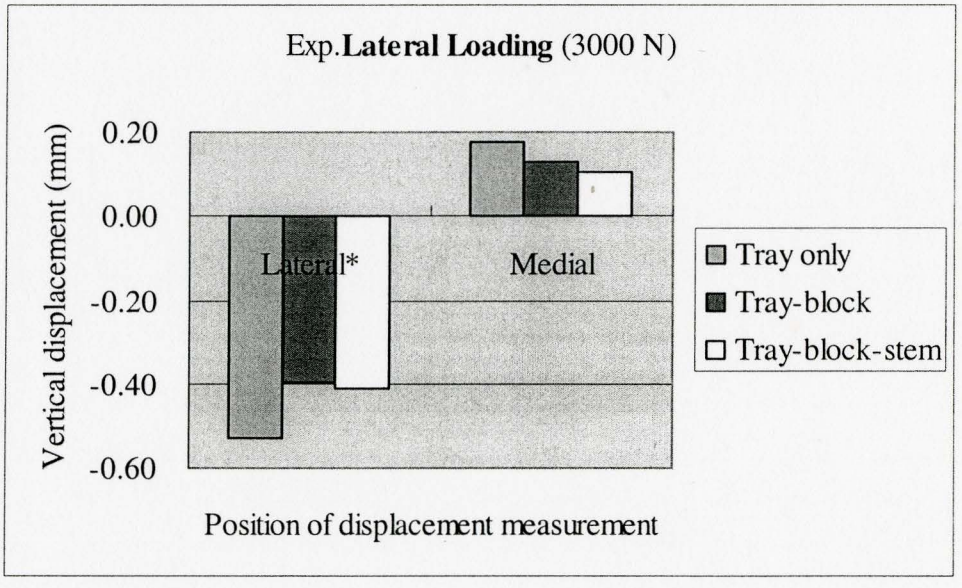

Figure 3.14 Vertical displacements of three cases under **lateral loading**

From the analysis of the experimental results, the following conclusions can be drawn:

1. Comparable stability is found between the case composed of the Deltafit Keel tibial tray without bone defect and the case of tray with block augment with bone defect assumed.

As discussed previously, case one and case two have very similar outcomes in effective strain and slight difference in displacement under central, medial and lateral loadings. This leads to a conclusion that a knee experiencing bone defect can experience almost the same post-operative outcome as that of a knee without bone defect, by means of using the tray with block configuration. This alone infers that when bone defect occurs, the block alone supplies enough stability to the system. However, this determination should be made on a case-by-case basis. Factors such as the severity of bone defect, the person's age, weight and medical condition all should be considered before making a decision.

2. Moderate increase in stability found in the case comprised of the Deltafit Keel tibial tray with both block and stem augments.

The introduction of the extended stem results in a significant reduction of effective strain at almost all the measured locations (Figure 3.9, Figure3.11 and Figure 3.13) but a relatively smaller degree of reduction on the displacements and also a slight improvement on tipping as compared to the other two cases (Figure 3.10, Figure3.12 and Figure 3.14). With these criteria combined, we can conclude that the stem augmentation

confers more stability. The strain decrease verifies that the stem offers moderate shielding from the loads to the tibia since the stem transmits the loads to the cortex further down the tibia.

Although more stability can be achieved, stress shielding is a potential problem when the stem is used. Bone that is used to a certain amount of strain is strong enough to bear that strain. If shielded sufficiently, the bone is likely to lose its load bearing properties and becomes atrophic.

Chapter 4

Geometric Modeling

4.1 Introduction

Geometric modeling of the human knee joint in this study includes the following aspects:

- Model the artificial knee parts such as the tray, the tray with augment and the tray with augment and extended stem.
- Model the tibia bone (outer cortical bone and inner cancellous bone) with or without bone defect, corresponding to the knee implants.
- Assemble the artificial knee implants onto the tibia bones.

The artificial knee components in this study are provided by Stryker Howmedica Osteonics and are shown in Figure 4.1. The keel tray has extended rippled wings at both side supporting the tray and increasing the area of the contact surface between the implant and the tibia bone. There are many tiny protuberances on the bottom surface of the tray as well as the top and bottom surfaces of the augment block for better contact and adhesion. The extended stem is connected to the tibia tray and fixed by a screw through

the center hole of the tray. Bone defect is considered at medial side of the knee so the block is located at this side. The assembled implant with the block and the extended stem augments is shown in Figure 4.2.

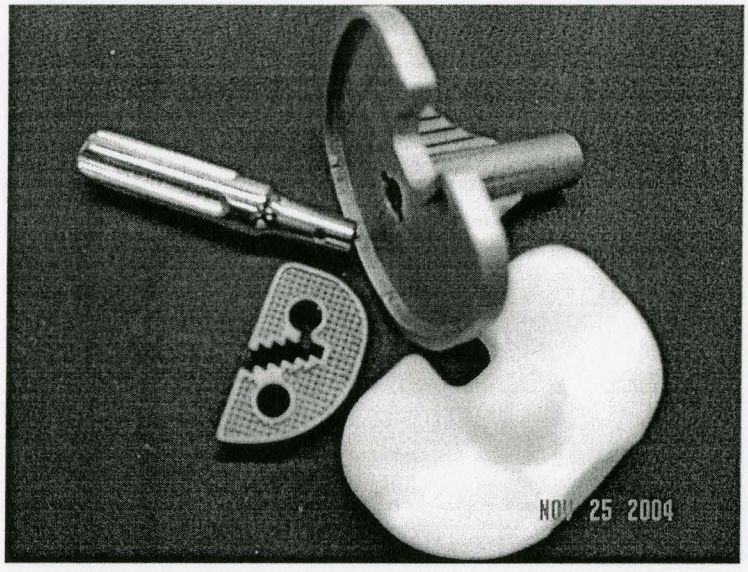

Figure 4.1 Artificial knee components

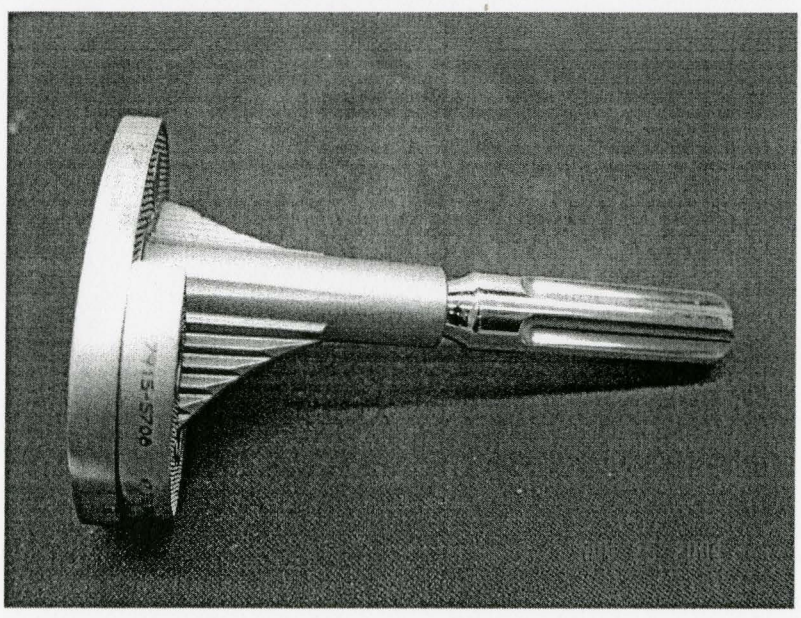

Figure 4.2 Implant with block and stem

4.2 Geometric modeling of artificial knee

All the modeled artificial knee components, manufactured by Stryker Howmedica Osteonics, are measured in detail in order to obtain the dimensions and are then geometrically modeled with CATIA. During modeling, the following simplifications have been made to model the artificial knee:

- The bottom surface of the tray as well as the top and bottom surfaces of the augment block with the tiny protuberances is simplified to flat surface. In order to simulate the effect of the tiny protuberances on the bottom surface of the tray as well as the top and bottom surfaces of the augment block, in the FE simulation, the assembled model (implant, cortical bone, cancellous bone) is treated as one single part with different material properties in different areas. In this way, all the interfaces are assumed to be completely contacted and bonded.
- For case 2, the tray and the block augment are integrated into one part since they are cemented together. In case 3, the extended stem is connected and fixed to the tray by a screw. Similarly, the tray, block and stem are modeled as one solid part since they are made from the same material.

  Figure 4.3 - Figure 4.5 display the geometric models for the three cases investigated in this study.

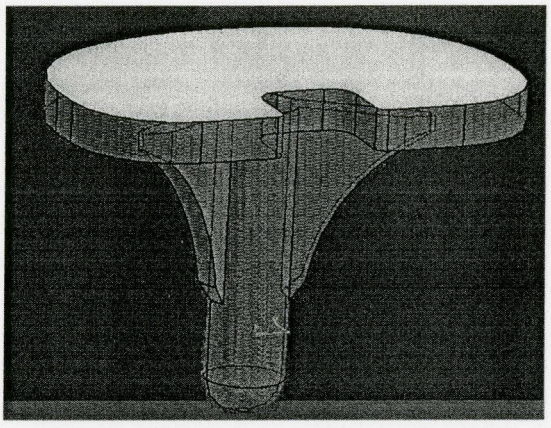

Figure 4.3 Geometric model of tibia tray

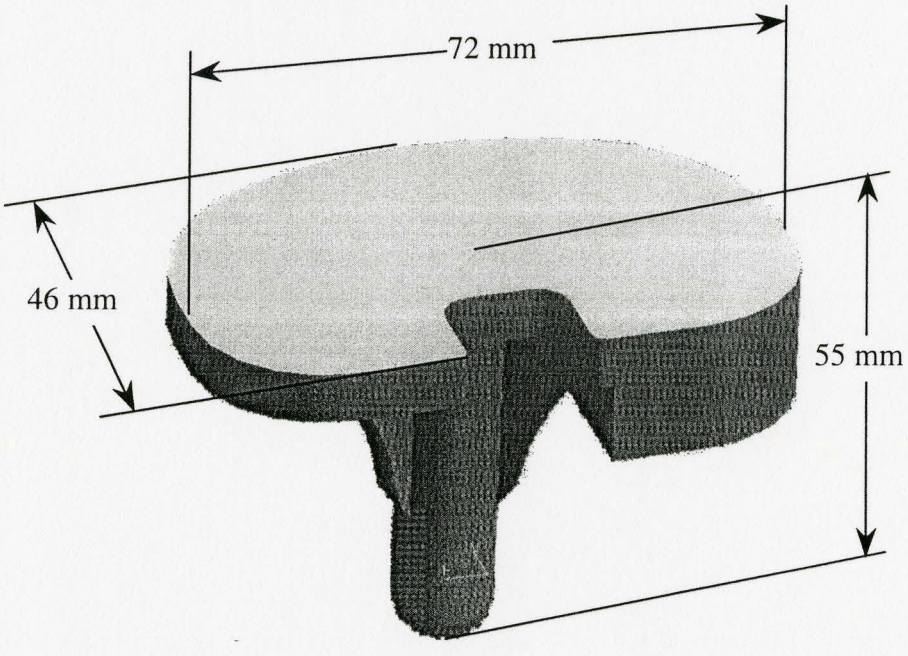

Figure 4.4 Geometric model of tibia tray with block

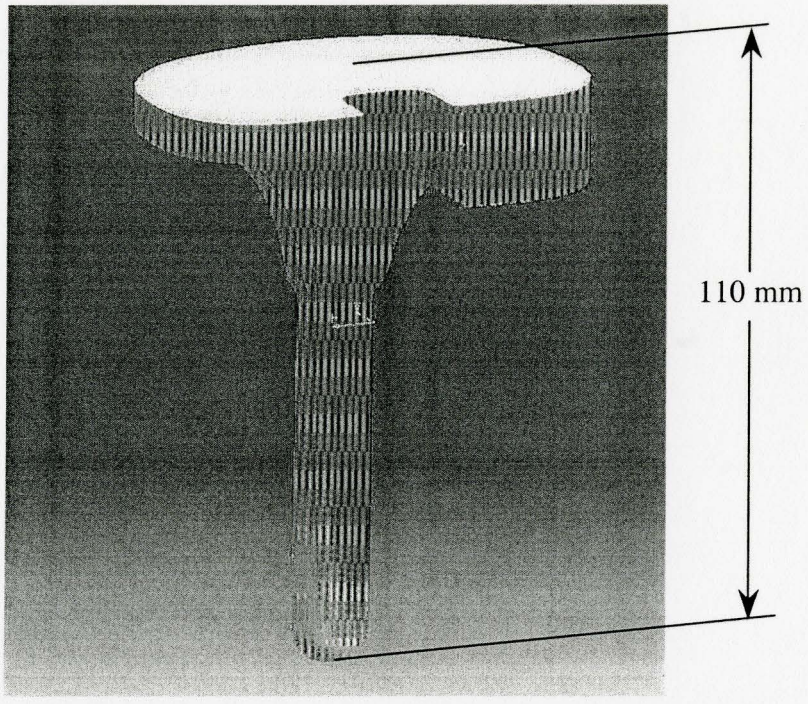

Figure 4.5 Geometric model of tibia tray with block and extended stem

4.3 Geometric modeling of tibia bone

The tibia bone shell was downloaded from Biomechanics European Laboratory (http://www.tecno.ior.it/VRLAB/researchers/repository/BEL_repository.html), and it is shown in Figure 4.6. This model is a preliminary model of a tibia bone and the shell is formed by six separate pieces, which cannot be directly used for our study.

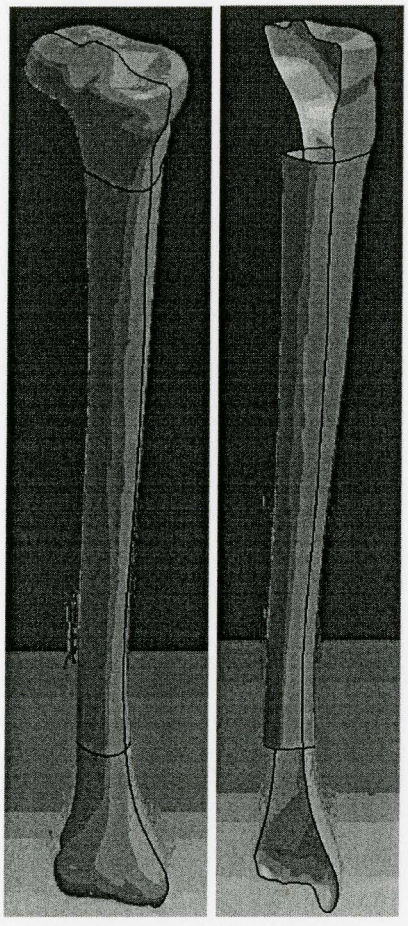

Figure 4.6 Tibia bone shell

In order to make use of it, the following tasks have been done:

1. Stitch the boundaries of the individual surfaces together to form the outer surface of the tibia bone.
2. Convert the tibia shell model from step 1 into a solid tibia bone model.
3. Rescale the solid tibia bone to match the size of the experimental composite bone.
4. Cut the top part of the solid tibia bone model to fit the keel tray.
5. Generate the interface loops of the cortical and cancellous bone from the model in step 4.

Since the tibia bone consists of outer cortical bone and inner cancellous bone, the boundary between them had to be formed manually. As a matter of fact, the thickness of the cortical bone varies along the axial direction (thin at top and thick at bottom), which makes the boundary formation very difficult and tedious. This task is achieved by making lots of cross-sectional cuts on the solid tibia model and then offsetting/shrinking the profile of the cross-section according to the thickness of the cortical bone at the corresponding location. In this way, the inner surface loops of cortical bone have been formed (see Figure 4.7).

6. The generated loops are then used to define the boundary surface between the cortical and cancellous bone in CATIA. The whole tibia bone geometric model, including cortical and cancellous bone, is shown in Figure 4.7.
7. In order to assemble the geometric models mentioned above, the intersection between the tibia bone and the implant must be formed first on the tibia bone. To achieve this, a Boolean subtraction is applied on the tibia bone by subtracting the contact surfaces of the implant (see Figure 4.8 b).
8. Then make a cut on the cortical and cancellous bone to fit the augment block shown in Figure 4.9.

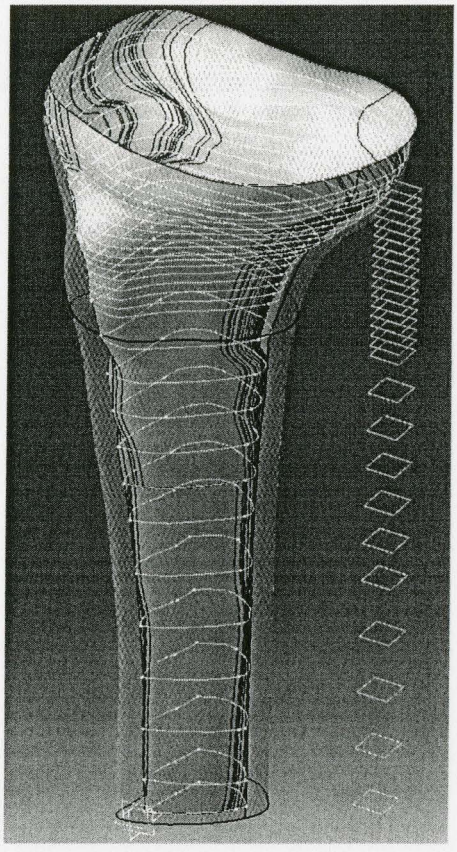

Figure 4.7 Cortical and cancellous bone construction

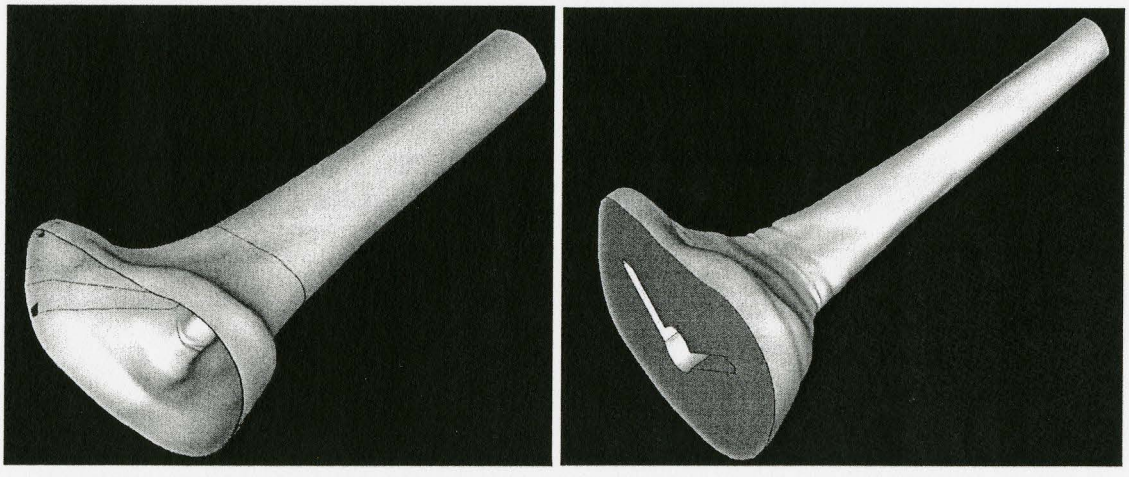

a. Cortical bone b. Cancellous bone

Figure 4.8 Geometric models of cortical and cancellous bone

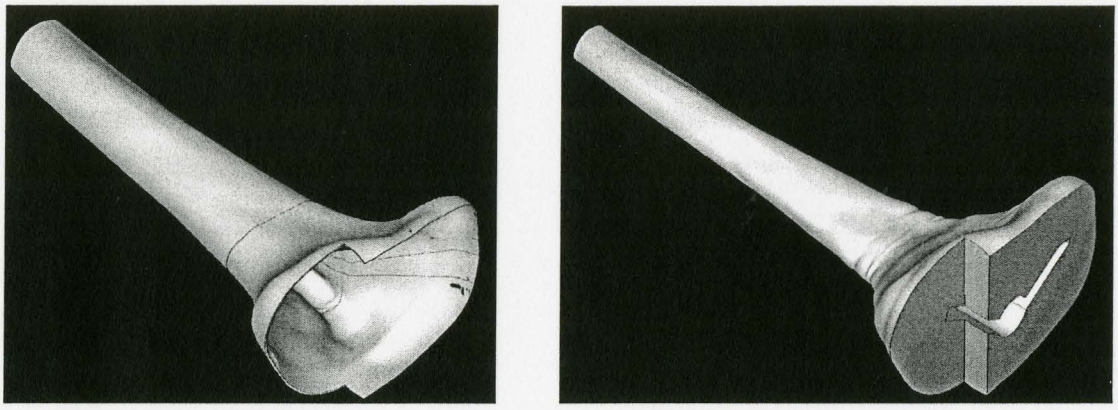

a. Cortical bone with bone defect b. Cancellous bone with bone defect

Figure 4.9 Geometric models of cortical and cancellous bone with bone defect

4.4 Model assembly

Once all the geometric models are prepared, they can be assembled in CATIA to form the assembled models for FEA simulation. Figure 4.10 shows the assembled models. The geometric models are saved as IGS/IGES files.

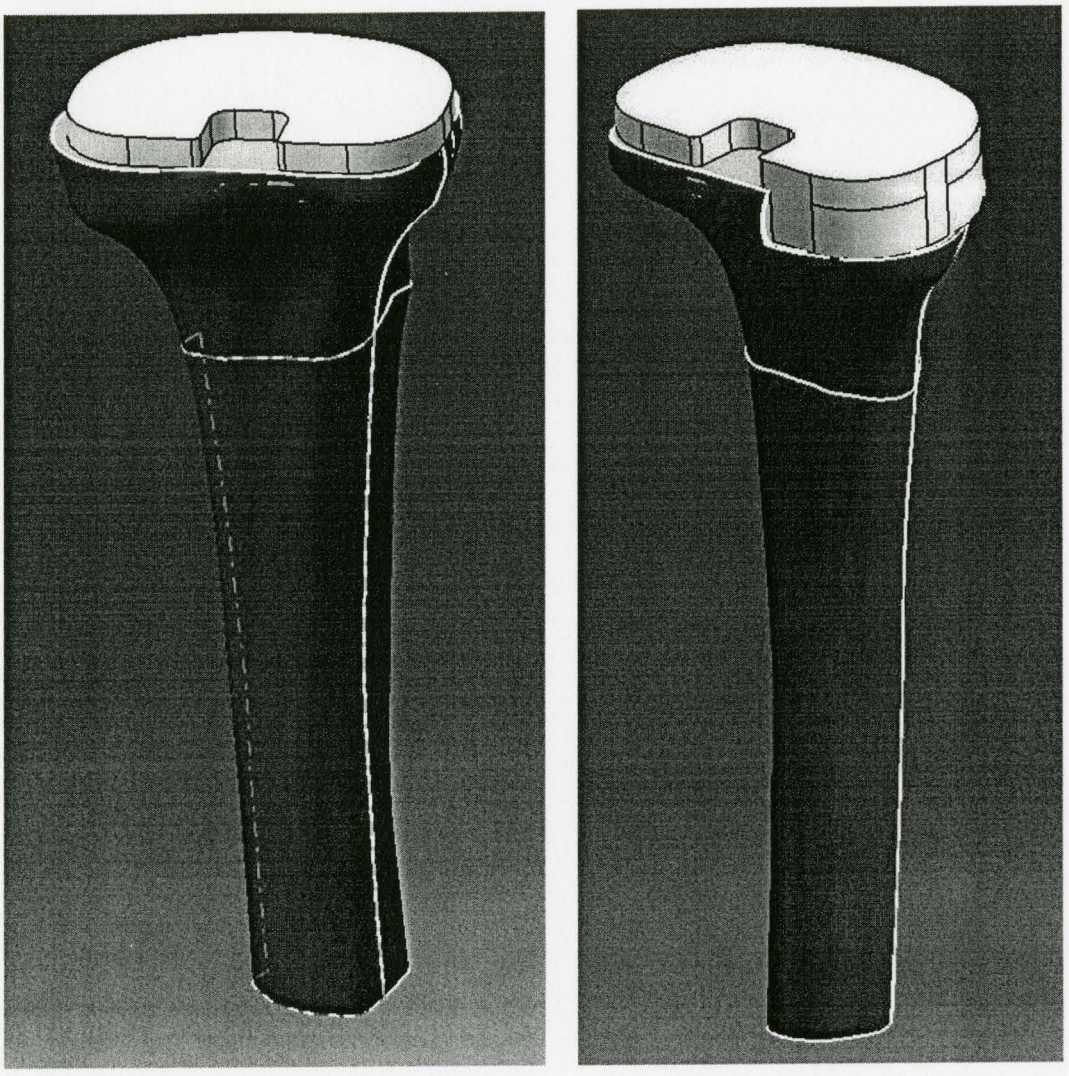

a. Tray only b. Tray with block

Figure 4.10 Assembled geometric models

Chapter 5

Finite Element Analysis

This chapter consists of FE modeling and simulations, result analysis and comparison, and discussions. Nine cases consisting of three configurations with lateral, medial and central loadings, separately imposed on each configuration, are simulated. Furthermore, the influence on simulation results due to small variations in the location of loading is also studied by offsetting the load in various directions. Moreover, the trend of the strain variation of the adjacent elements in posterior, medial proximal, medial distal, anterior and lateral areas is investigated as well.

5.1 FE modeling

FE modeling includes meshing the geometric model of all the components, setting the material properties for all the parts, constraining the model, imposing the load on the model, requesting the output, running the model and outputting the results. Since this study involves static stress/displacement analysis, Abaqus/Standard 6.4 is used for simulation.

5.1.1 Meshing

The geometric model of the knee developed using CATIA system has been described in the previous chapter. The next critical task is to properly mesh the components. In general, the assembled geometric models (IGES files) can be directly imported into Abaqus system, and Abaqus mesh generator can generate mesh for the components involved. However, in our case, which is a complicated geometric model, Abaqus is not able to hex mesh it, especially the cortical and the cancellous bones. Figure 5.1 is a transparent assembled geometric model. It is seen that the wall thickness of the cortical bone changes from top to bottom. Instead of relying on Abaqus mesh generator, a specific meshing tool, TrueGrid mesh generator (XYZ Scientific Application Inc.), which is able to tackle the components with very complicated shapes, is employed to create the hexahedral mesh from IGES geometry files representing the three components. The outer and/inner surfaces of the block structure mesh of each component was projected on to the IGES surfaces and mating surfaces nodes between the outer and inner bone, and between the inner bone and implant were then merged resulting in a mesh with approximately 48000 nodes and 45000 elements. The meshed parts and the assembled model are shown in Figure 5.2.

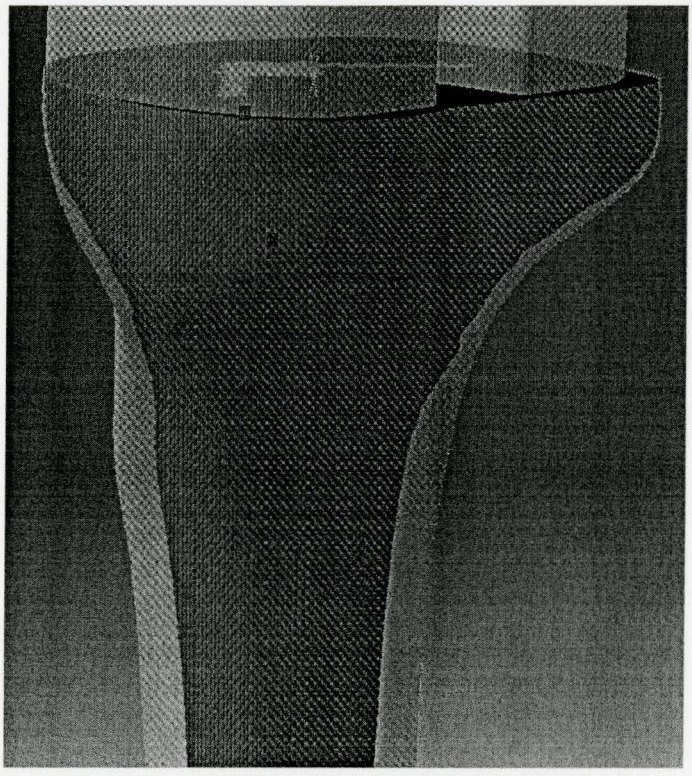

Figure 5.1 Cortical bone and cancellous bone

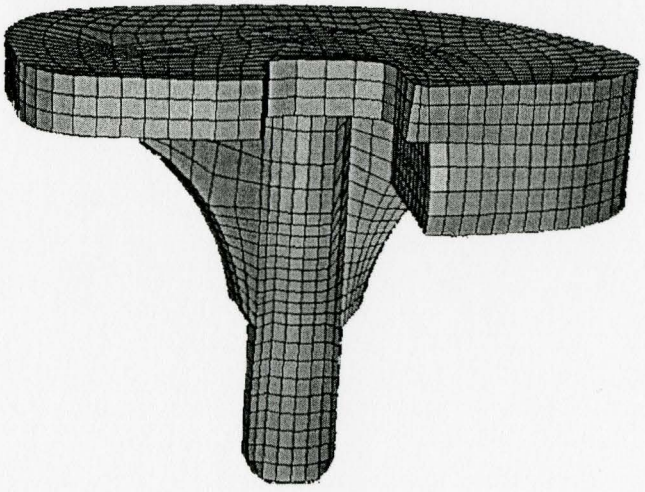

a) Tray with block

b) Cancellous bone

c) Cortical bone

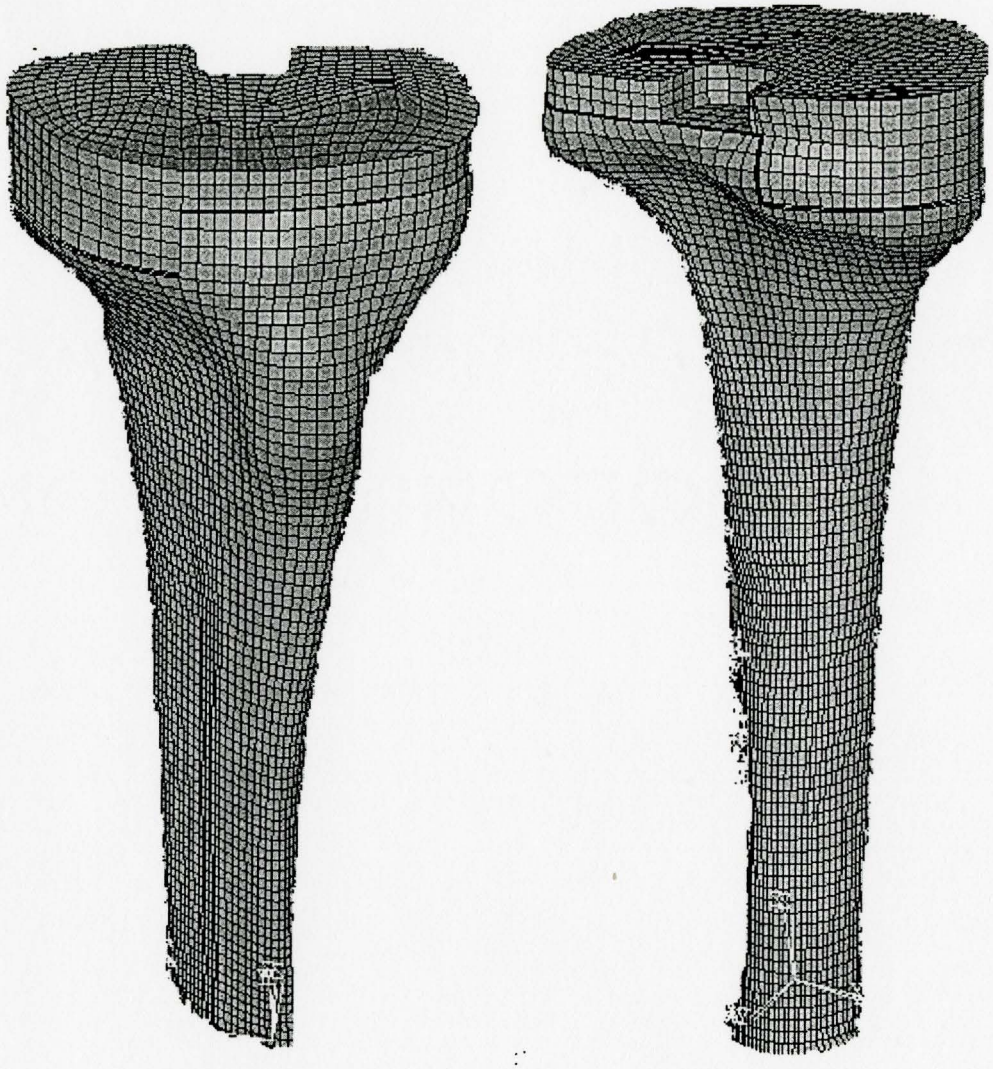

d) Assembled model (front and side view)

Figure 5.2 Meshed parts and assembled model

5.1.2 Abaqus model structure

Abaqus model is organized into an assembly of part instances. The FE model basically consists of part definition, assembly, material properties, boundary conditions and analysis steps. Figure 5.3 shows the scheme of the input file of the model.

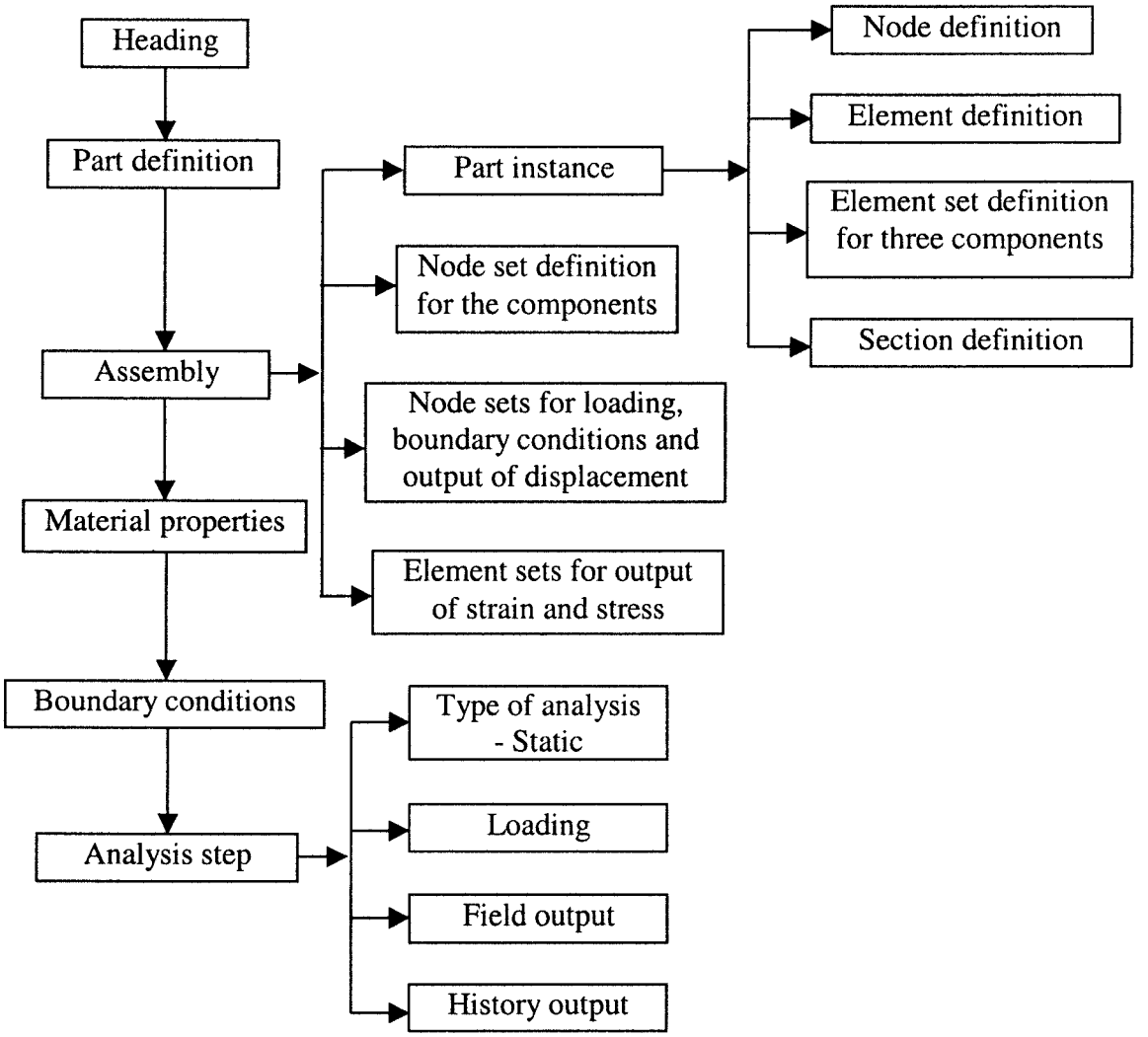

Figure 5.3 the scheme of the input file of the FEA model

In this study, cortical bone, cancellous bone and implant are assembled into one model and the model is treated as one part in the input file. In order to separate them, the nodes and the elements of each component are defined as a node set and an element set respectively and then different material properties are assigned to different element sets corresponding to the components. Other element sets are defined for the output of strain

and stress at the interested locations corresponding to the locations of the strain gages in the experiments. In addition, node sets are defined for imposing the loads, constraining the boundary and outputting the specific displacements corresponding to the measured locations in experiments.

5.1.3 Material properties

In this study, the material properties of the composite bones and the implants were provided by the manufacturers. In this project, a lower bone mass was used comparable to the one on an old age where the implant is frequently used. These properties are listed in Table 5.1.

Table 5.1 Material properties

Part name	Material	Elastic modulus (MPa)	Poisson's ratio
Tray, block and stem augments	Titanium	220,000	0.3
Cortical bone	Composite material	14,200	0.3
Cancellous bone	Composite material	137	0.3

As in previous studies, all the materials are considered as isotropic and only elastic properties under room temperature are employed. The unit of Young's modulus is MPa and the dimension unit of the geometric model is millimeter so that the units of the

output are as follows: displacement is in millimeter; the stress is in MPa; and the reaction or contact forces are in Newton.

5.1.4 Boundary conditions

Corresponding to Figure 3.6 (a) that shows how the composite bone is fixed during the experiment, in the FE model, the bottom surface of the tibia bone is fixed while the other nodes are free to move (see Figure 5.4).

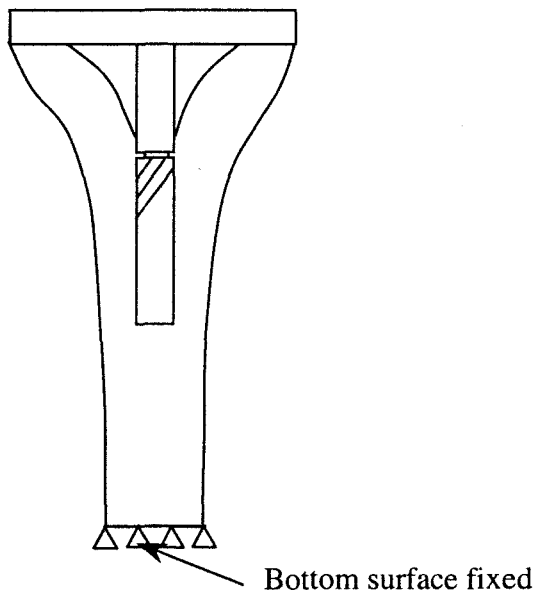

Figure 5.4 Boundary conditions

5.1.5 Loading

A compressive concentrated nodal force of 3000 N is imposed on the nodes that correspond to the medial, central and lateral locations on the tray, respectively. Figure 5.4 shows the three loading locations in FE model. In order to investigate the sensitivity of

the knee to small variations of the loading locations, an investigation in which the locations of the loadings are given small offsets from the original medial, central and lateral locations is carried out.

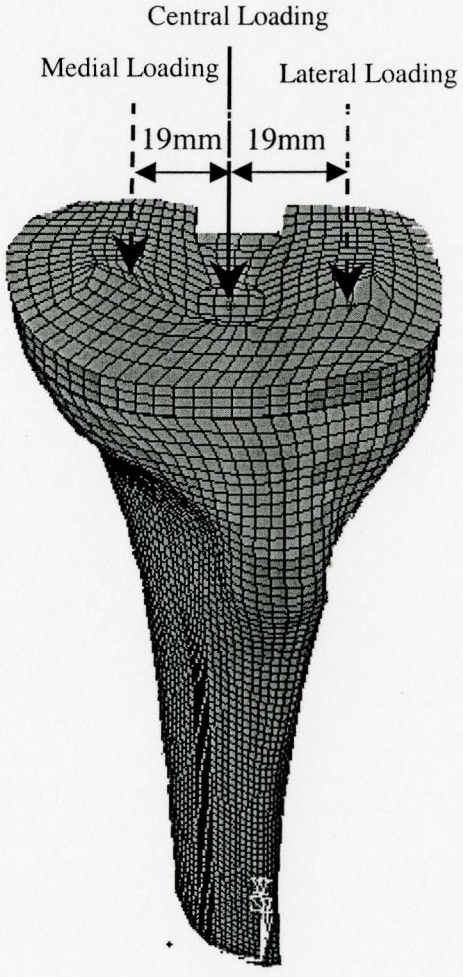

Figure 5.5 Loading locations in FE model

5.1.6 Output request

Field output is requested in FEA model for viewing the strain/stress contour and history output is requested for some node sets and element sets so that the history data from FEA simulation can be used to compare with the experimental results. The required history output from FE simulation is as follows:

- Strain/stress at the areas of posterior, medial proximal, medial distal, anterior and lateral. Figure 5.6 shows their locations in FE model. And the average values of the adjacent elements in these areas are used to represent the results.
- Similar to strain, the displacements at the lateral, central and medial locations corresponding to the experiments are requested in the FEA model. Figure 5.7 shows the locations of displacement output.
- In order to utilize Abaqus/Viewer to display the simulation results, job-name.**odb** file needs to be established by requesting field output and history output using *OUTPUT option.

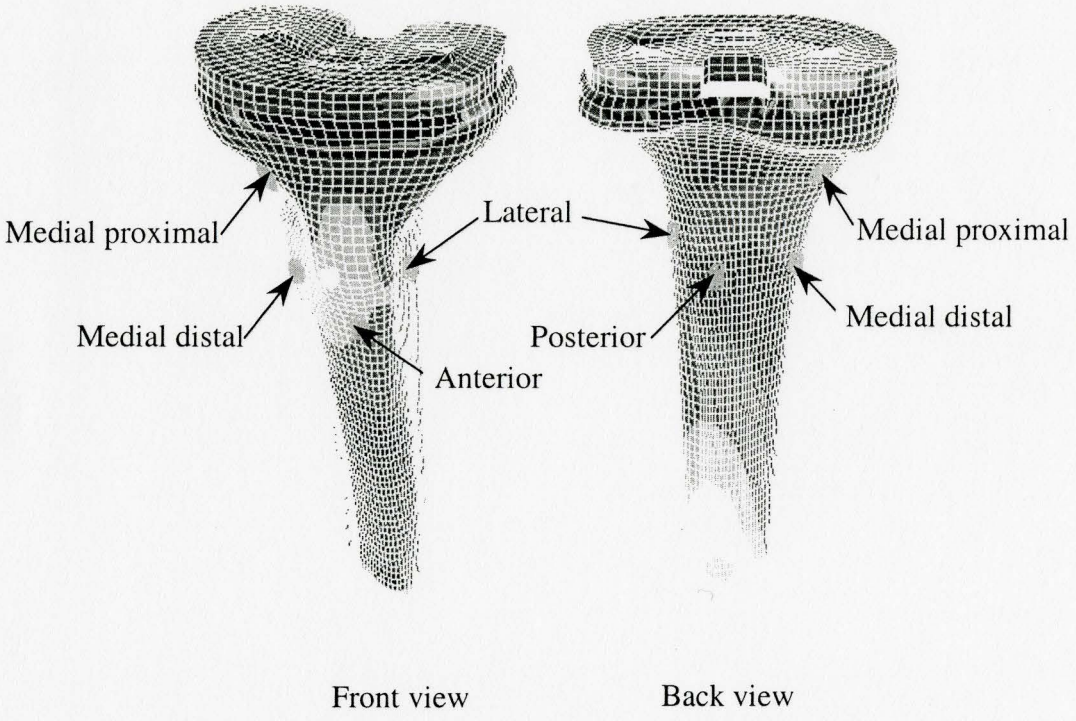

Figure 5.6 Five sites corresponding to the places of strain rosettes

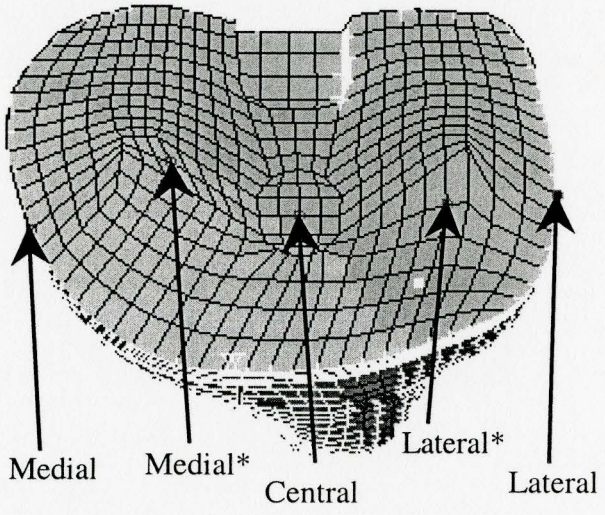

Figure 5.7 Locations for displacement output

The history output data, directly obtained from simulation, include principal strains, principal stresses and displacements. In order to obtain simulated effective strain and equivalent stress, equations 5.1 and 5.2 are employed, respectively.

The effective strain: $$\varepsilon_e = \frac{\sqrt{2}}{3}\sqrt{(\varepsilon_a - \varepsilon_b)^2 + (\varepsilon_b - \varepsilon_c)^2 + (\varepsilon_c - \varepsilon_a)^2} \quad (5.1)$$

where ε_a, ε_b and ε_c are principal strains.

The equivalent stress: $$\sigma_e = \frac{1}{\sqrt{2}}\sqrt{(\sigma_a - \sigma_b)^2 + (\sigma_b - \sigma_c)^2 + (\sigma_c - \sigma_a)^2} \quad (5.2)$$

where σ_a, σ_b and σ_c are principal stresses.

5.2 Investigation of strain gradient at measurement locations

Before determining how many elements should be included to represent the FEA simulation results for the five small regions on cortical bone shown in Figure 5.6, the strain variation of the adjacent elements surrounding posterior, medial proximal, medial distal, anterior and lateral locations are investigated. By varying the configurations under the same loading and varying the loadings on one configuration, the following cases are studied:

$$Medial\ loading \begin{cases} tray\ only \\ tray - block \\ tray - block - stem \end{cases}$$

$$Tray-block\begin{cases} medial\ loading \\ central\ loading \\ lateral\ loading \end{cases}$$

Figures 5.8-5.10 show the results of tray only, tray-block and tray-block-stem under medial loading respectively, while the results of tray-block under the medial, central and lateral loadings are exhibited in Figure 5.9 and Figures 5.11-5.12, respectively. All the results, shown in these figures demonstrate that the strain distributions are relatively flat at the selected locations of measurements. The average value of these elements at each location is therefore expected to provide reliable results. Further results related to the strain contour surrounding posterior, medial proximal, medial distal, anterior and lateral under central loading can be found in Appendix C.

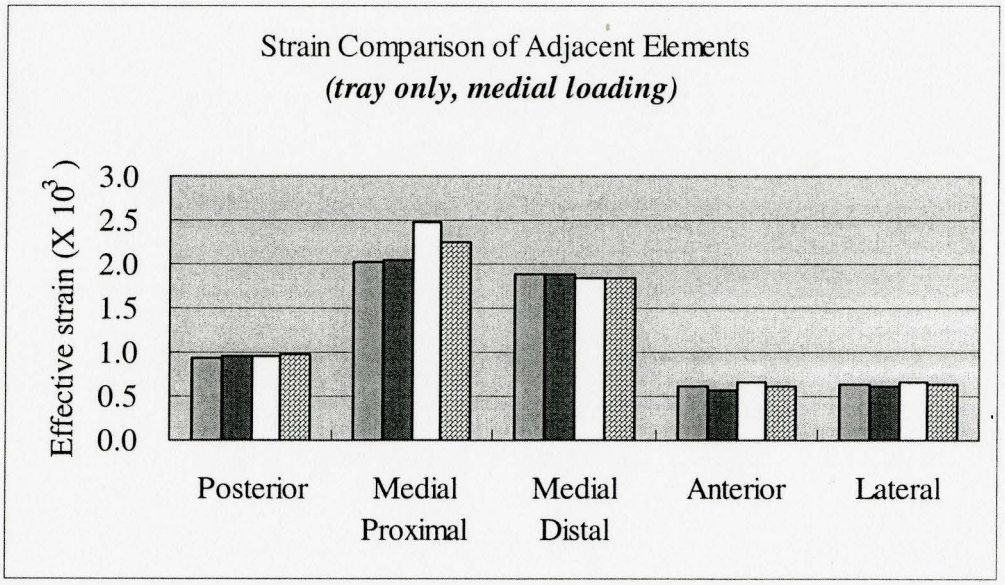

Figure 5.8 Effective strains of adjacent elements under medial loading **(tray only)**

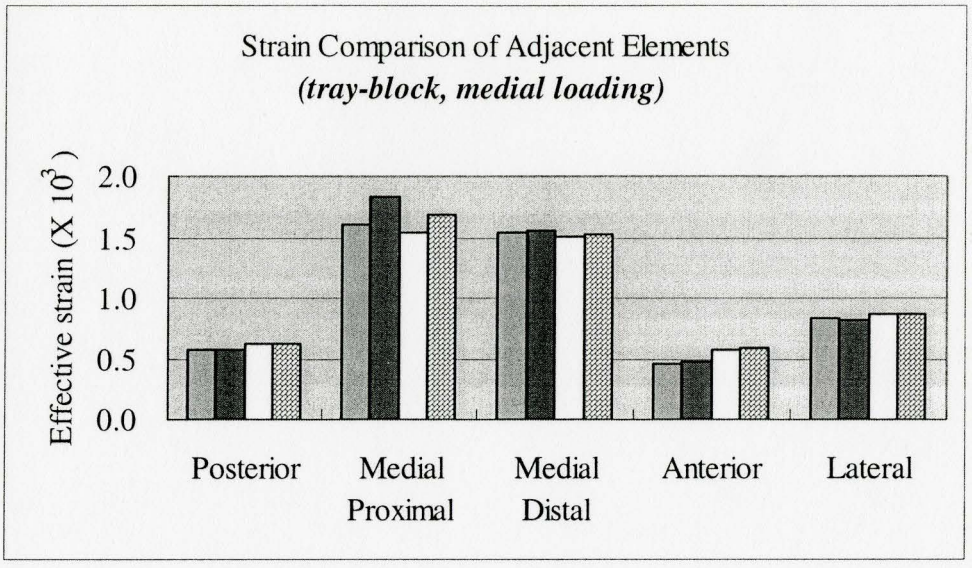

Figure 5.9 Effective strains of adjacent elements under medial loading **(tray-block)**

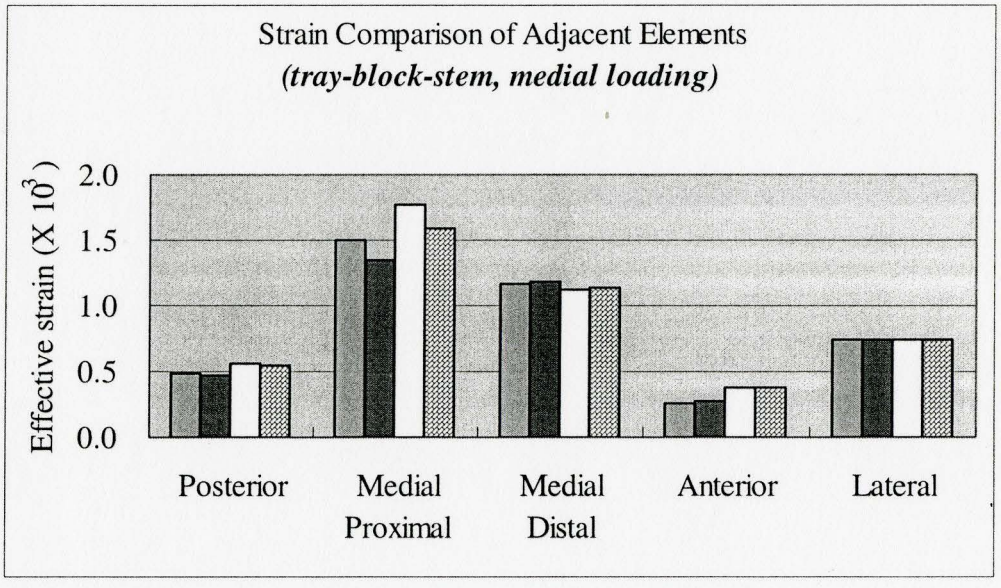

Figure 5.10 Effective strains of adjacent elements under medial loading **(tray-block-stem)**

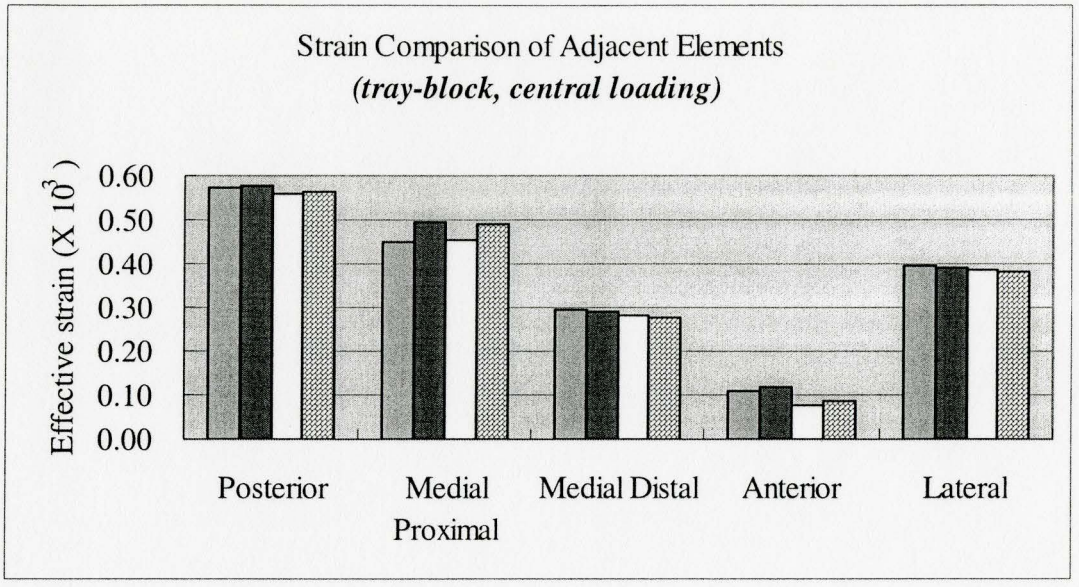

Figure 5.11 Effective strains of adjacent elements under central loading **(tray-block)**

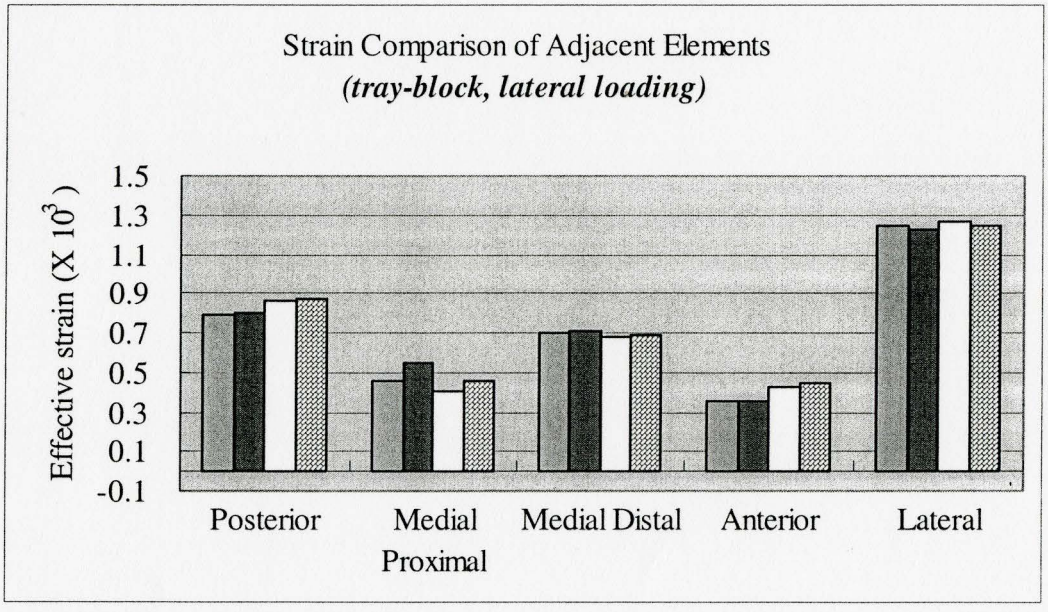

Figure 5.12 Effective strains of adjacent elements under lateral loading **(tray-block)**

5.3 Sensitivity to location of loading

The purpose of this section is to investigate how sensitive the elements on the composite knee are to a slight offset of the loading location. The studied cases are:

$$Medial\ loading \begin{cases} tray\ only \\ tray - block \\ tray - block - stem \end{cases}$$

In these cases, the location of the medial load has a slight offset in four directions (left, right, front and back) as shown in Figure 5.13. The offset is in a range of 2.74 to 2.84 mm for the three cases. The simulation results of strain and displacement are shown from Figures 5.14 to 5.19.

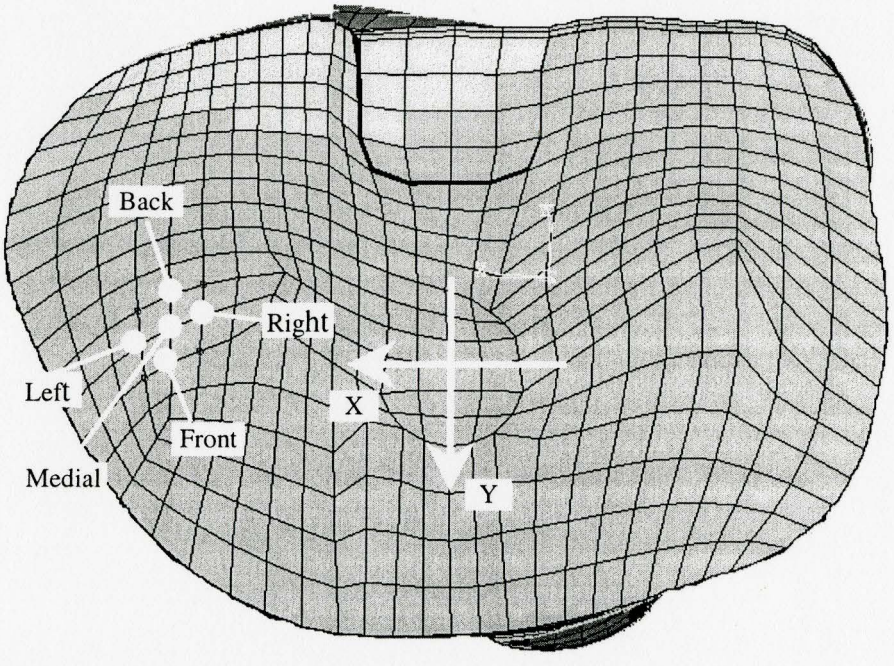

Figure 5.13 Load offsetting in medial side

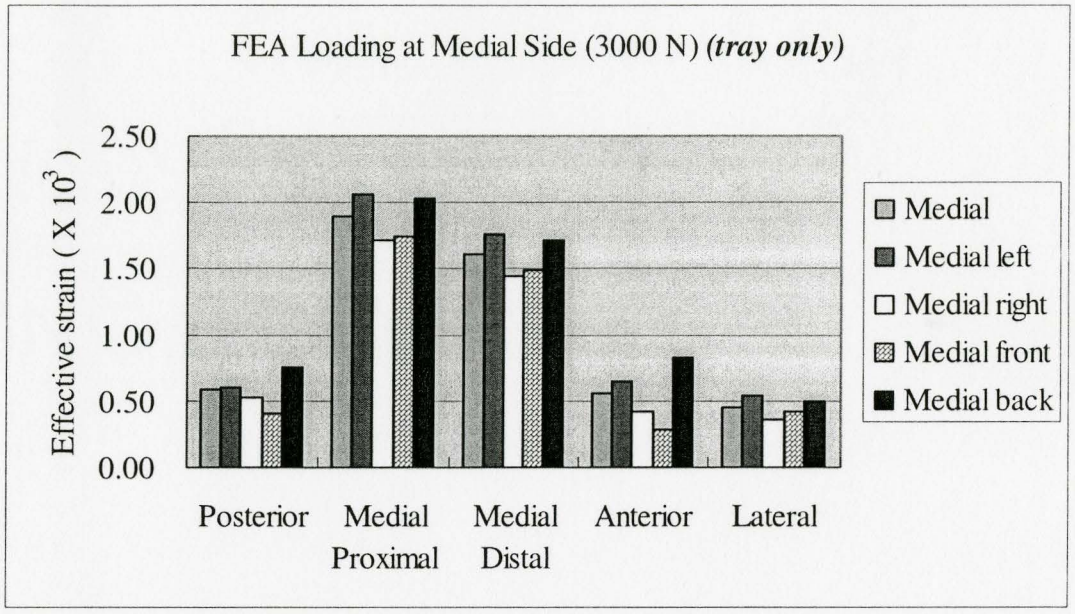

Figure 5.14 Effective strain versus loading offset in the case of **tray only**

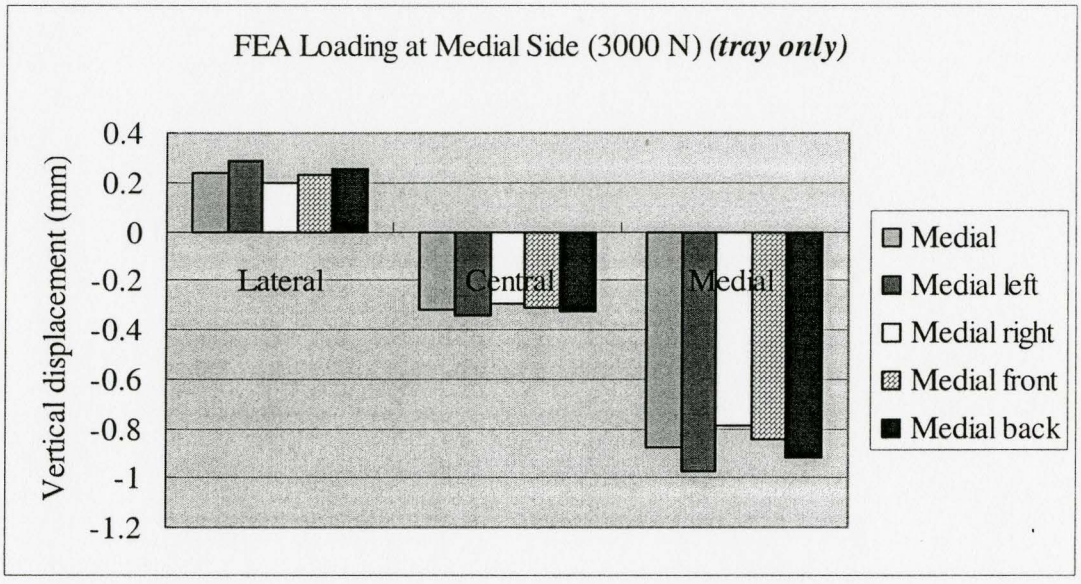

Figure 5.15 Vertical displacement versus loading offset in the case of **tray only**

From Figure 5.14 and 5.15 we can see that the loading offset along either the direction of left-right or the direction of front-back (Figure 5.13), in this tray only case, only causes slight changes in effective strain and vertical displacement. When the loading

has a slight offset in right or front directions, a slight decrease in both strain and displacement can be observed. When the loading offsets in left and back directions, there is a slight increase in both strain and displacement.

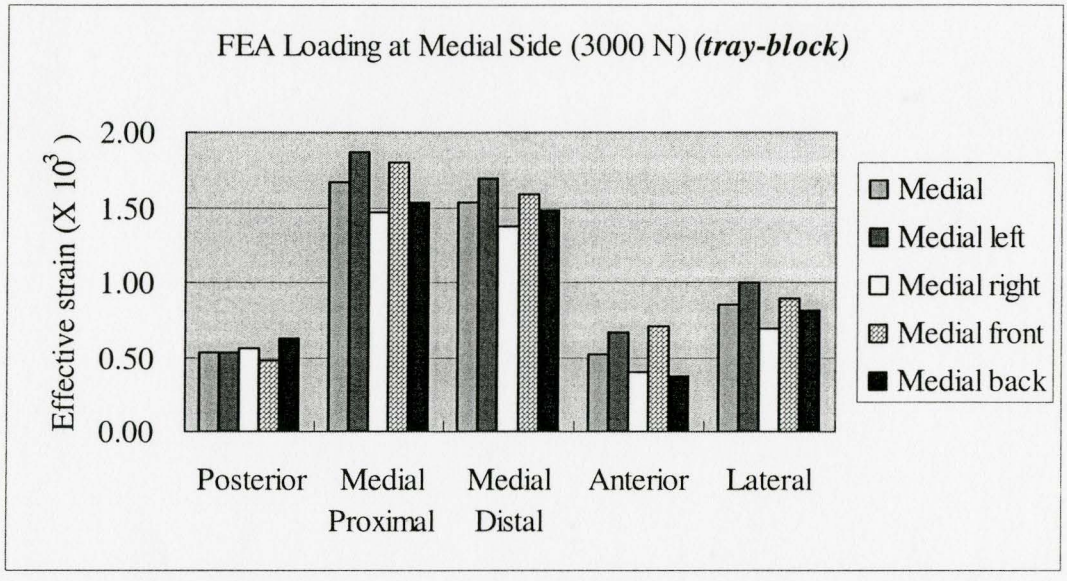

Figure 5.16 Effective strain versus loading offset in the case of **tray-block**

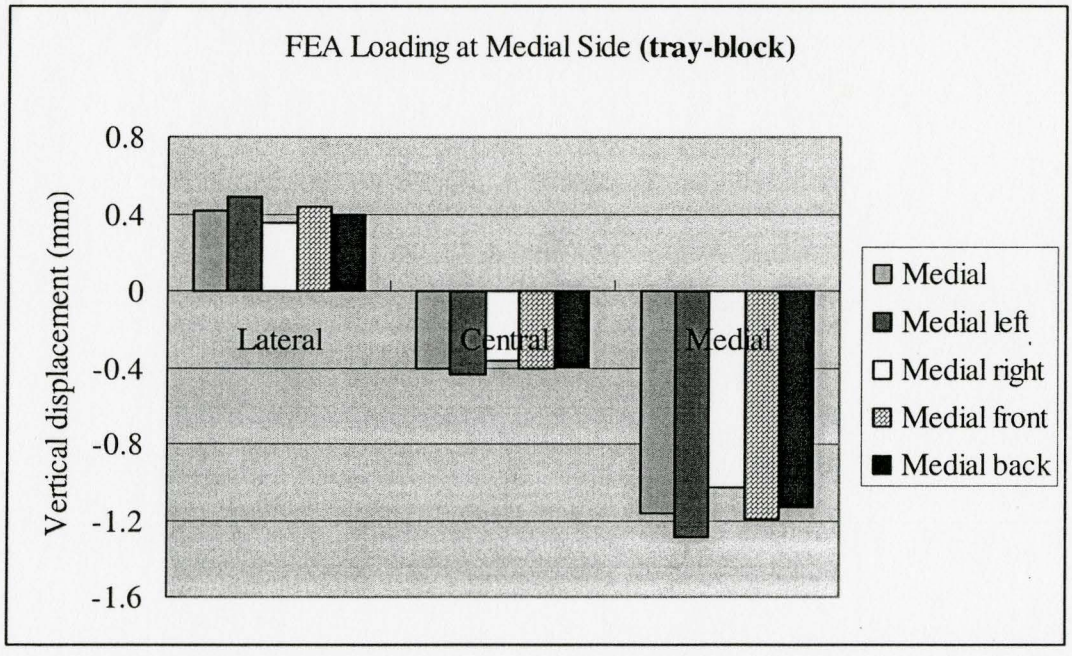

Figure 5.17 Vertical displacement versus loading offset in the case of **tray-block**

Similar to the case of tray only, the strain change is still limited in the case of tray-block when the loading was offset from the original loading spot at both X and Y direction. The loading offsetting in left and front direction can cause a very slight increase in both strain and displacement while in the rest of the directions the strain and displacement have a slight decrease or remain the same (Figure 5.16 and 5.17).

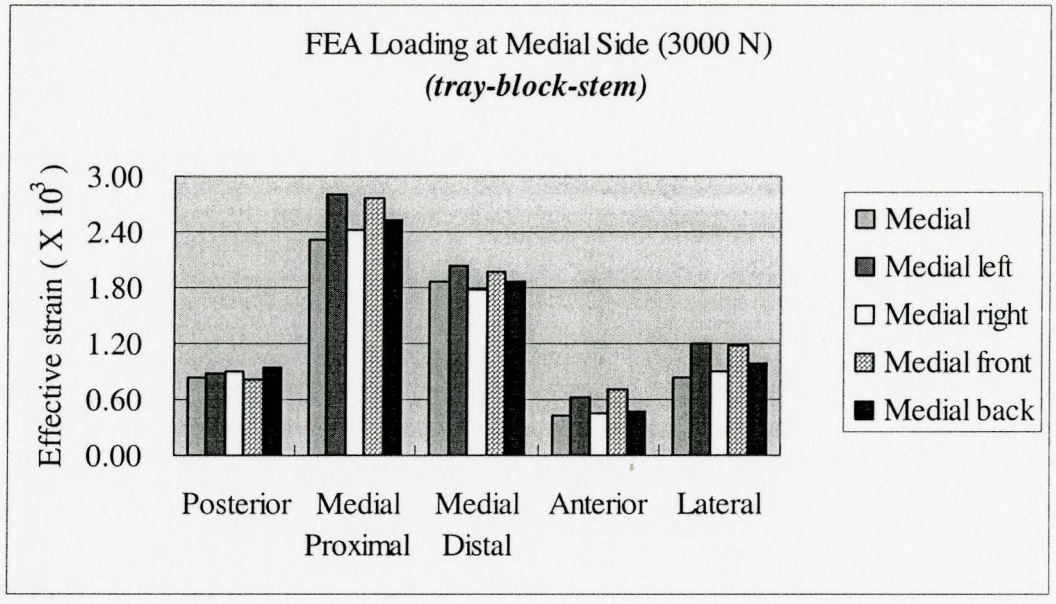

Figure 5.18 Effective strain versus loading offset in the case of **tray-block-stem**

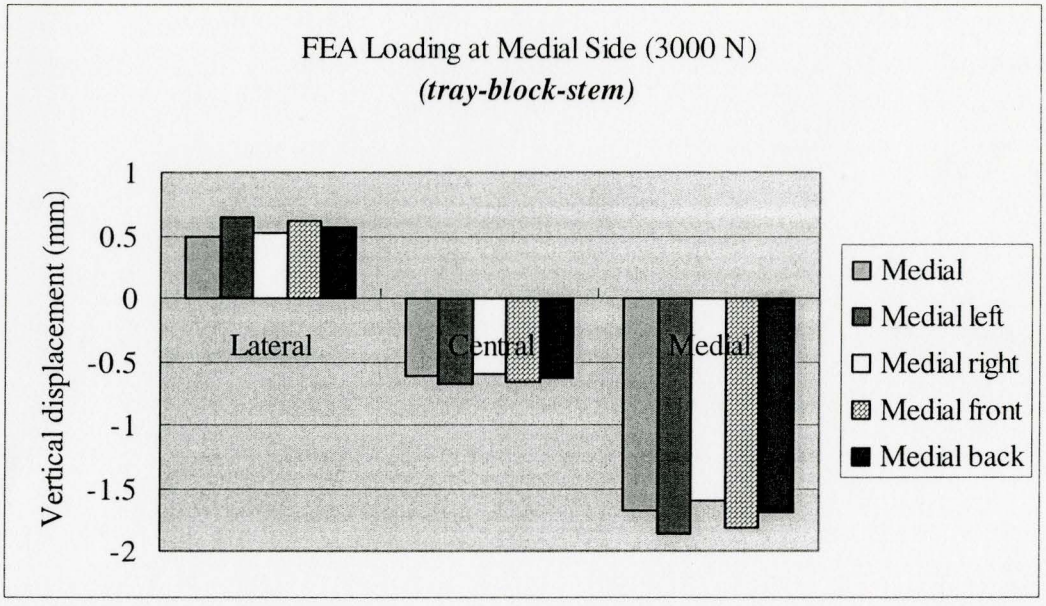

Figure 5.19 Vertical displacement versus loading offset in the case of **tray-block-stem**

In the case of tray-block-stem, the strain change due to the change of loading location exhibits a similar trend as in the case of tray-block and tray only. Figure 5.18 and Figure 5.19 show that moving the loading away from the location of original medial loading point does not result in a significant change in terms of strain and displacement, respectively.

5.4 FEA results

For the purpose of comparison, the following nine cases are simulated by FEA.

$$Central\ loading \begin{cases} tray\ only \\ tray-block \\ tray-block-stem \end{cases}$$

$$Medial\ loading \begin{cases} tray\ only \\ tray - block \\ tray - block - stem \end{cases}$$

$$Lateral\ loading \begin{cases} tray\ only \\ tray - block \\ tray - block - stem \end{cases}$$

In the FEA of these cases above, the history output of the adjacent elements surrounding posterior, medial proximal, medial distal, anterior and lateral locations are requested. As discussed in section 5.2, the average of their outputs in each small region represents the output at each location. The simulation results are shown in the following sections.

5.4.1 Central loading

In the case of central loading, a slight change is noted in strain (Figure 5.20) between the first case of tray only and the second case of tray and block, while the strain decreases more significantly at all locations except anterior central in the third case with the addition of the stem. The largest strain occurs at posterior followed by proximal medial and lateral side. Obvious decrease in strain can be observed with the introduction of extended stem. As shown in Figure 5.21, the equivalent stress follows the same trend as the strain. Regarding the displacement (Figure 5.22), there is no significant change between case one and case two. However, the extended stem results in a decrease of the displacements in all locations.

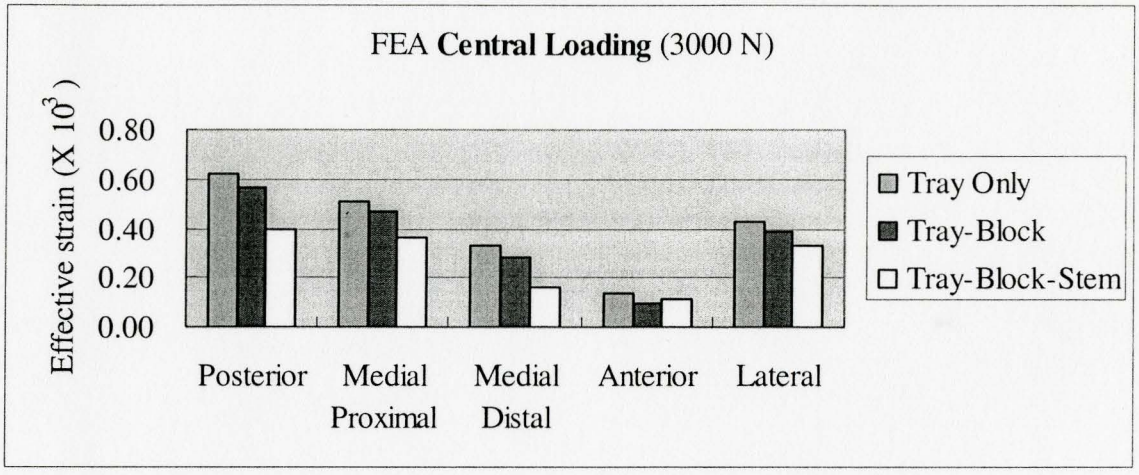

Figure 5.20 Effective strains of three cases under **central loading** (FEA)

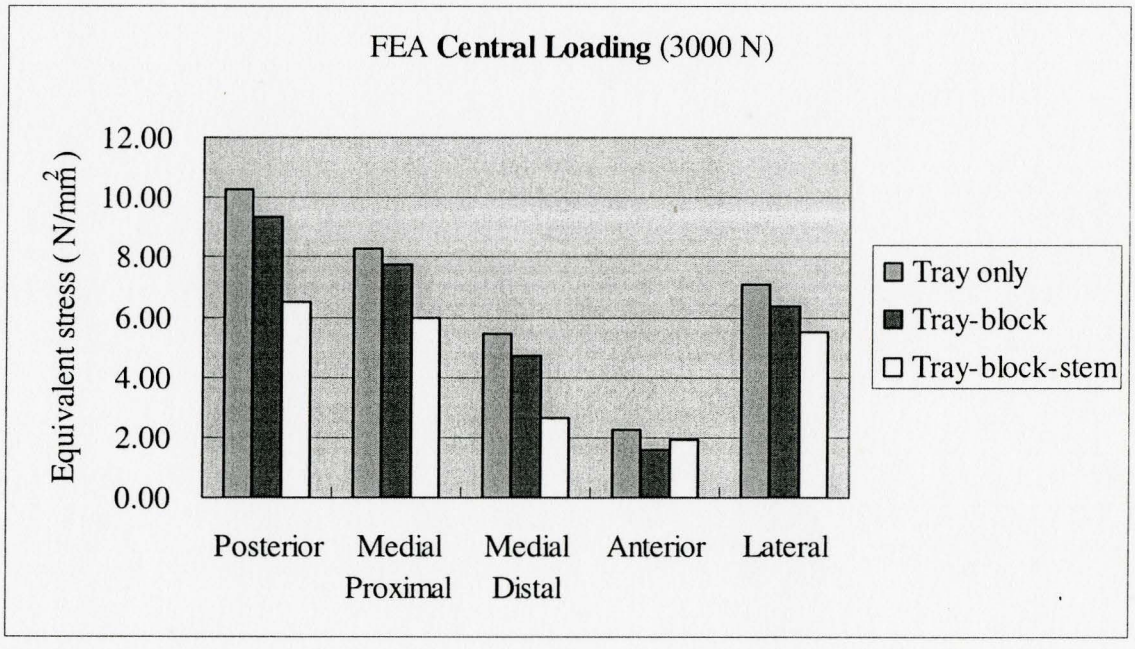

Figure 5.21 Equivalent stress of three cases under **central loading** (FEA)

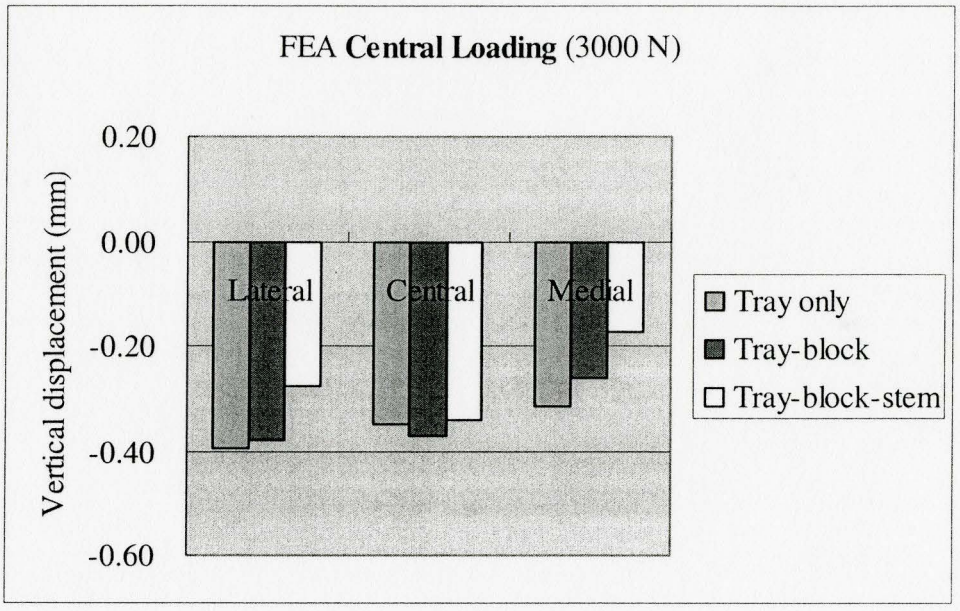

Figure 5.22 Vertical displacement of three cases under **central loading** (FEA)

5.4.2 Medial loading

In the case of medial loading, no significant change in displacement (Figure 5.25) is found between the first case and the second case, which is similar to the experimental results. But a noticeable decrease in strain/stress (Figures 5.23 and 5.24) is noted at distal medial, proximal medial, posterior and a strain/stress increase at lateral side from the first case to the second case, which is similar to the experimental results as well. A further decrease in strain/stress is observed with the addition of stem in case three.

Similar to the experimental results, the largest strain/stress and displacement occur at the medial side and the results show a tipping effect in displacement as the lateral side actually displaces in the opposite direction of the displacement at the medial side.

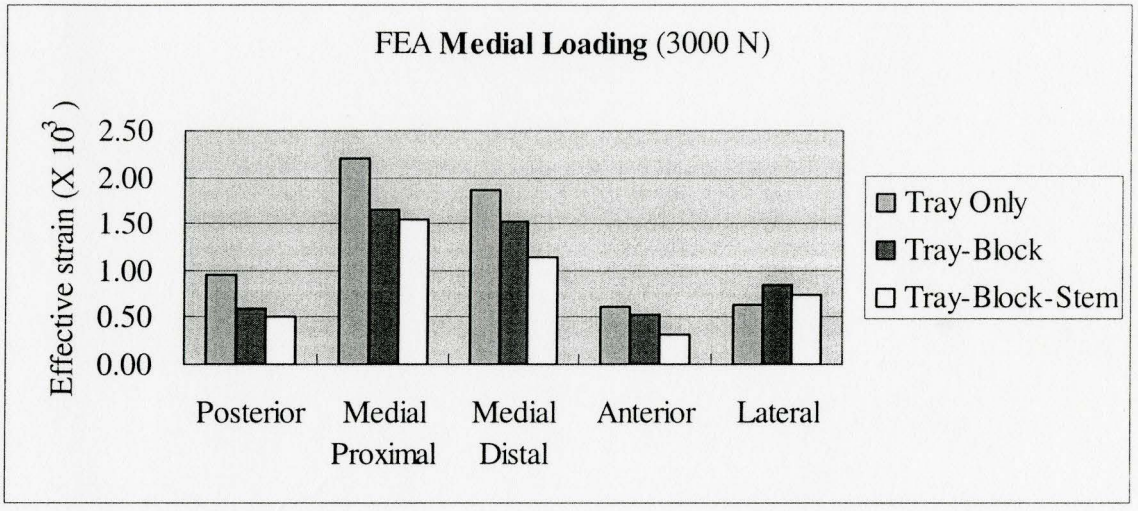

Figure5.23 Effective strains of three cases under **medial loading** (FEA)

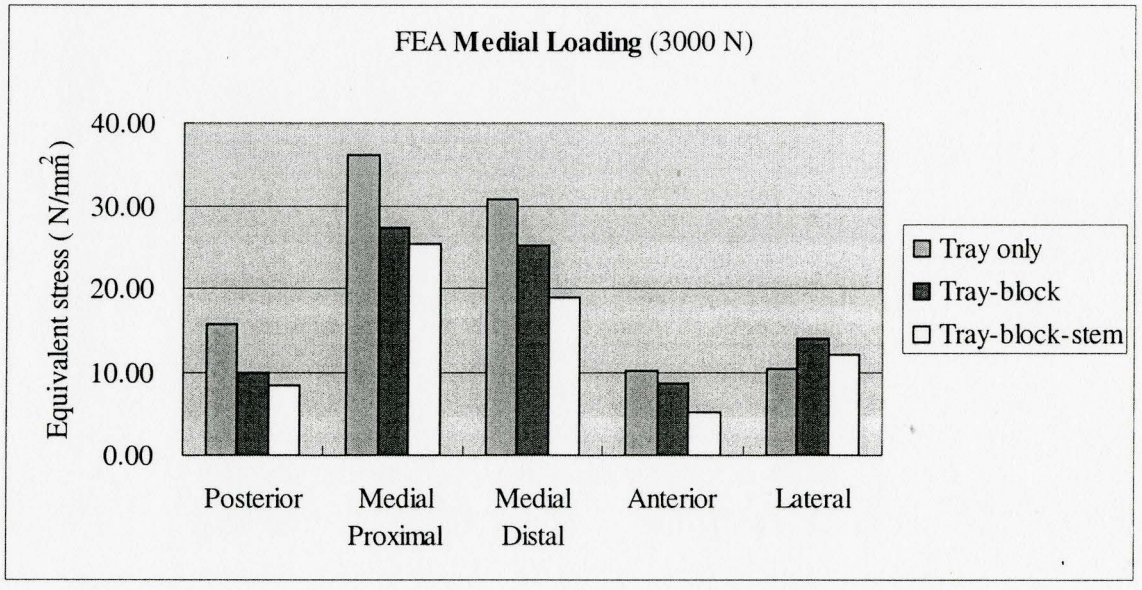

Figure 5.24 Equivalent stresses of three cases under **medial loading** (FEA)

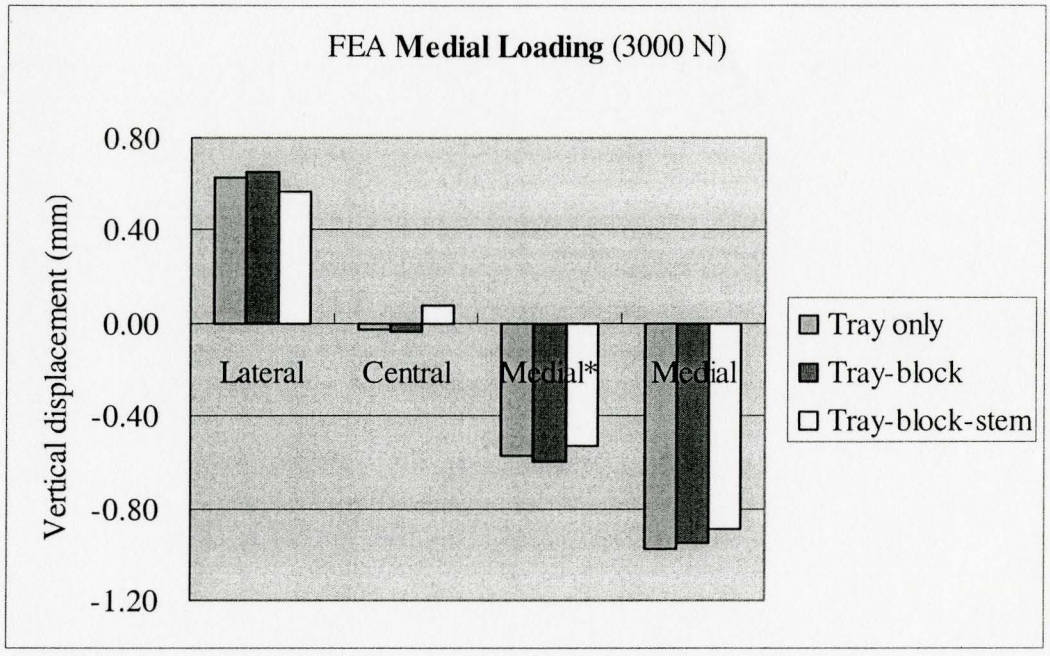

Figure 5.25 Vertical displacements of three cases under **medial loading** (FEA)

5.4.3 Lateral loading

In the case of lateral loading, a significant decrease in strain/stress is noted in the case with stem as compared to the cases without the inclusion of stem augment, and a slight displacement drop can be seen in the third case (Figures 5.26-5.28). Comparing the second case with the first case, we can see a slight decrease in strain /stress (Figures 5.26 – 5.27) at lateral side and anterior central and a noticeable drop at posterior and medial side but a negligible change in displacement (Figure 5.28). The largest strain/ stress and displacement occur in lateral side. Again, a tipping effect in displacement is observed. Although the block augment in FEA simulation results in a slightly higher degree of decrease as compared to the experiment, the trend is the same.

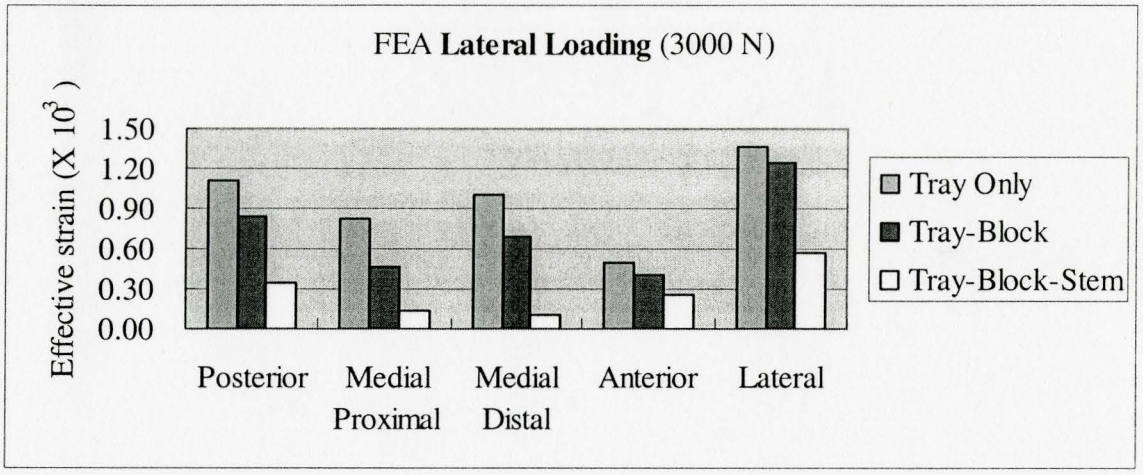

Figure 5.26 Effective strains of three cases under **lateral loading** (FEA)

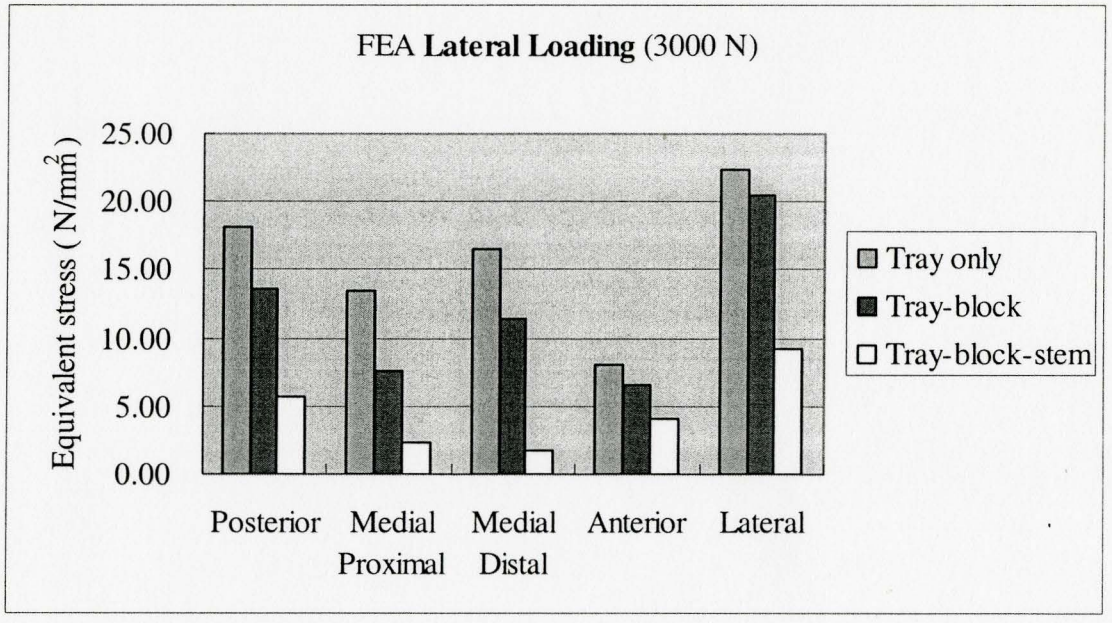

Figure 5.27 Equivalent stresses of three cases under **lateral loading** (FEA)

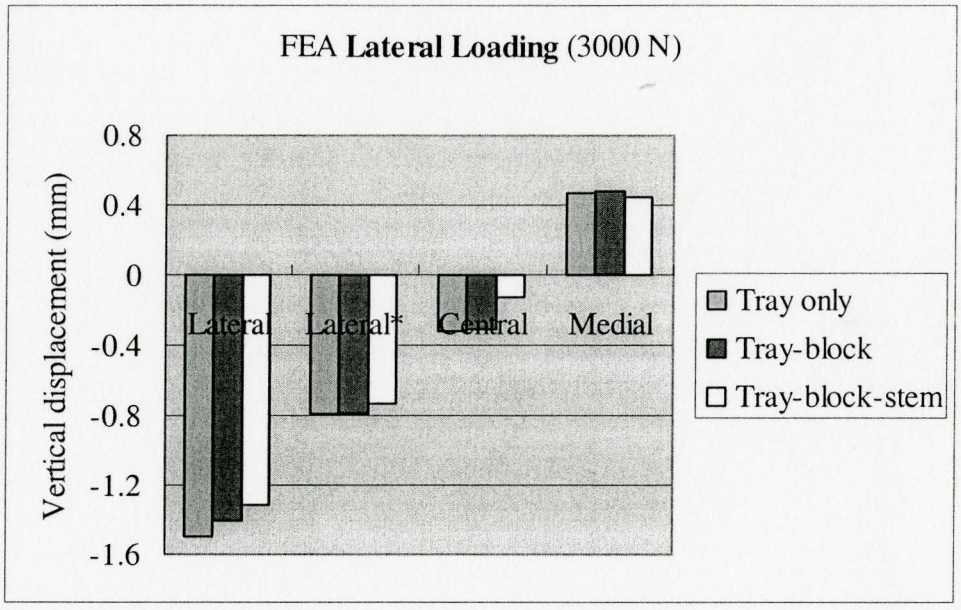

Figure 5.28 Vertical displacements of three cases under **lateral loading** (FEA)

5.5 Stress contours

The stress contours of the implants, cortical and cancellous bone are obtained by FEA simulation. Figures 5.29-5.31 show the stress contour of the model under medial loading of 3000 N. Detailed stress contours for each component in three configurations under different loadings can be found in Appendices E, F and G.

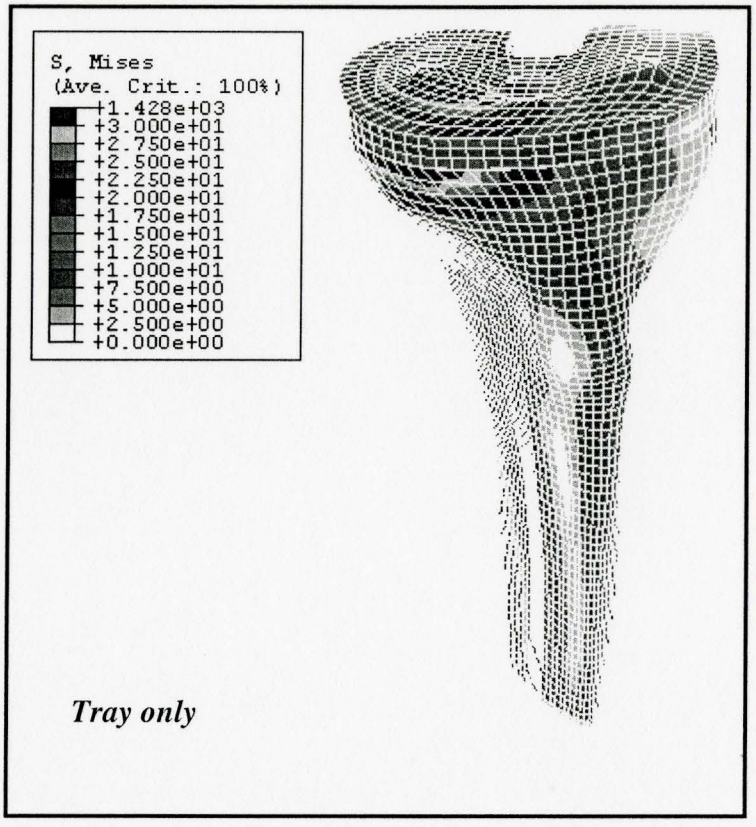

Figure 5.29 Von Mises stress contour under medial loading **(tray only)**

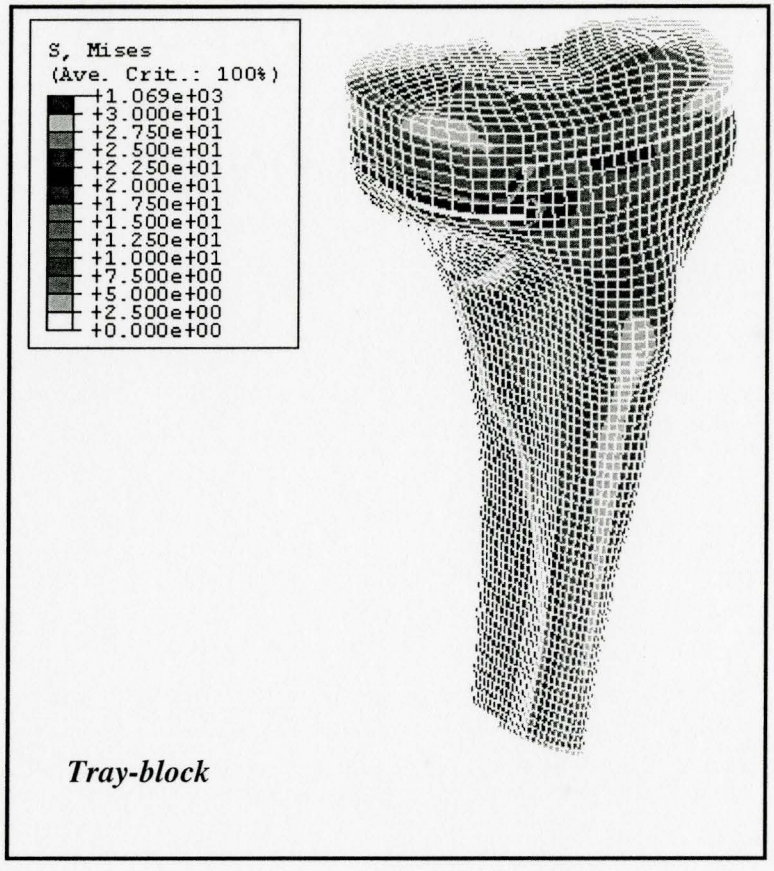

Figure 5.30 Von Mises stress contour under medial loading **(tray-block)**

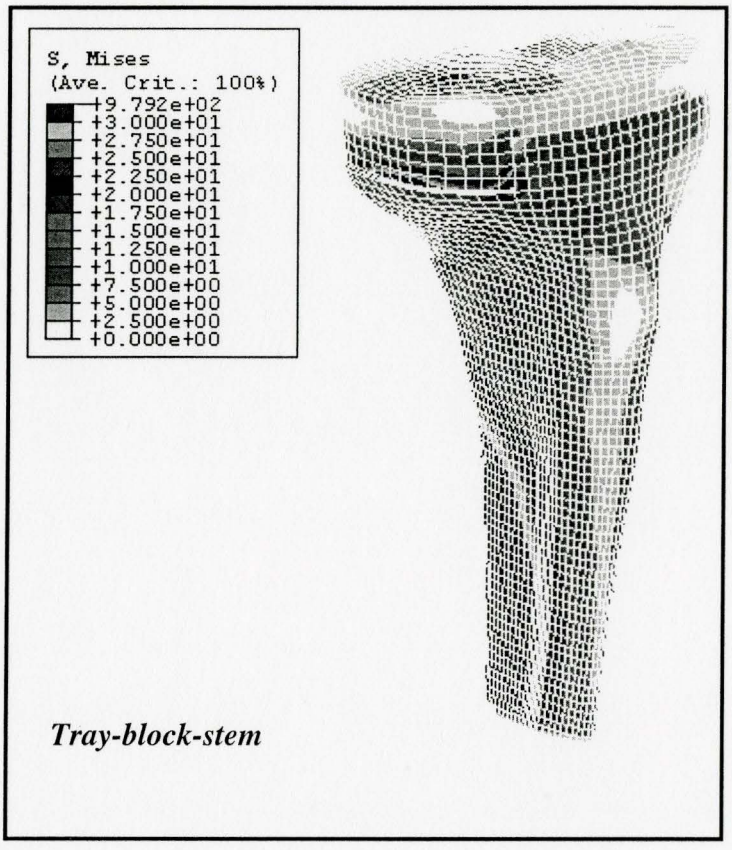

Figure 5.31 Von Mises stress contour under medial loading **(tray-block-stem)**

By analyzing the stress contours (appendices D, E and F), it is found that:

- The maximum stress of the cortical bone in case one generally occurs on the top surface because the contact surface on the top is small. In cases two and three, the maximum stresses are located at the corner of bone defect cut because this is the place where the stress concentration occurs.
- Maximum stress of the cancellous bone is always located at the bottom surface of the central hole where the tip of the implant makes contact. When the medial or lateral loading is imposed, the second largest stress occurs on the cancellous bone directly

to the side of the maximum stress, which may be caused by the effect of bending on the implant.

- The maximum stress of the implant always occurs at the place where the load is imposed because of stress concentration.

5.6 Result comparison and discussions

Comparing the simulation and experimental results, the same trend can be observed in all the investigated cases in terms of strains (Figures 5.32-5.34) and displacements (Figures 5.35-5.37). However, there are substantial differences between the absolute values of the experimental and FEA simulation results. The reasons for these deviations may be caused by the following factors:

- Geometric model simplifications
- Material property assumptions
- Implant position in the bone during experiments
- Model constraints and knee clamping in the fixture
- Loading locations
- Output positions
- Cements omited

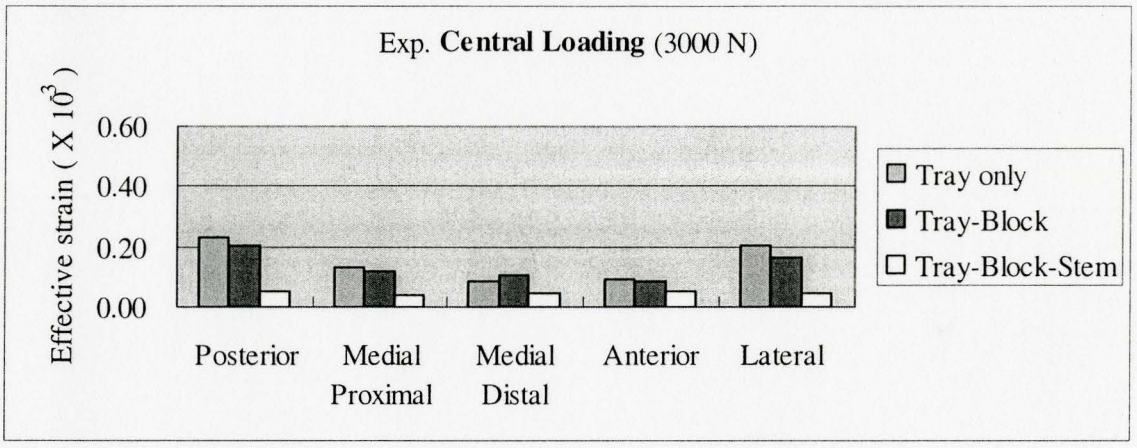

a) Experimental results

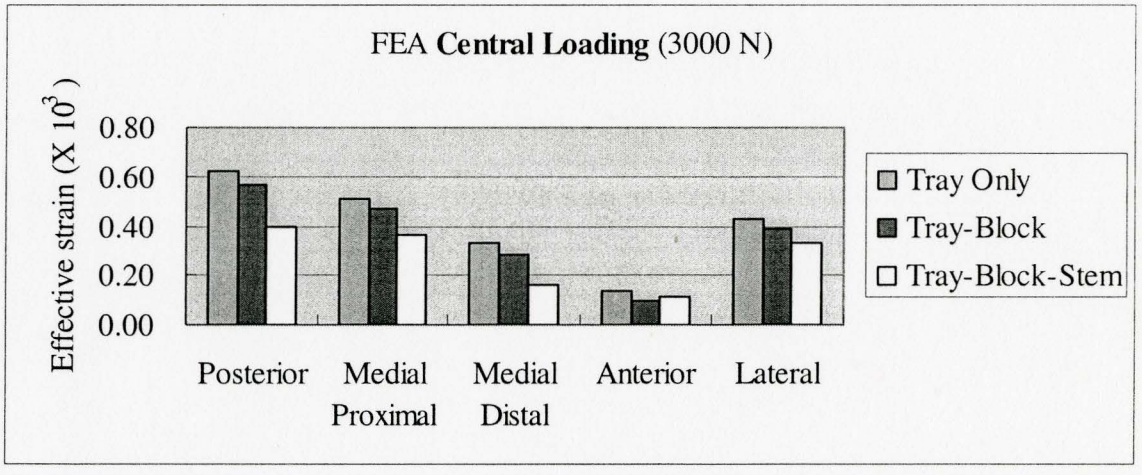

b) **FEA results**

Figure 5.32 Experimental and simulation effective strain under **central loading**

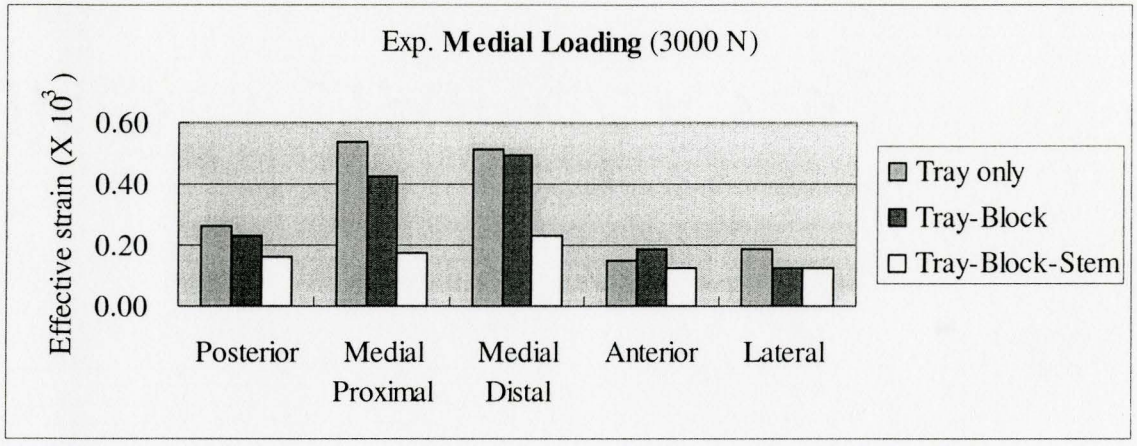

a) **Experimental results**

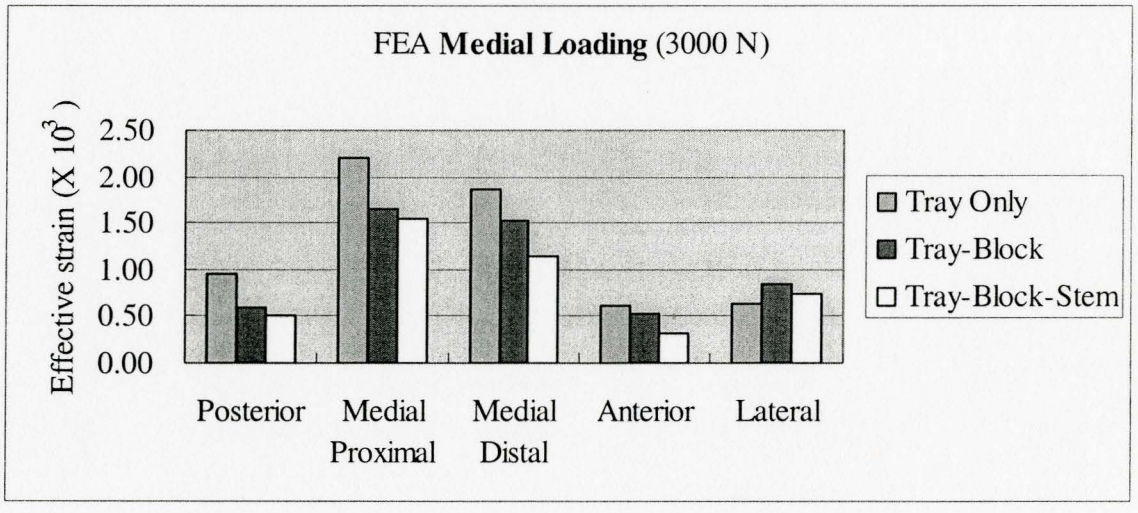

b) **FEA results**

Figure 5.33 Experimental and simulation effective strain under **medial loading**

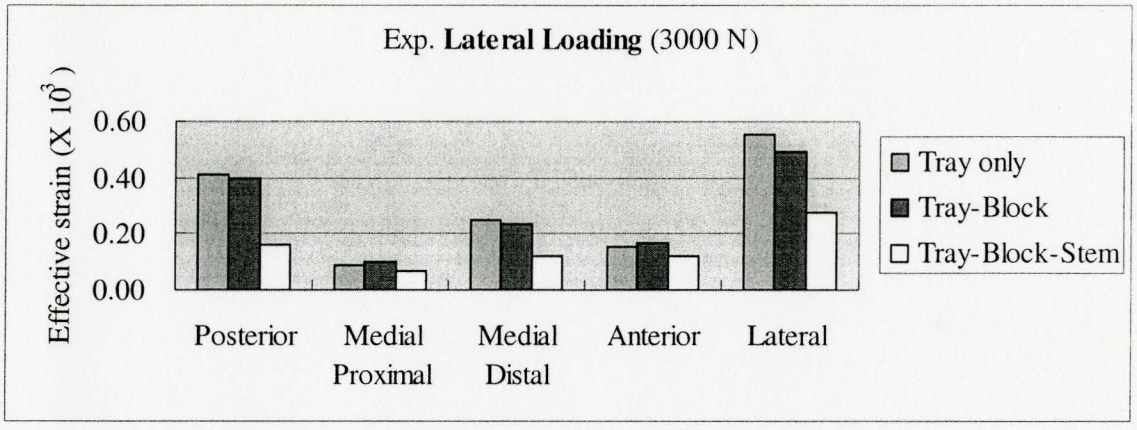

a) Experimental results

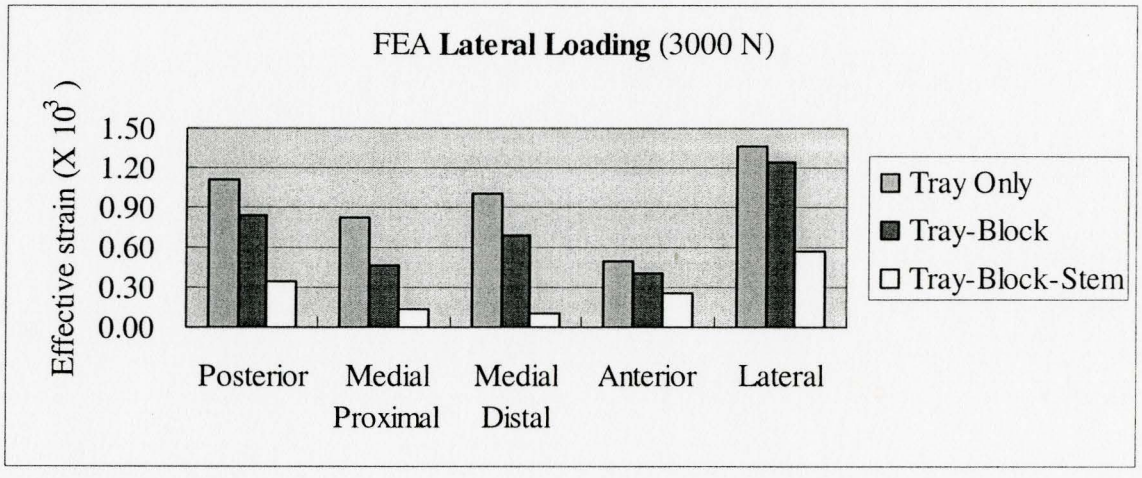

b) FEA results

Figure 5.34 Experimental and simulation effective strain under **lateral loading**

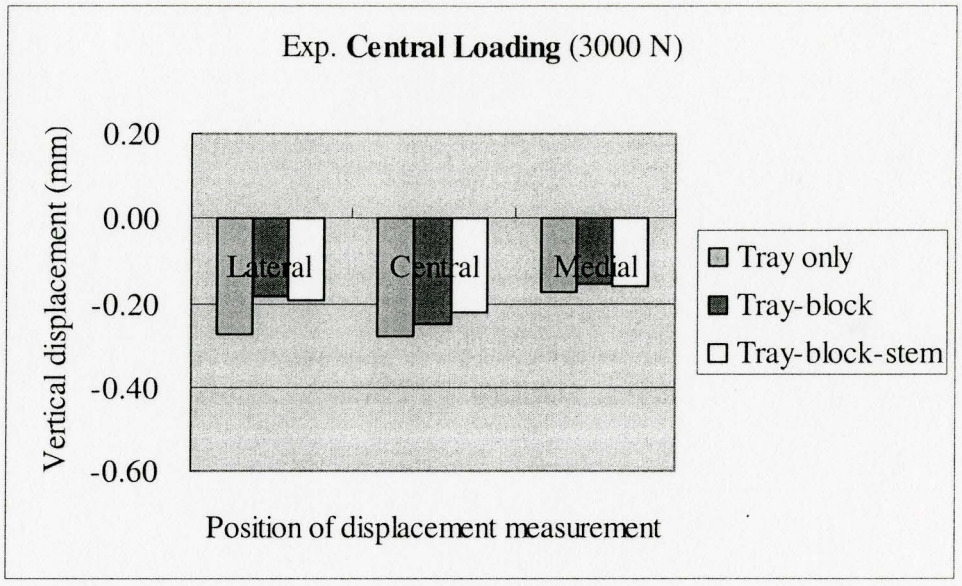

a) Experimental results

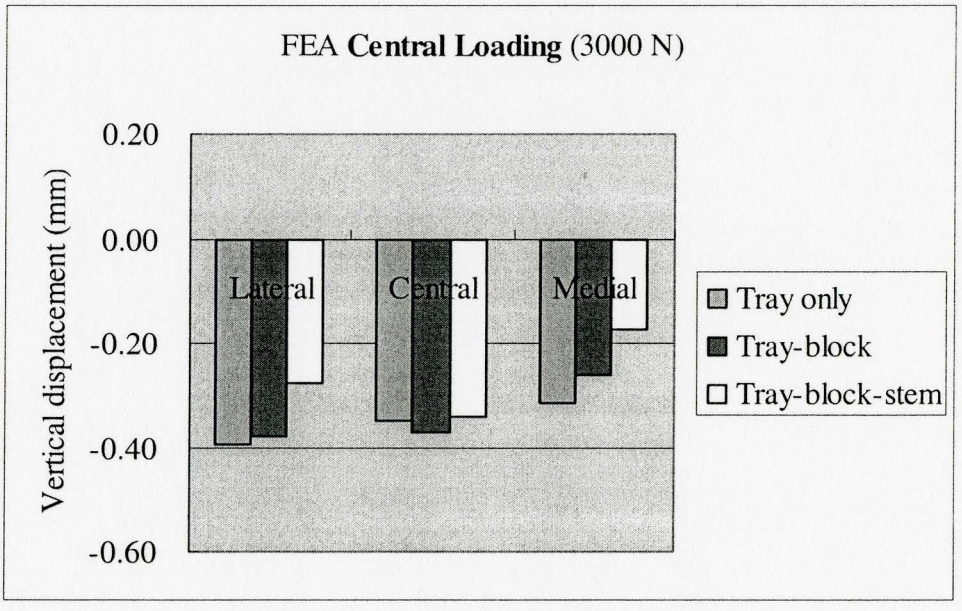

b) FEA results

Figure 5.35 Experimental and FEA vertical displacement under **central loading**

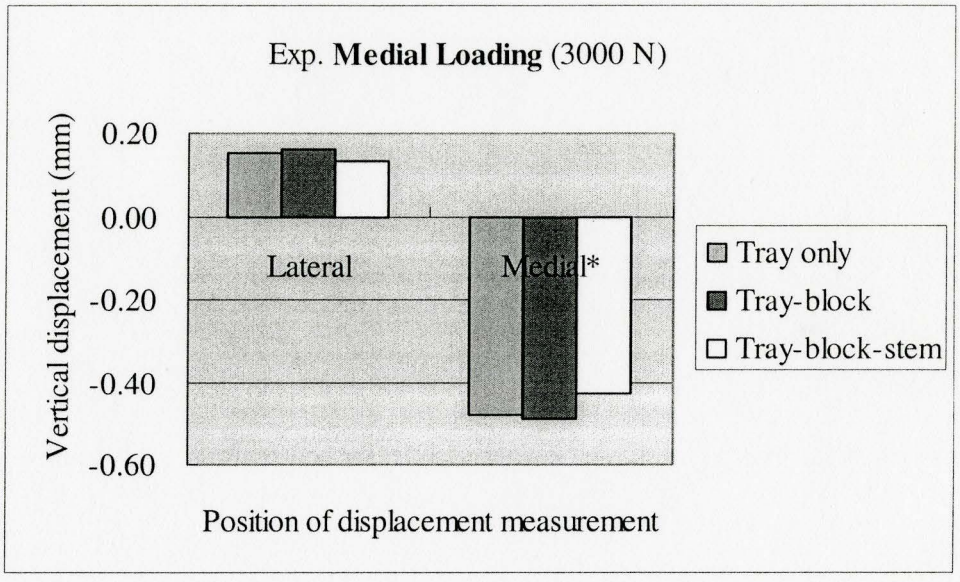

a) Experimental results

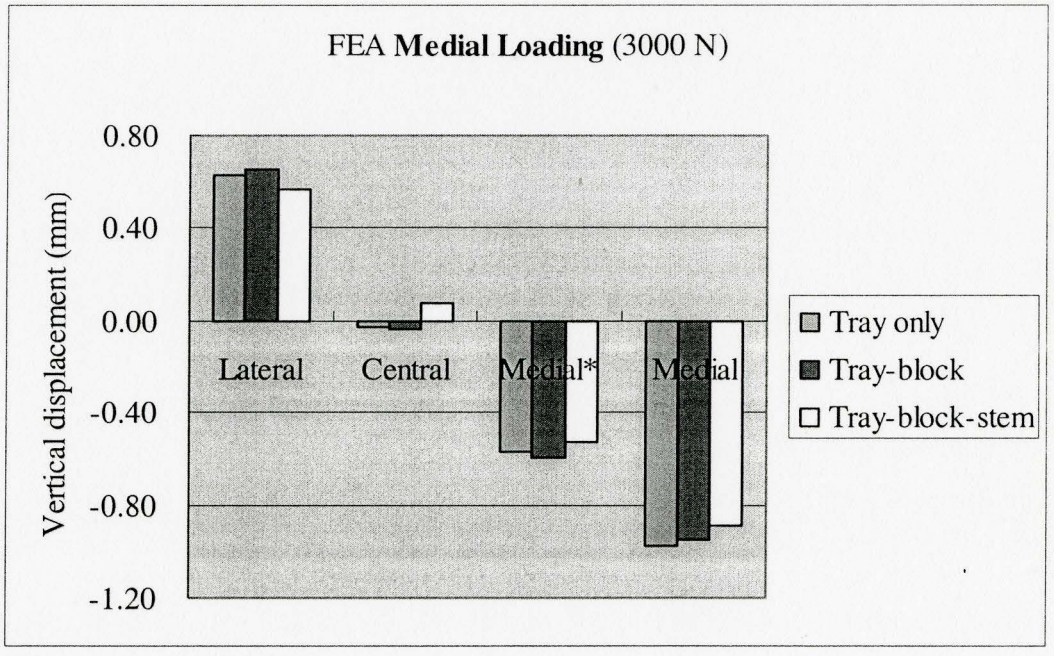

b) FEA results

Figure 5.36 Experimental and FEA vertical displacement under **medial loading**

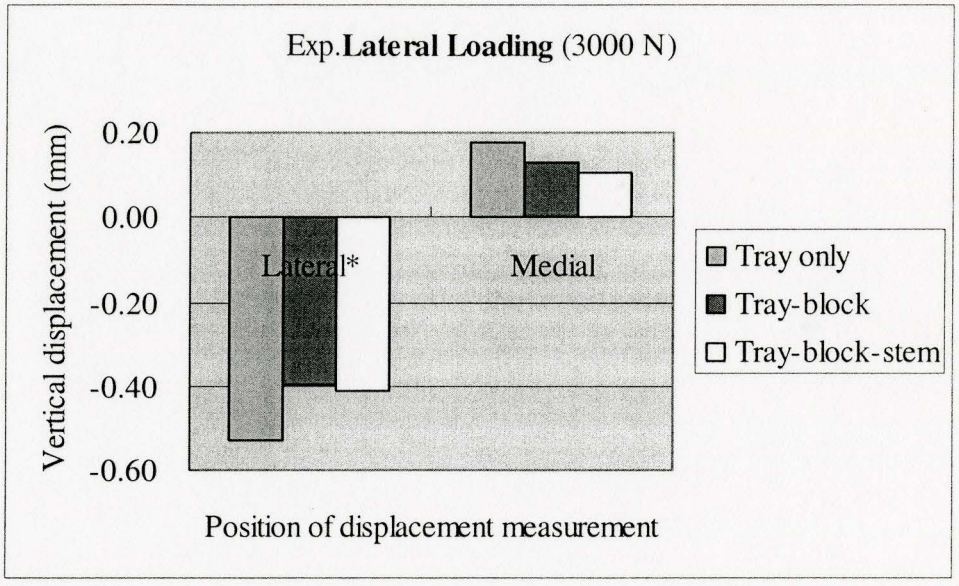

a) Experimental results

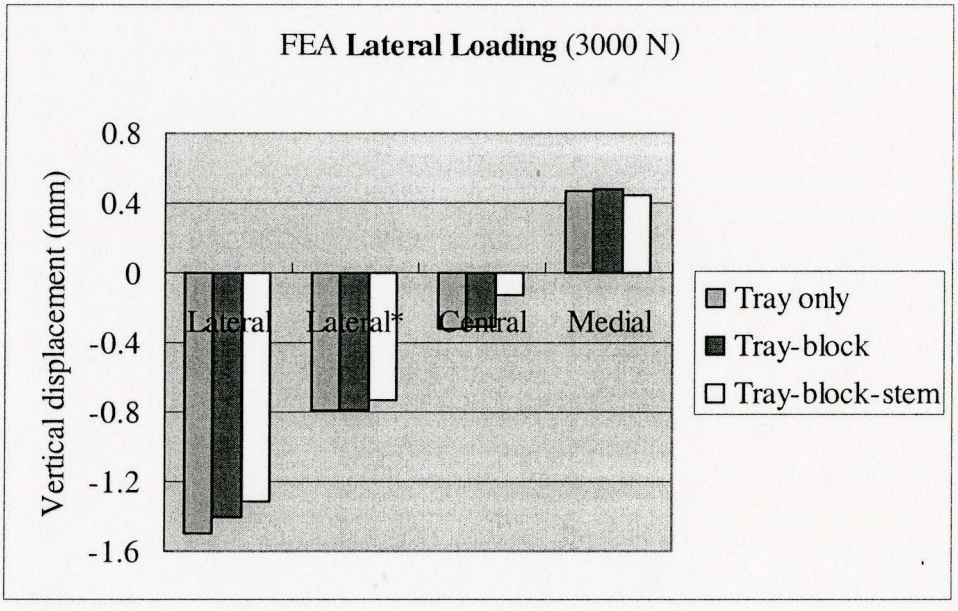

b) FEA results

Figure 5.37 Experimental and FEA vertical displacement under **lateral loading**

In addition to the trend, both experimental and FEA results reveal the following important observations:

1. The addition of stem augment leads to a stability increase of the knee. But the fact of stress reduction may cause stress shielding. Figures 5.32-5.37 above show a significant decrease at most of the recorded locations in the configuration of tray-block-stem as compared to the other two cases. However, a significant reduction in strain/stress may cause a potential problem, referred to as stress shielding.

2. The block does not seem to increase stresses or displacements. Comparing the configuration of tray-block with the one of tray only (Figures 5.32-5.34), the addition of block results in a negligible or a slight reduction in strain, which indicates that stress shielding for the configuration of tray-block would not be a problem. Moreover, the displacements (Figures 5.35-5.37) at the recorded locations under the three loadings stay roughly the same or a slight decrease, which is observed in both experimental and simulation results.

From the results of adjacent elements in the five regions corresponding to the experiments, no sudden change is observed and the strain gradients are relatively flat. This validates the use of the mean value of several elements to represent the simulation results at these areas.

The investigation of loading offset shows that a slight movement of the load either forward and backward or left and right does not have a significant affect on the results.

FEA simulation overcomes the disadvantage of experiments in which only limited data can be obtained. From the FEA simulation, we are able to obtain the strain, stress and displacement contours for all the components involved in the FEA model and more analysis can be carried out. We can also find the location of the maximum strain/stress and displacement. Because of the introduction of augments, which have higher strength and rigidity than human bone material, a larger portion of the loading is transmitted by the augment and a smaller portion is transferred to the top of the tibia bone, which results in lower strain/stress in the tibia bone. The long term effect of this stress reduction is that the bone structure will become atrophic.

Chapter 6

Conclusions and Future Work

6.1 Research summary and conclusions

Based on the new design of the Deltafit Keel tibial tray, an investigation of three configurations, tray only (without bone defect), tray with block augment and tray with block and extended stem augments (bone defect assumed) has been conducted by means of experiments and FE simulations. In this study, composite bones with isotropic material properties are utilized. For each configuration, 3000 N static compressive load was imposed on the top surface of the tray at central, medial and lateral locations and then the strains and displacements at the designated locations were measured using strain rosettes (strain gages) and DVRT (Differential Variable Reluctance Transducer) displacement transducers. FEA model is established by employing several advanced software including CATIA, TrueGrid Mesh generator and Abaqus. In order to compare the FE simulation results with the experimental ones, nine cases (three configurations with three different loadings for each configuration) have been simulated using Abaqus/Standard 6.4.

Moreover, the influence of loading offset on FE simulation results is also investigated and the discrepancy of the outputs from the adjacent elements is checked as well. The results from the experiments and FEA simulations provide the following conclusions:

1. Comparable stability is found between case 2 and case 1 as the strains/stresses and displacements from case 2 are slightly lower than the ones from case 1 for the studied loading locations.
2. All the results from both experiment and FE simulation show that case 3 with extended stem offers the highest stability among the three cases because of lower strain/stress and displacement. However, stress shielding might be a potential problem that may result from using the extended stem.

However, contrary to expectation, the extended stem configuration does not produce significant improvement of tipping. Obviously, excessive reduction in stress causes stress shielding that may eventually results in atrophy. Moreover, the extended stem causes more difficulties to the surgery as well as more suffering to the patients.

3. The results from FEA simulation follow similar trends as those observed from the experimental results. Therefore, the FEA model can be used for more in-depth analysis to reveal the performance of the studied artificial knees under various loadings.
4. No sensitive directions of loading motion have been found. A slight load offset would not cause any significant strain increase or decrease. Since nodal force is used in FE model, even if the node on which the load is imposed may not be exactly at the same location as the one in experiment, it should not result in a tremendous difference,

no matter the offset is in medial-lateral or anterior-posterior directions. But we still suggest using an evenly distributed load in the small area in FEA model corresponding to the small contact surface between the loading rod and the tray.

5. Equivalent stress values at adjacent elements do not show any sudden changes on the FE results. The discrepancy of their output is negligible. Therefore, the value of the adjacent elements could be used to represent the average stress over a small region to compare with the experimental strain measured by strain rosettes.
6. Finally, when employing the new design of Deltafit Keel tibial tray in cases of bone defect, tibia tray with block augment only should be the first choice. With large amount of bone defect, extended stem may need to be considered. In this case the relationship between the amount of bone defect and the knee stability under the configuration of extended stem should be further investigated by FEA simulation.
7. Strain is higher in the model than that of experiment. This is because of the lower cortical thickness in the model than that of experiment as well as an ideal fixation in the FE model.

6.2 Future research work

Based on the existing experimental device and FEA model, further research can be carried out to improve our understanding of the following aspects:

1. Investigate the relationship between the amount of bone defect and the knee stability under the configuration of extended stem by FEA simulation.

2. Investigate the responses of these three configurations under other loading conditions may cause instability such as shear force, impact force, etc. and compare the results.
3. Perform the same experimental and FEA investigation on the traditional design of tibia tray.
4. Study the performance under bending and torsion loads.
5. In the case of bone defect, the retained bone structure around the block augment should be slightly weaker than the normal bone. In order to simulate bone defect closer to reality, the retained bone should be assigned different material properties from the normal bone.
6. Simulate bone fracture/failure by considering the materials as elastic-plastic ones.
7. Simulate cementless cases of TKA. In the cases of this study, cement is used between the implant and the bone in our FEA model, no surface contact is considered. However, cementless TKA is now implemented in real surgery in order to avoid the problems caused by cement. In this case, surface contact (surface contact definition, friction model) needs to be included in FEA model. And hence the effect of surface contact on the knee performance including stability would be interesting.
8. Modeling the anisotropic material properties and implementing into FEA simulation for more realistic simulation is an interesting research project too.
9. We have less inter specimen variability in the experiment. It would be good to use more specimens and it is even better to use human specimens instead of using composite bones.

Appendix A

Preparation of Tibia Bones to Experimental Setup

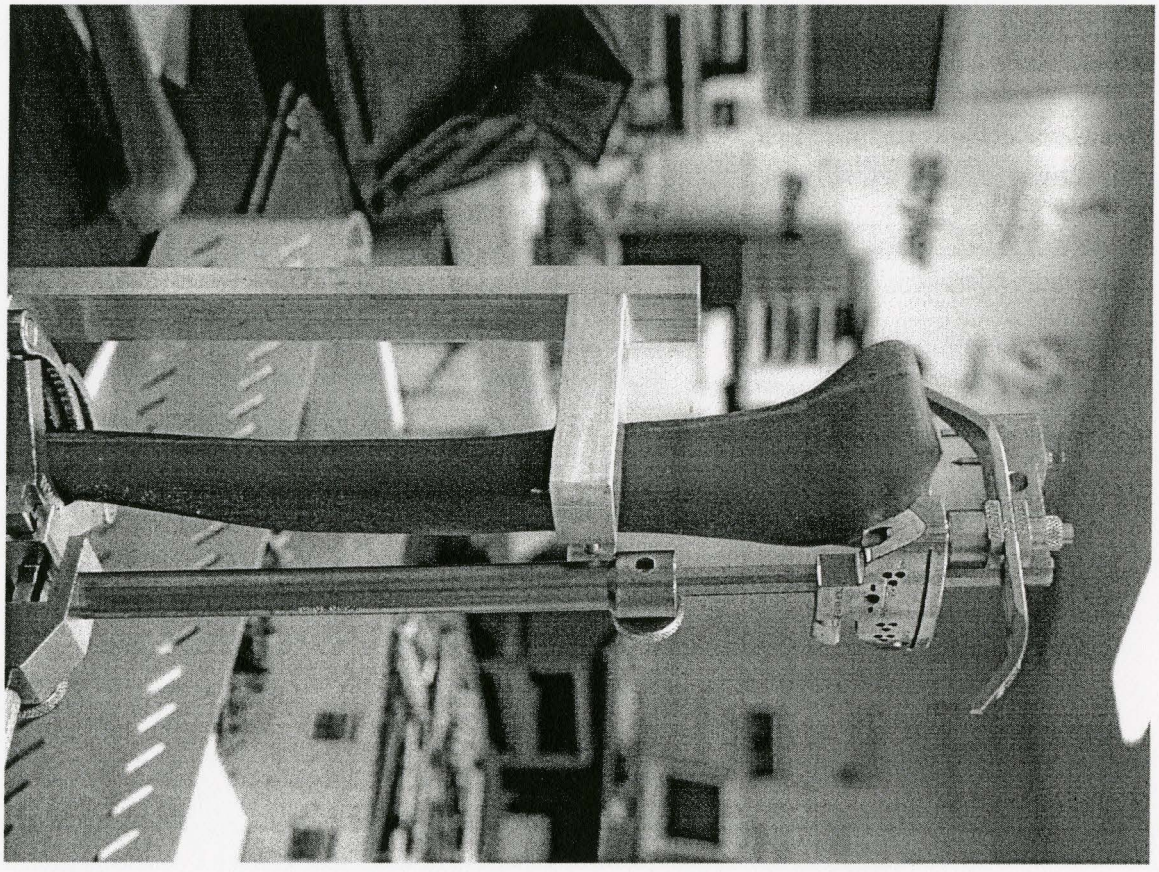

Figure A.1 Clamping the composite tibia bone

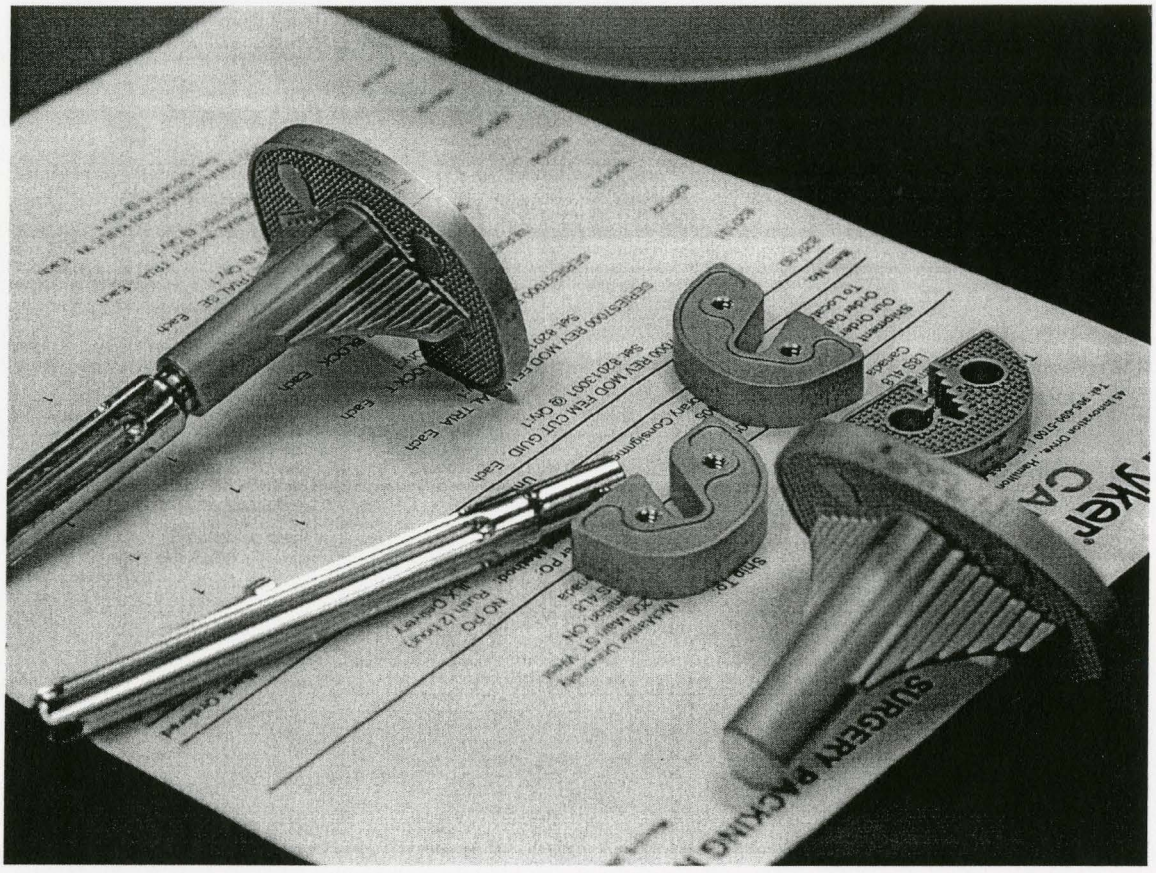

Figure A.2 Implant components: keel tray, block and extended stem augments

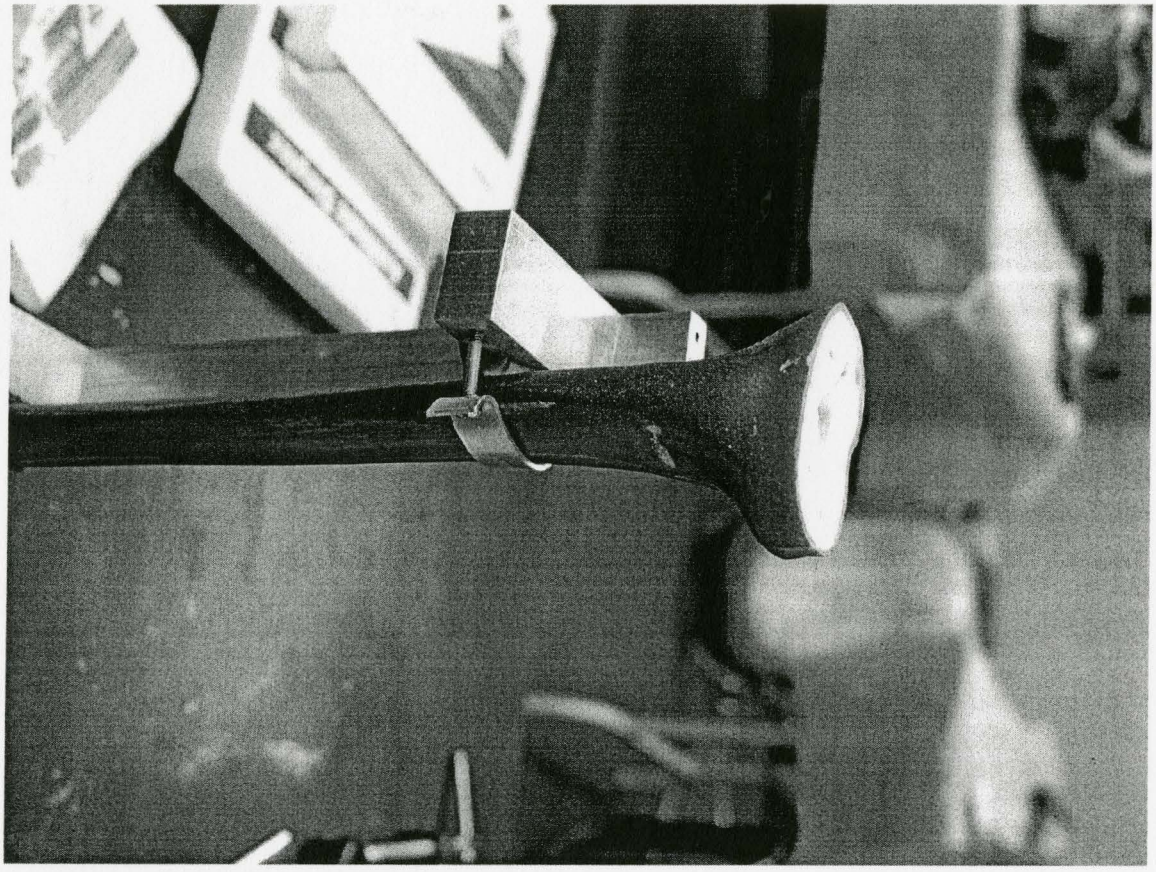

Figure A.3 Tibia bone after cutting

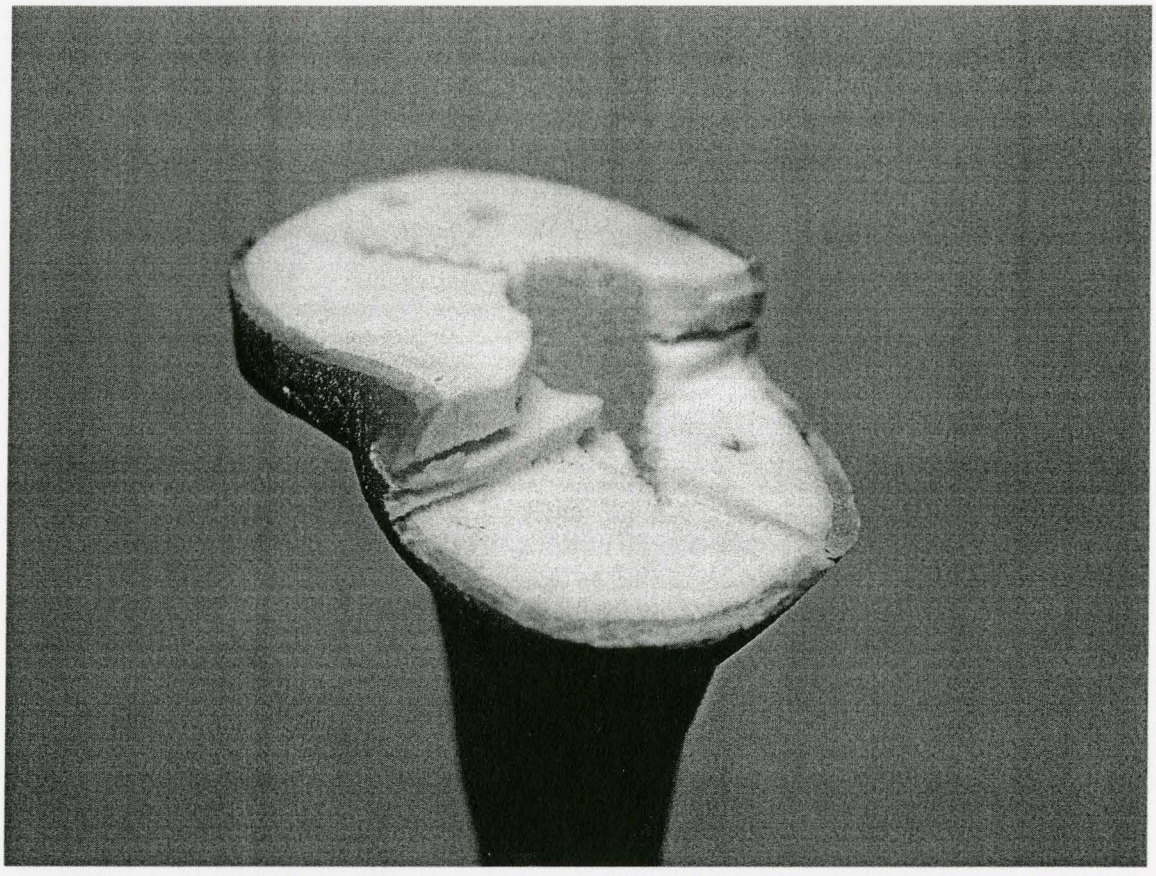

Figure A.4 Tibia bone after cutting (bone defect assumed)

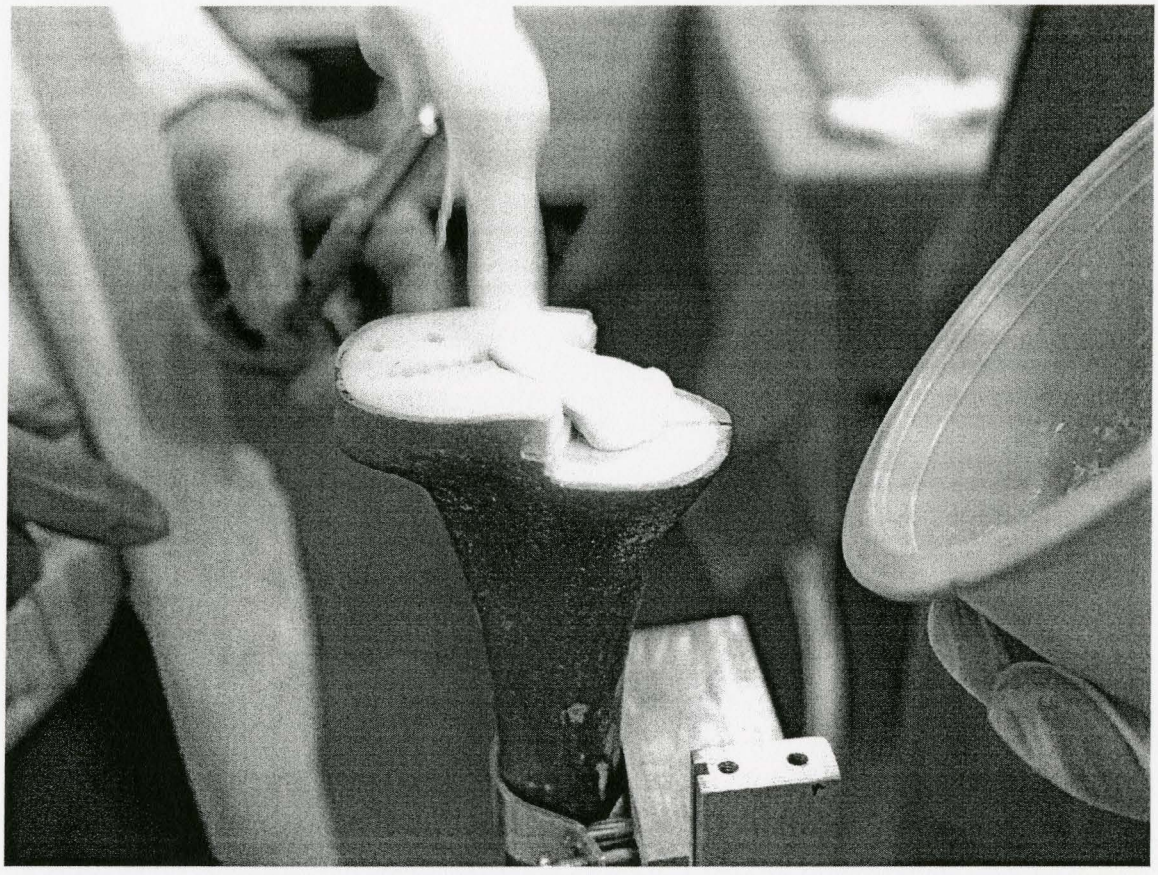

Figure A.5 Adding cement

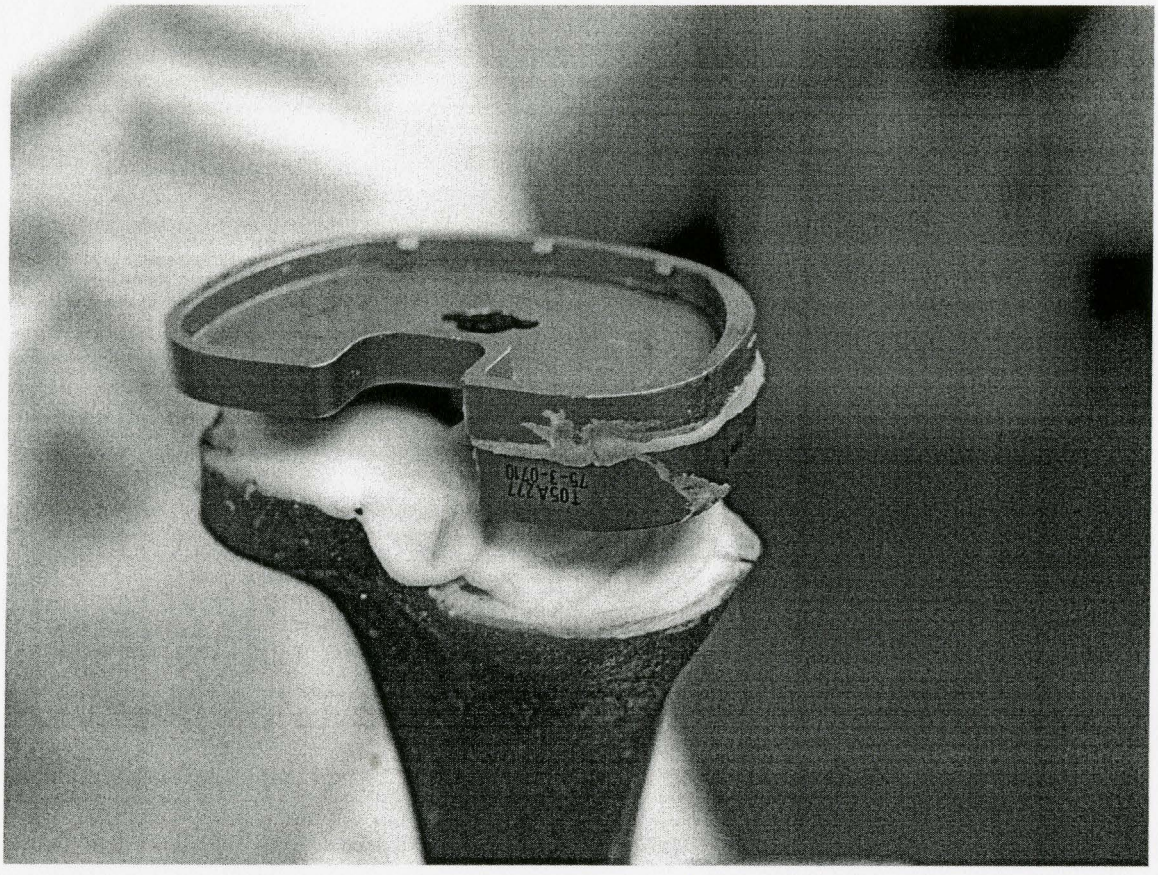

Figure A.6 Assembly of implant and tibia bone (1)

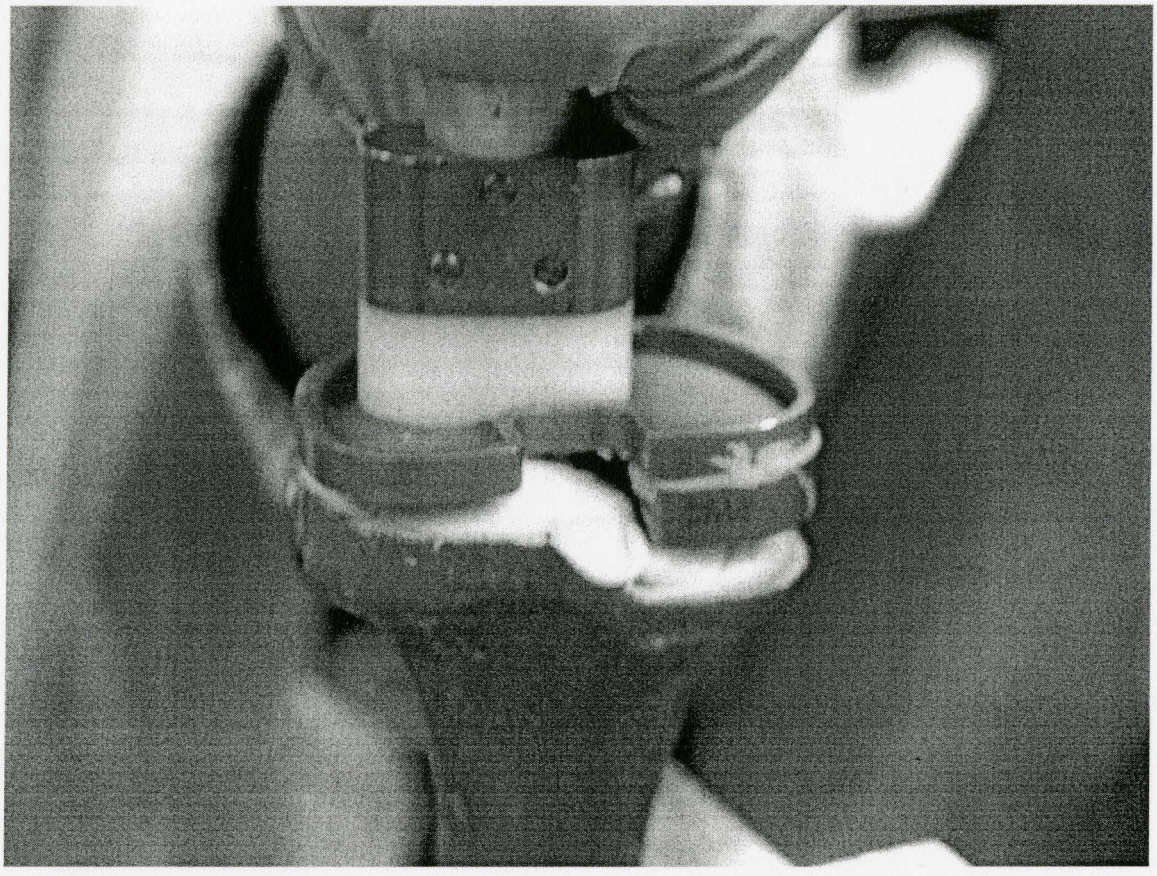

Figure A.7 Assembly of implant and tibia bone (2)

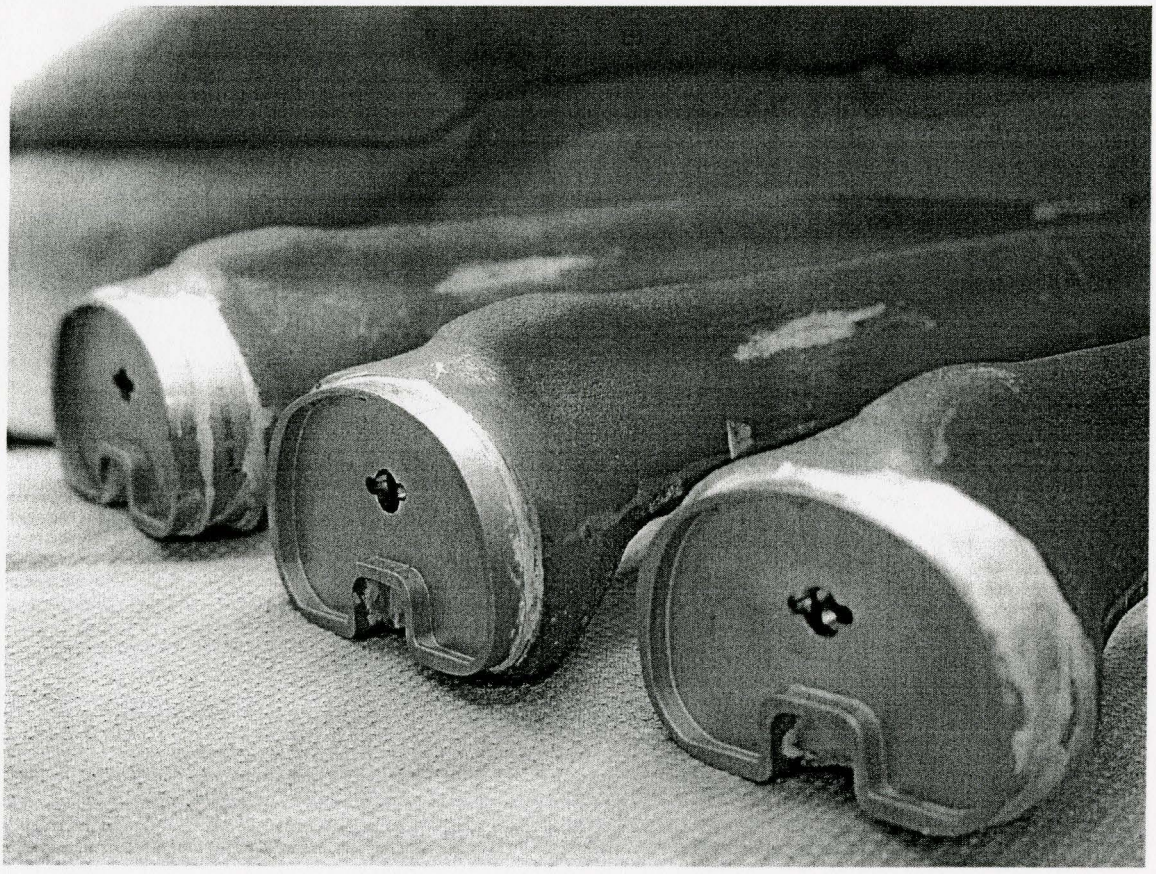

Figure A.8 Tibia bones with implants

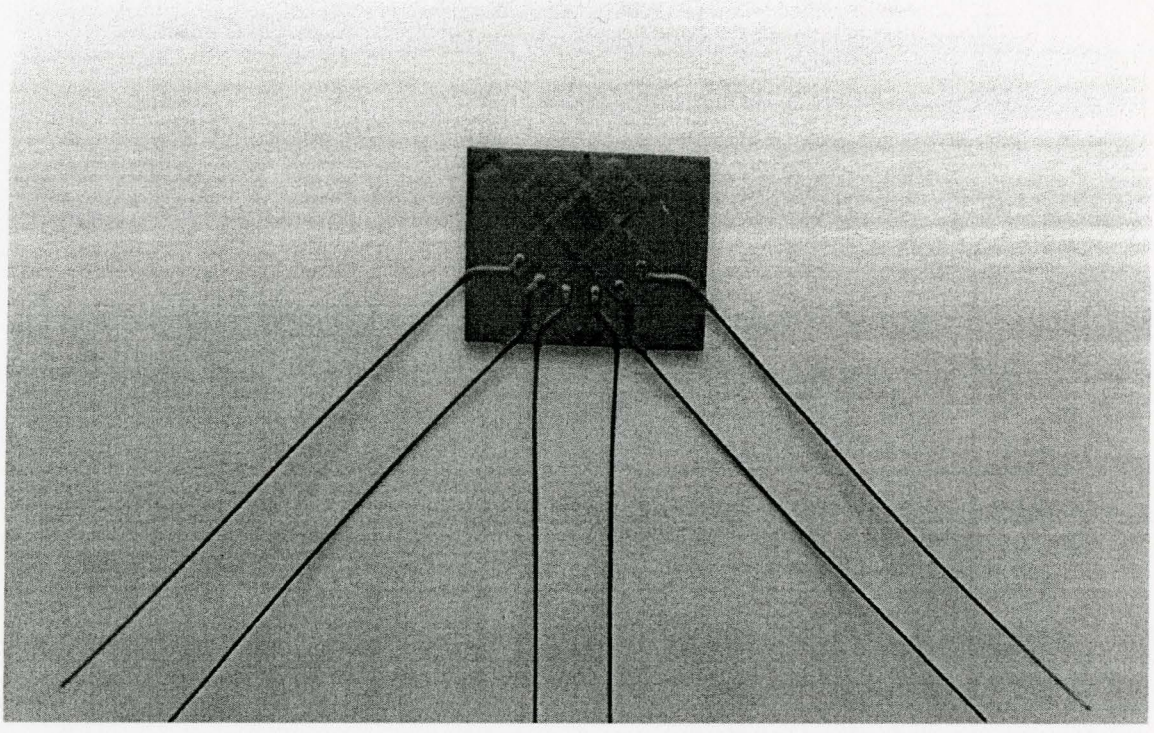

Figure A.9 Strain rosette

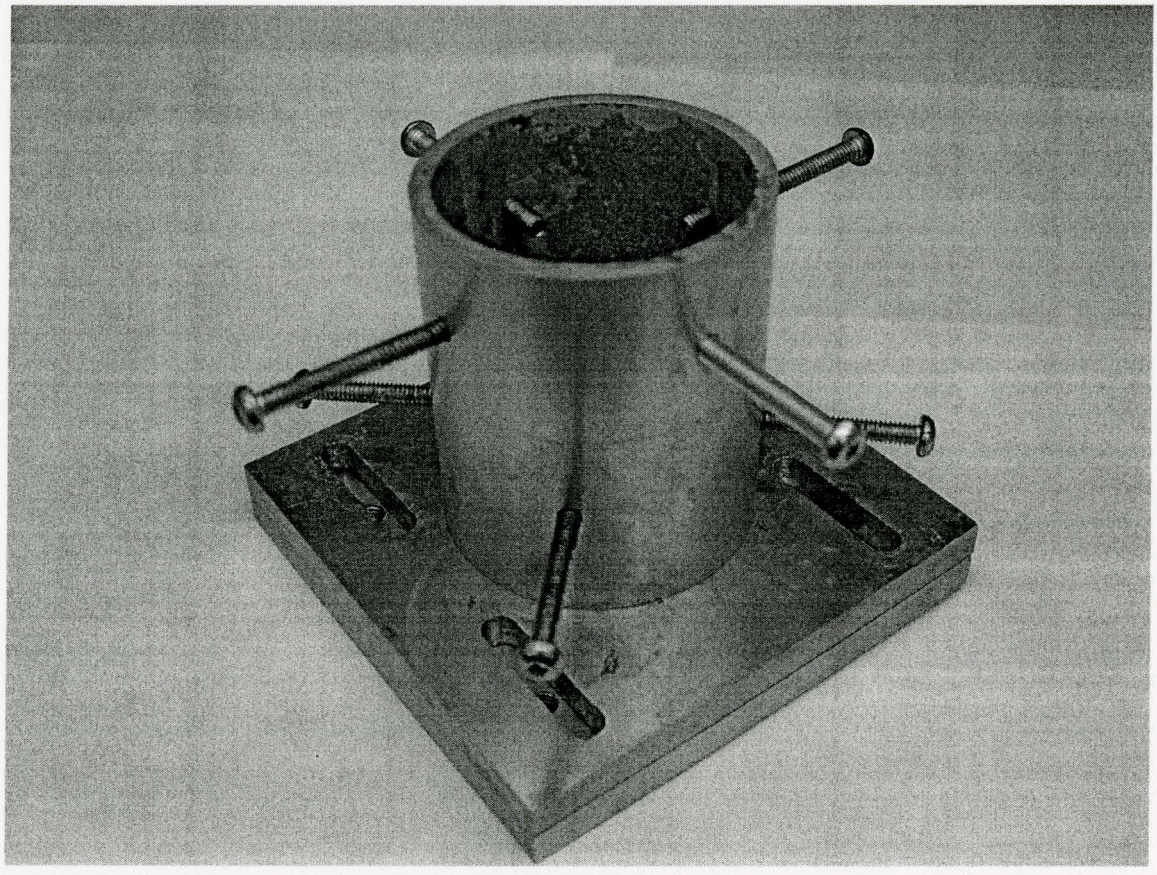

Figure A.10 Fixture for clamping the tibia bones

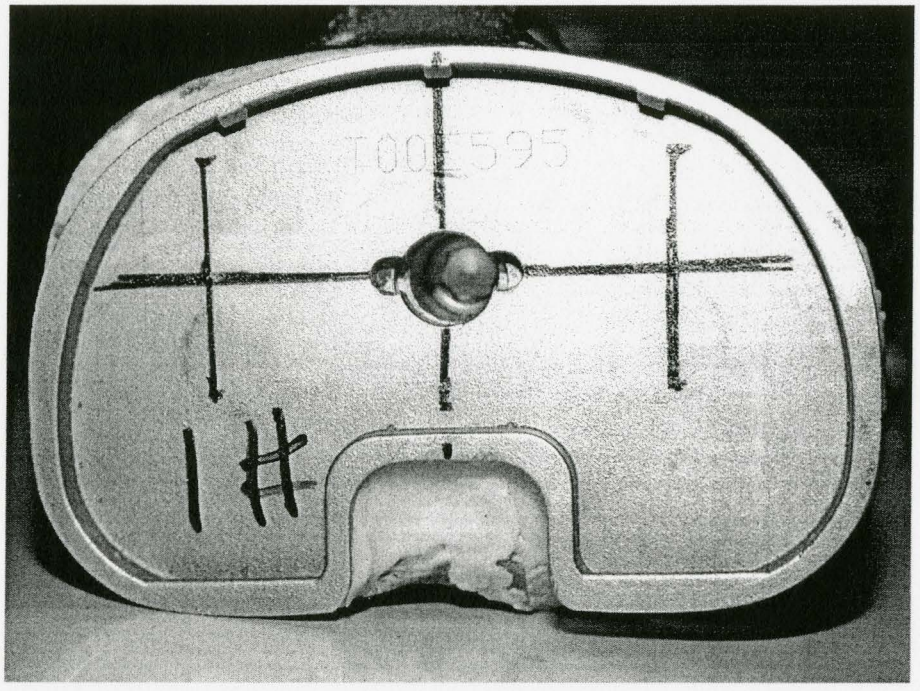

Figure A.11 Loading locations (lateral, central and medial from left to right)

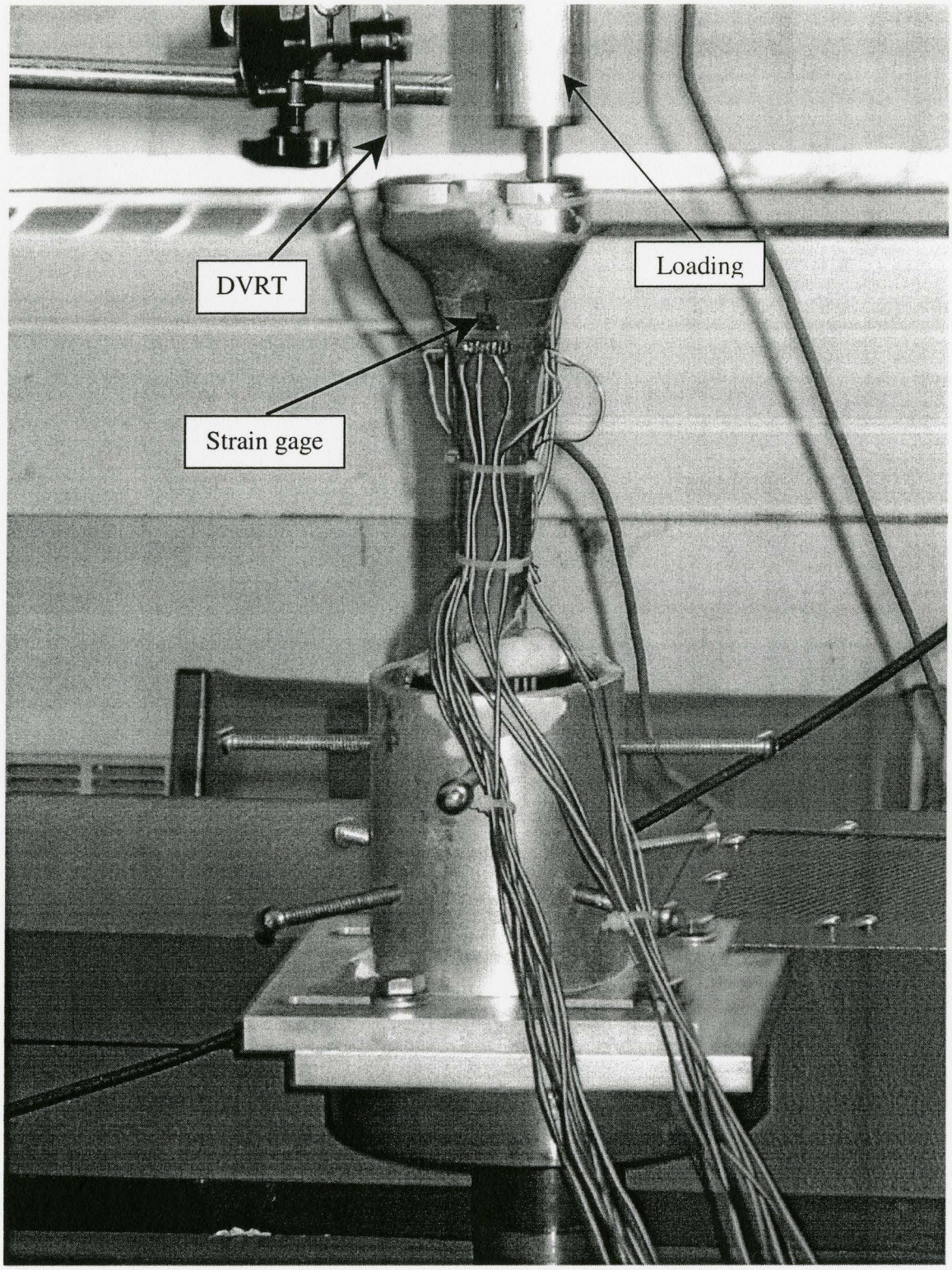

Figure A.12 Experimental setup

Appendix B

Sensor Calibrations

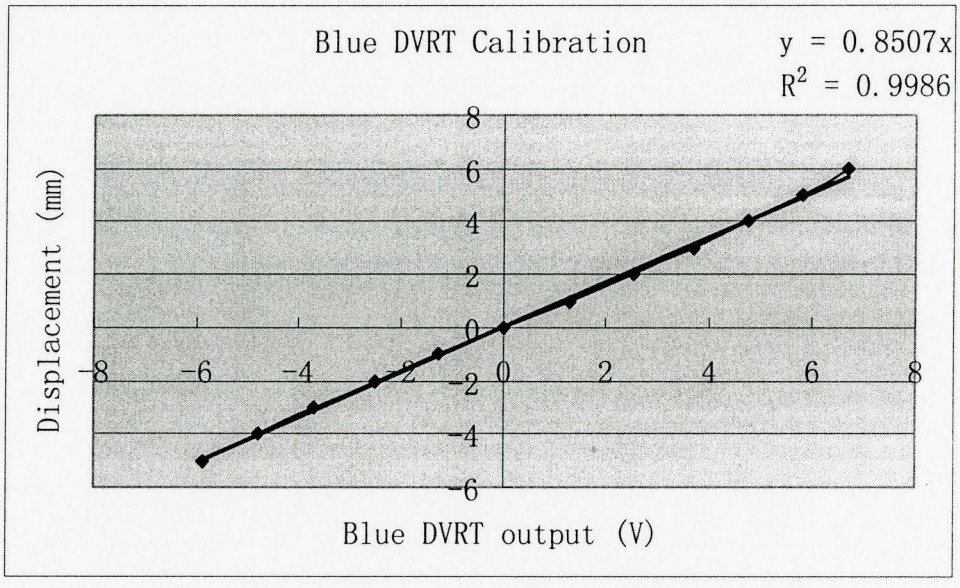

Figure B.1 Blue DVRT calibration curve

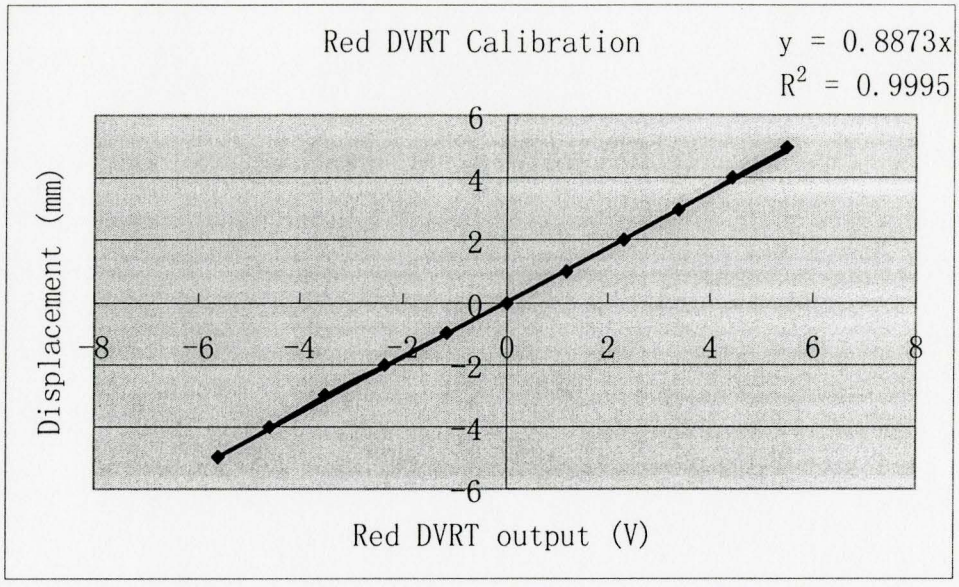

Figure B.2 Red DVRT calibration curve

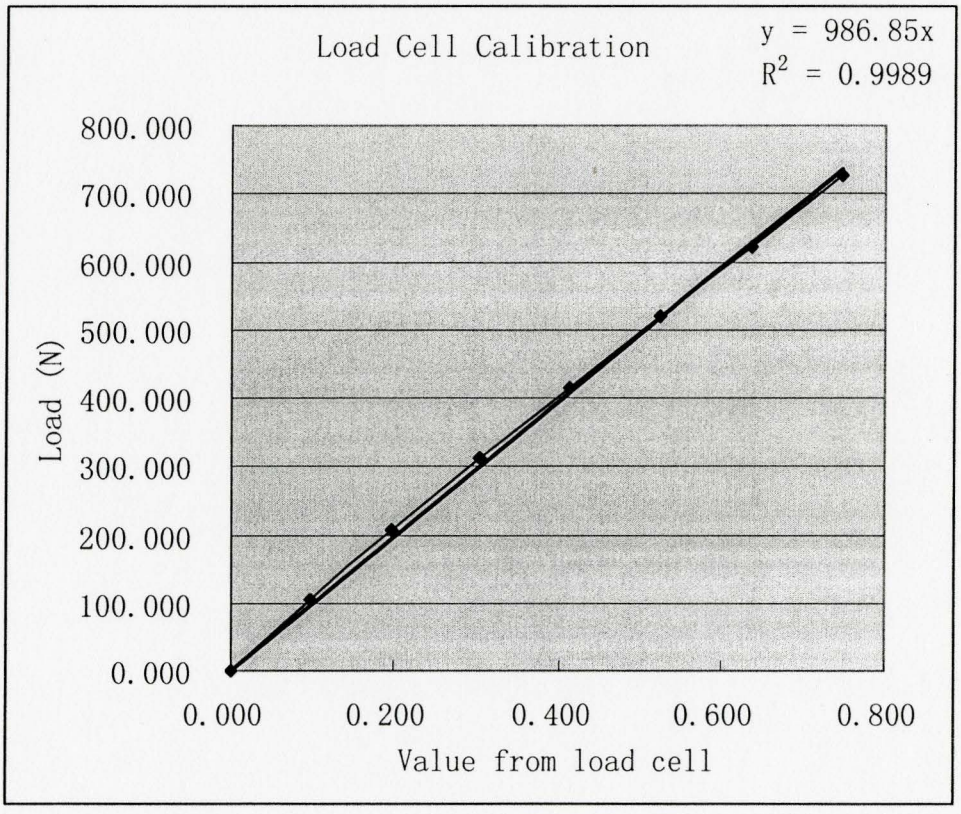

Figure B.3 Load calibration curve

Appendix C

Principal Strain Contours on Cortical Bone

----Under Central Loading

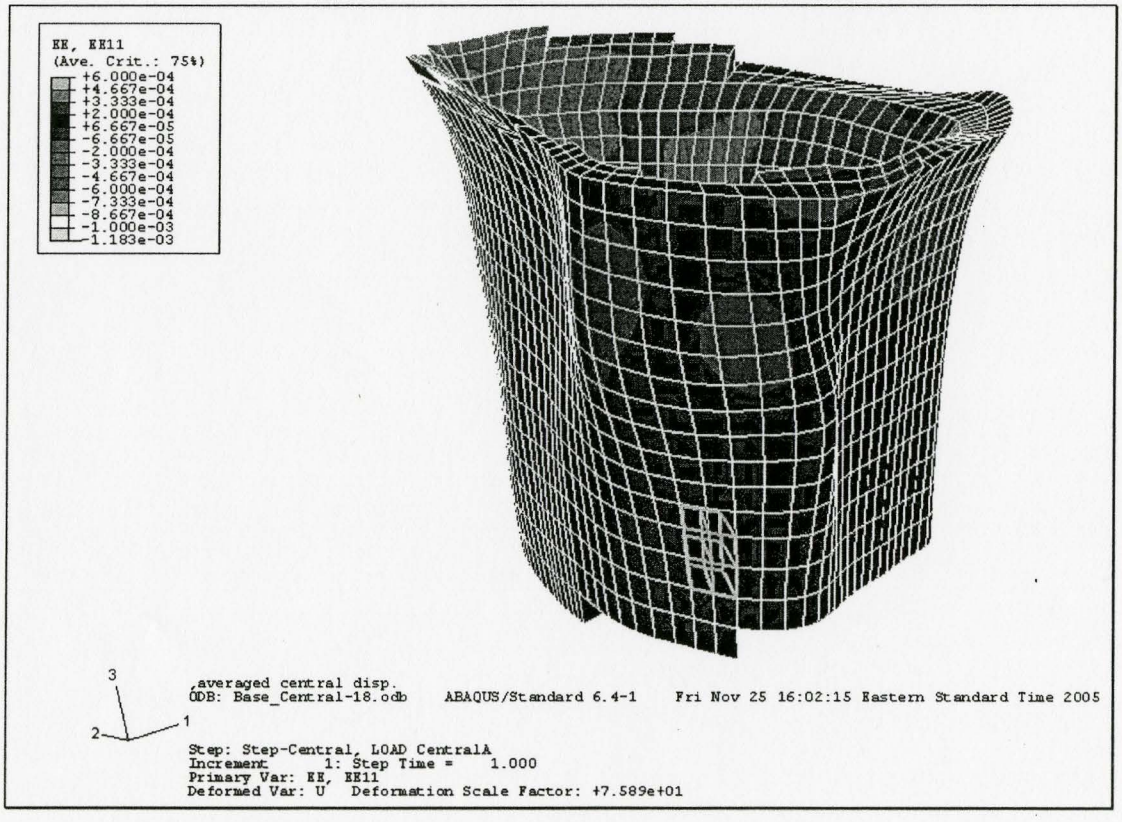

Figure C.1 Strain contour of anterior view (**tray only**)

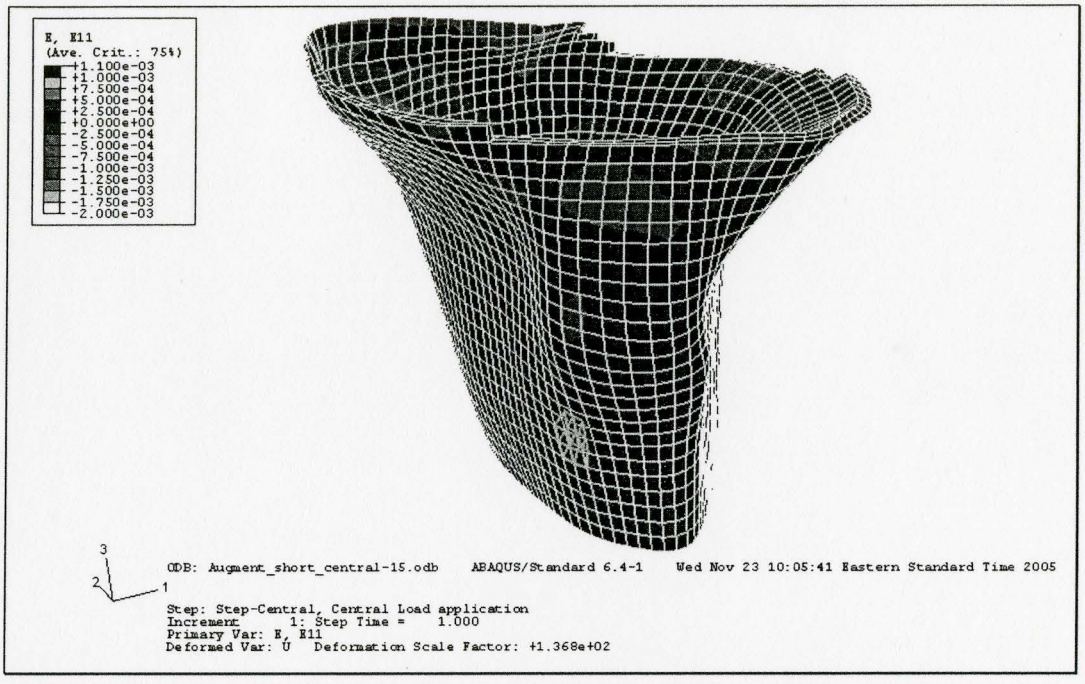

Figure C.2 Strain contour of anterior view (**tray-block**)

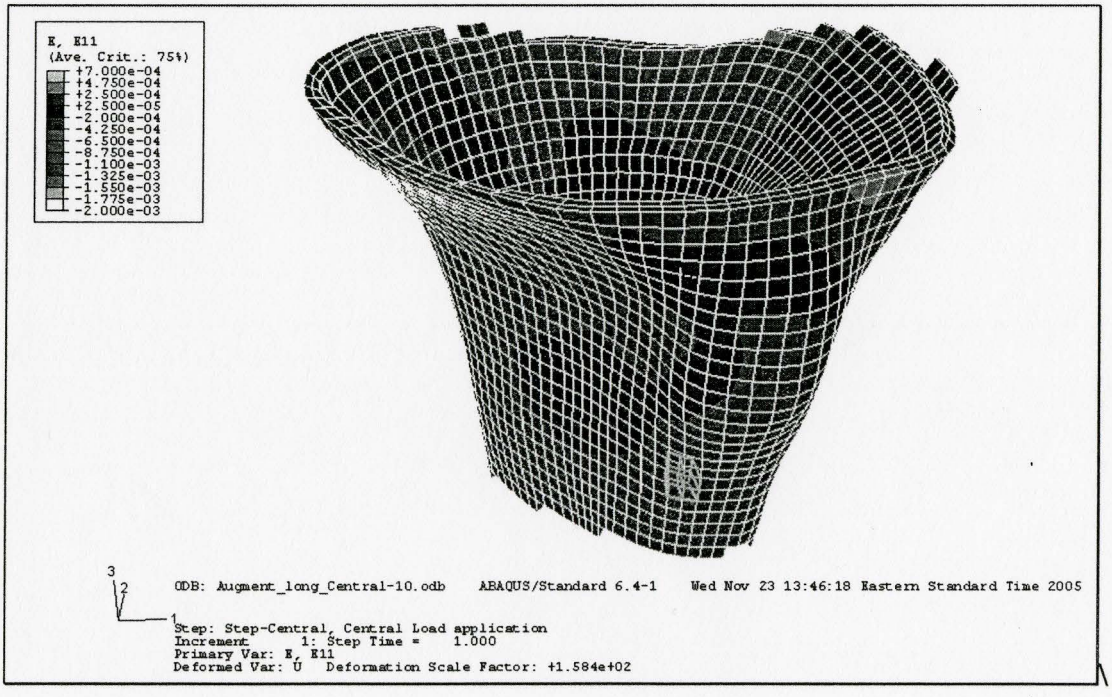

Figure C.3 Strain contour of anterior view (**tray-block-stem**)

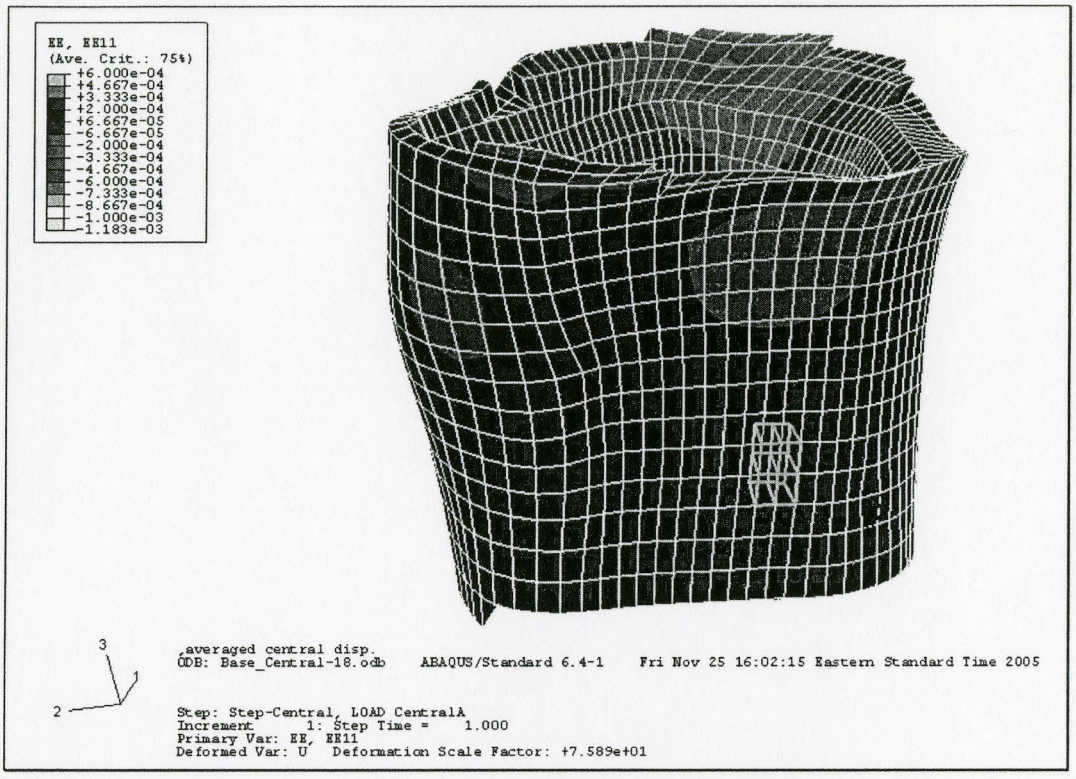

Figure C.4 Strain contour of lateral view (**tray only**)

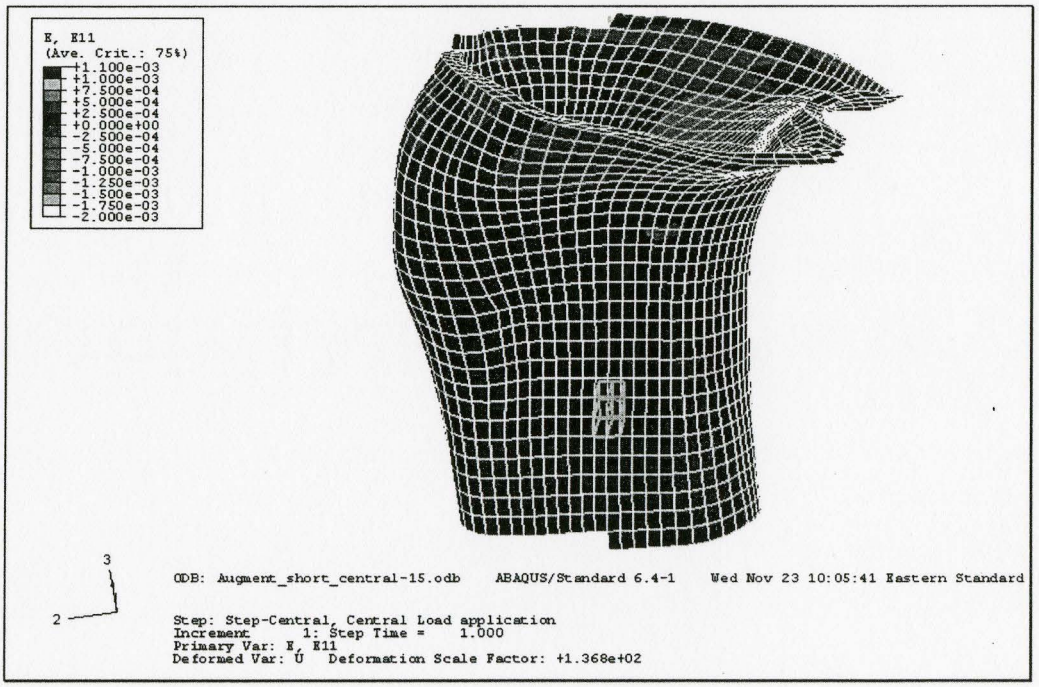

Figure C.5 Strain contour of lateral view (**tray-block**)

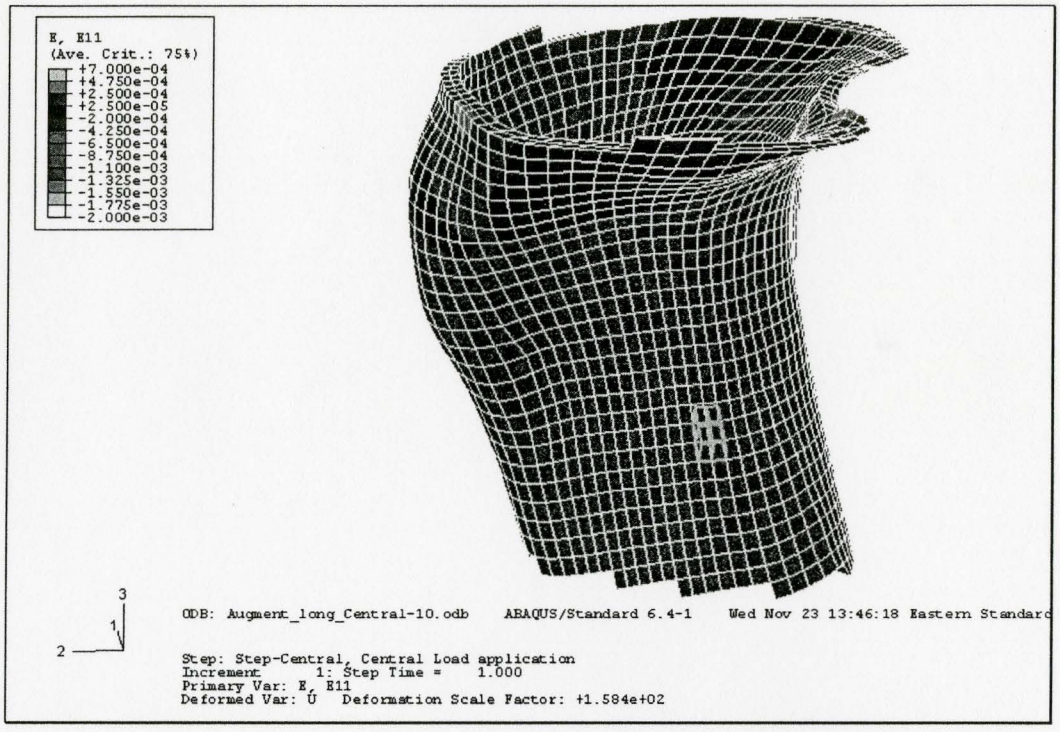

Figure C.6 Strain contour of lateral view (**tray-block-stem**)

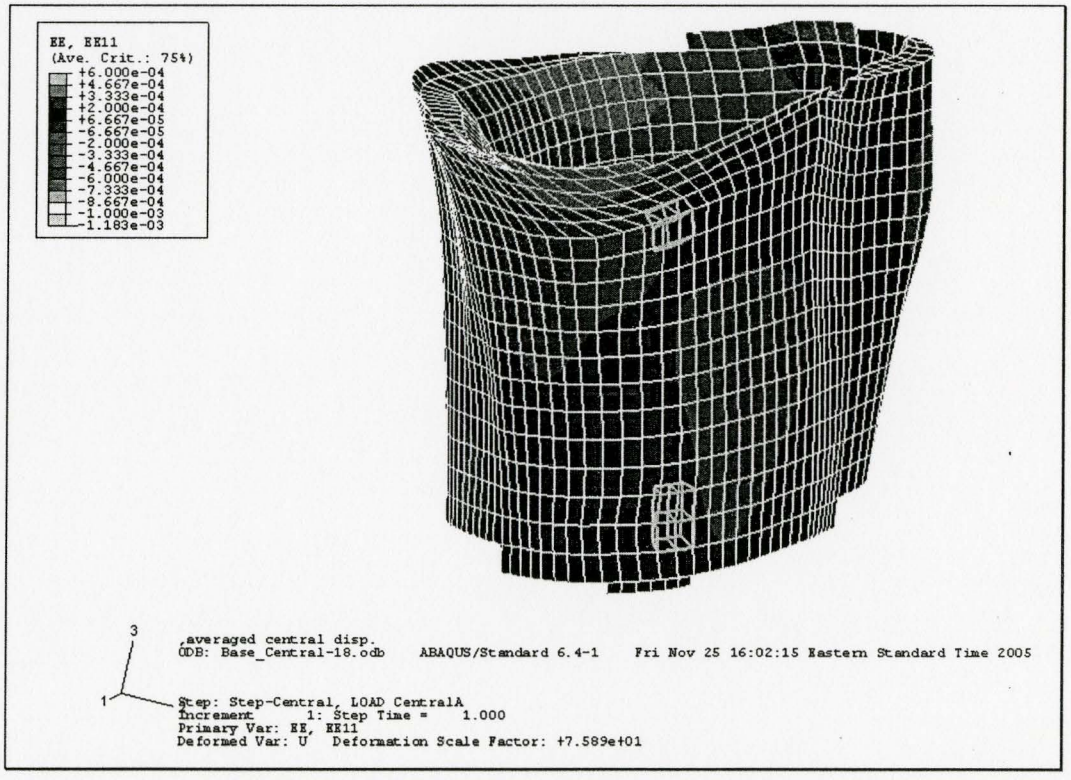

Figure C.7 Strain contour of medial view (**tray only**)

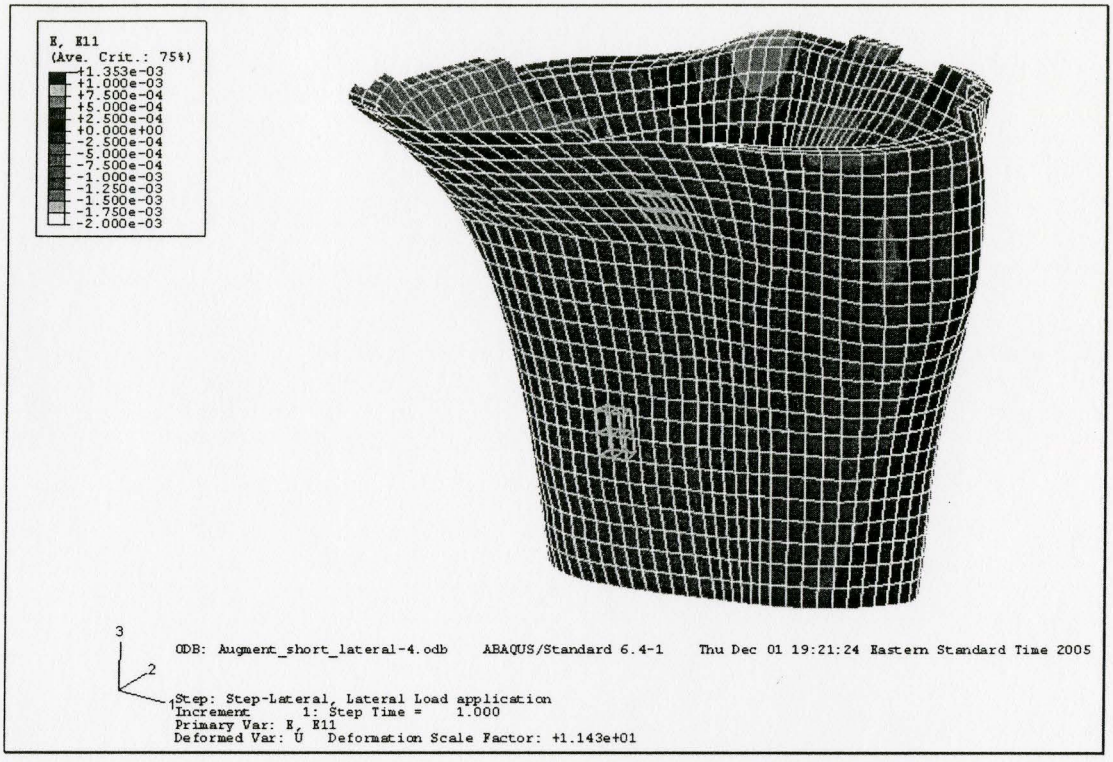

Figure C.8 Strain contour of medial view (t**ray-block**)

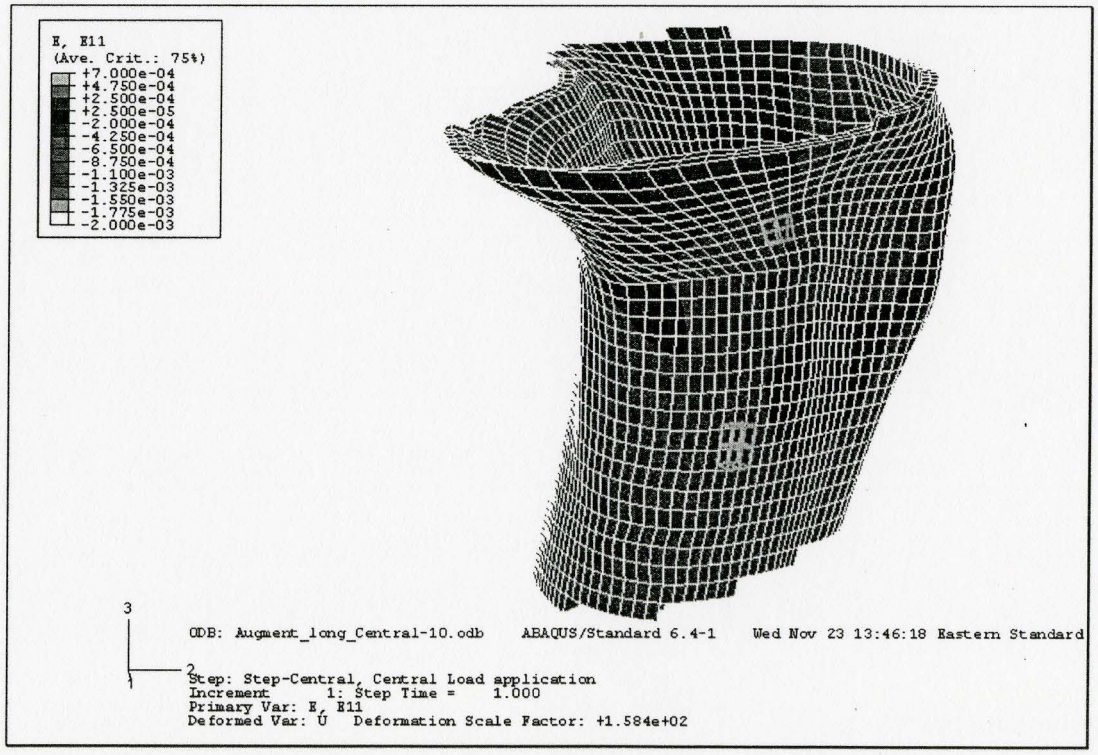

Figure C.9 Strain contour of medial view (**tray-block-stem**)

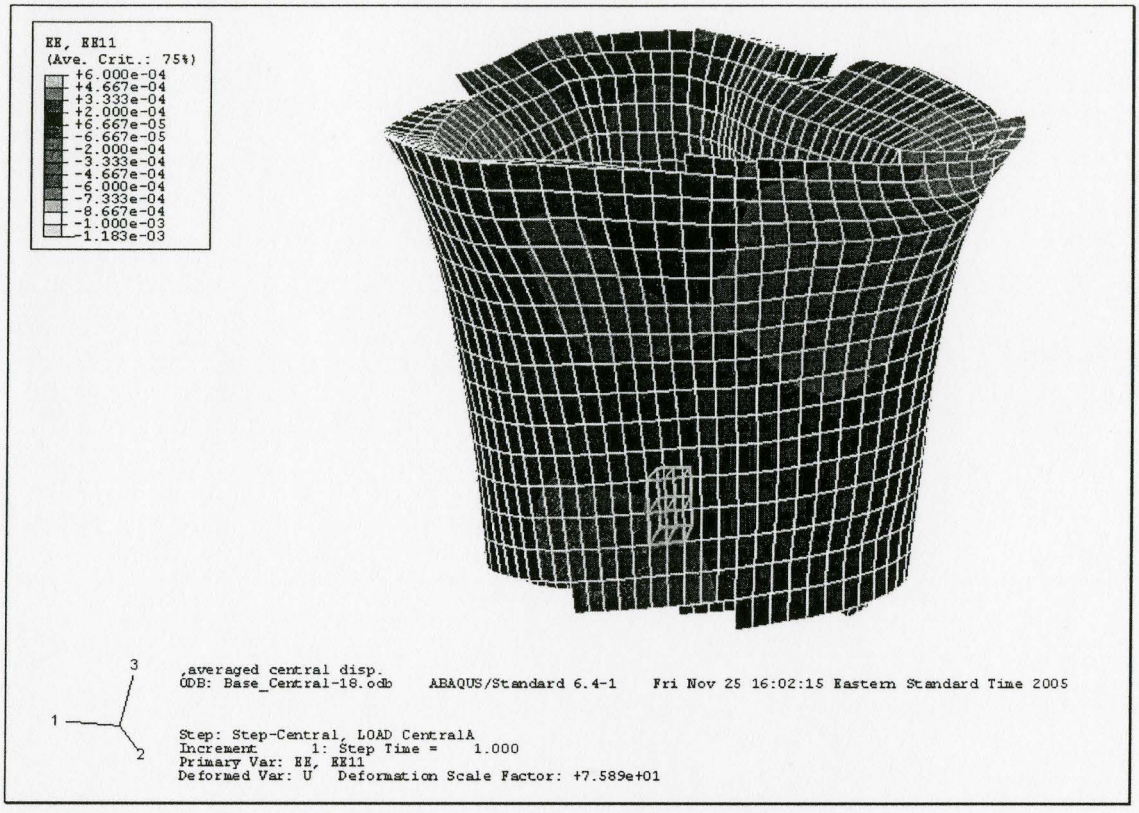

Figure C.10 Strain contour of posterior view (t**ray only**)

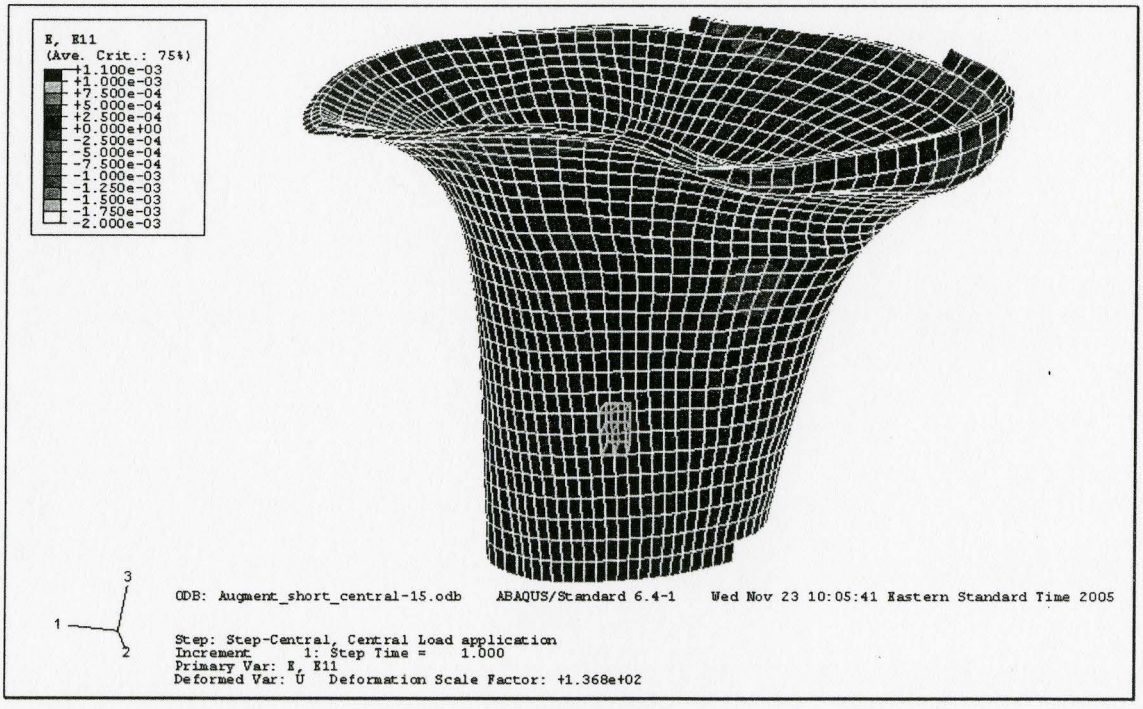

Figure C.11 Strain contour of posterior view (**tray-block**)

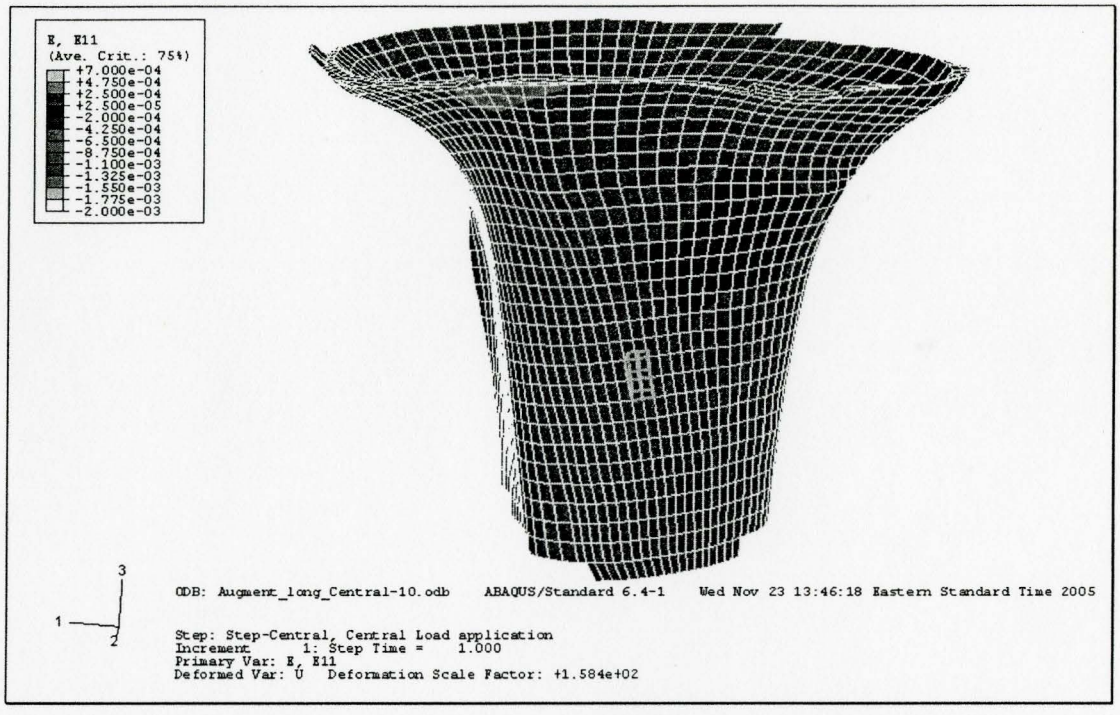

Figure C.12 Strain contour of posterior view (**tray-block-stem**)

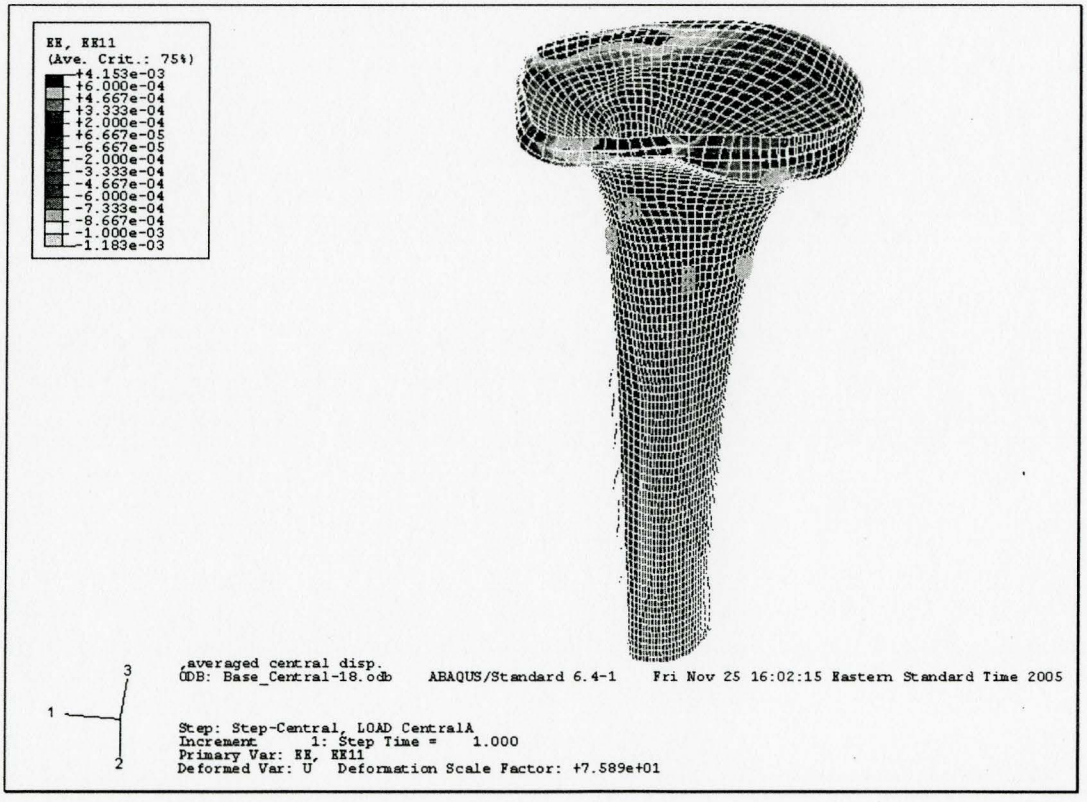

Figure C.13 Strain contour of whole view (**tray only**)

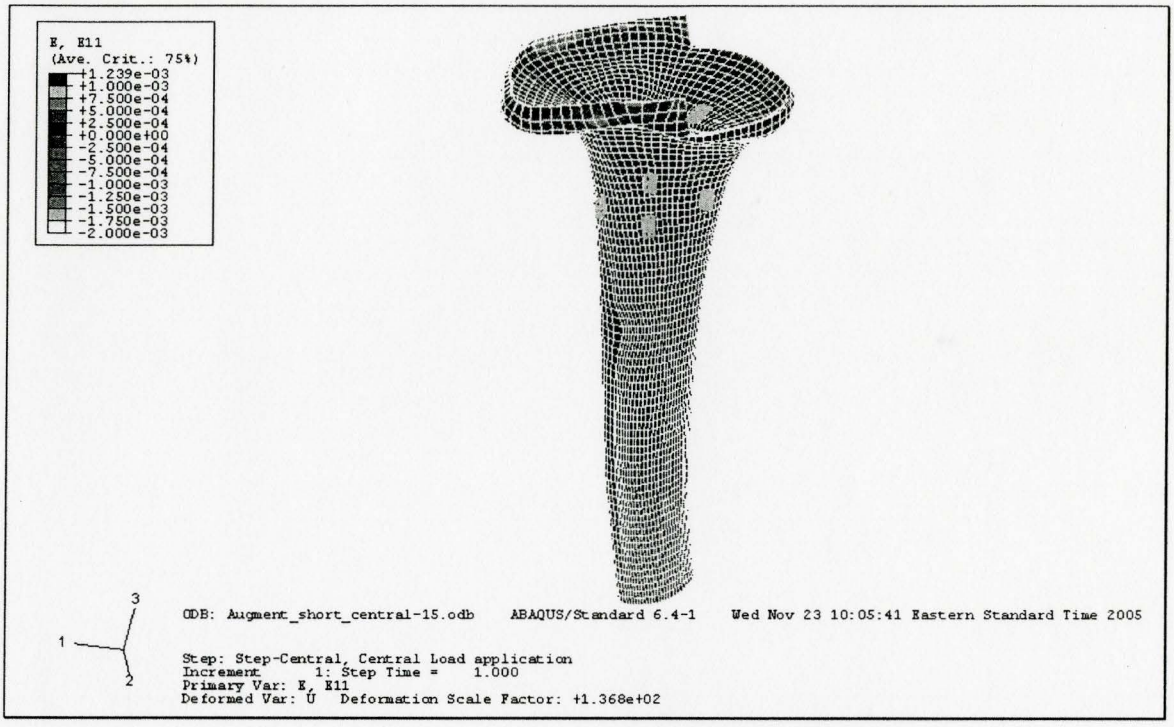

Figure C.14 Strain contour of whole view (**tray-block**)

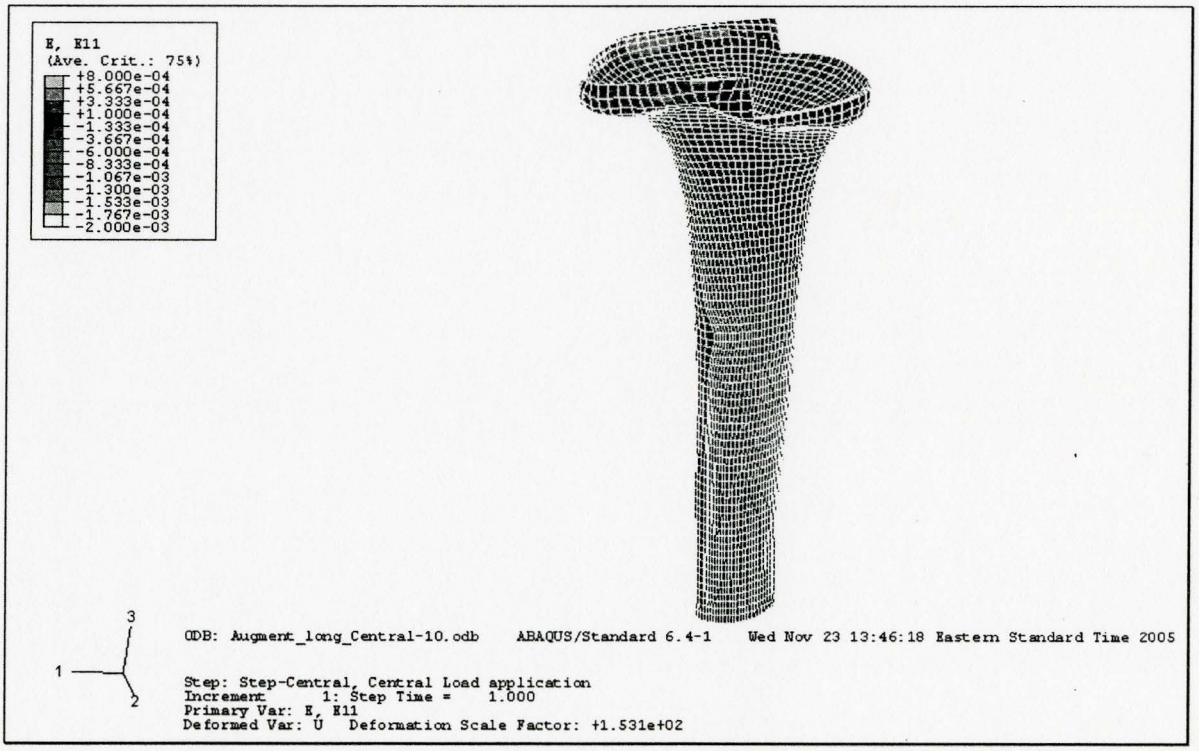

Figure C.15 Strain contour of whole view (**tray-block-stem**)

Appendix D

Von Mises Stress Contours (central loading)

D.1 Configuration of tray only

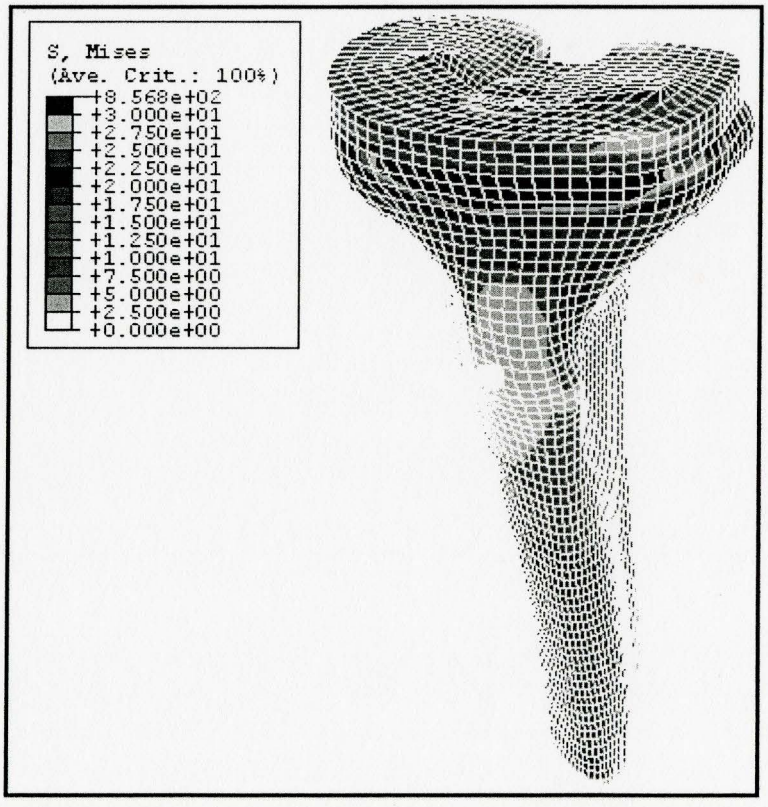

Figure D.1 Von Mises stress contour of the whole model (**tray only, central loading**)

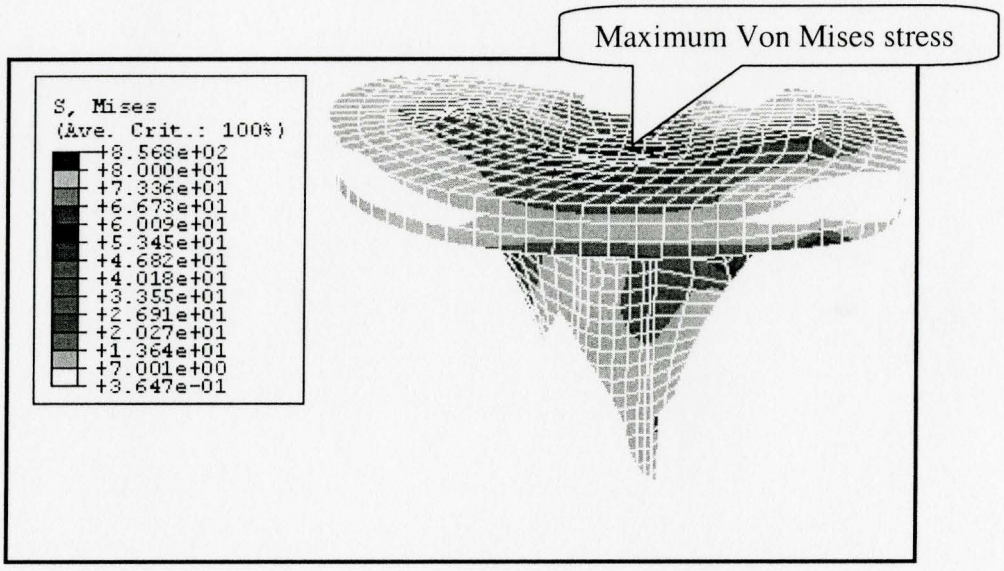

Figure D.2 Von Mises stress contour of the implant (**tray only, central loading**)

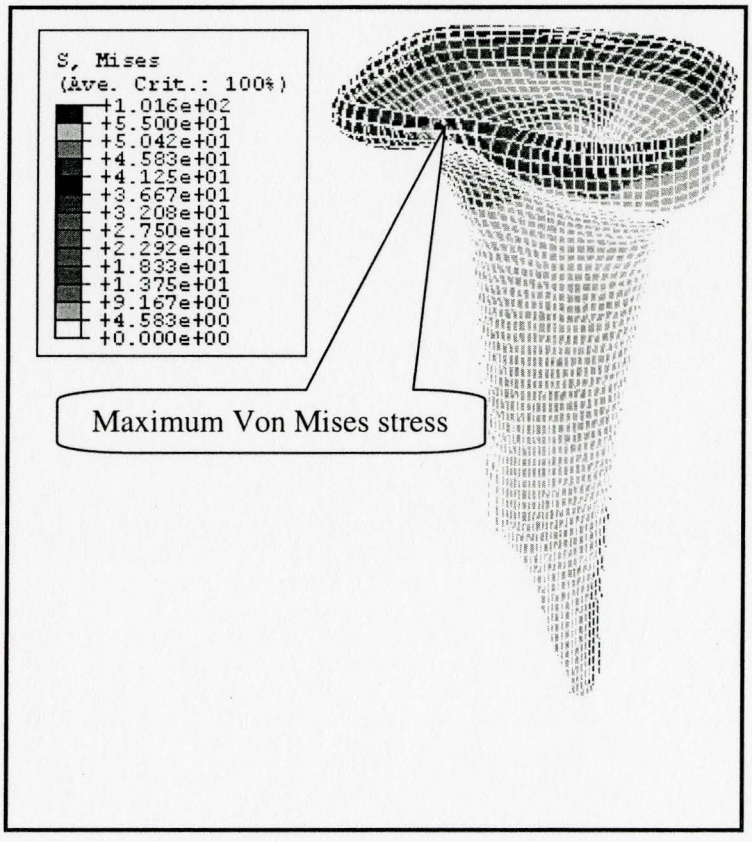

Figure D.3 Von Mises stress contour of the cortical bone (**tray only, central loading**)

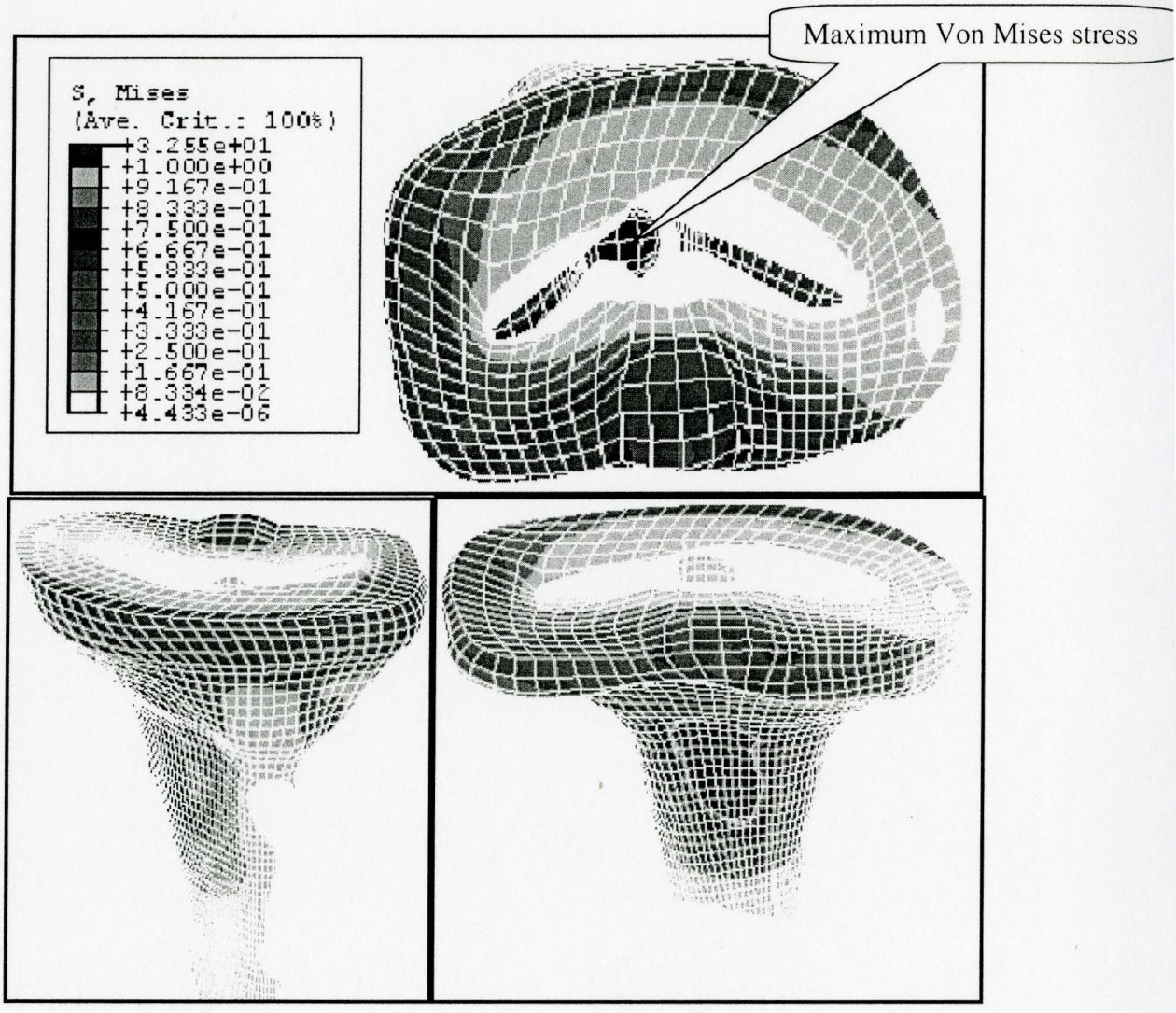

Figure D.4 Von Mises stress contour of the cancellous bone (**tray only, central loading**)

D.2 Configuration of tray-block

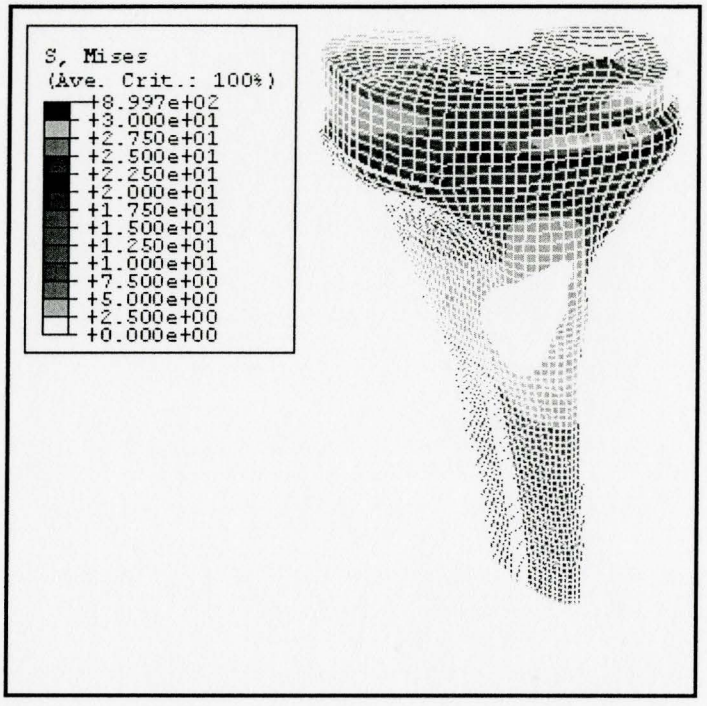

Figure D.5 Von Mises stress contour of the whole model (**tray-block, central loading**)

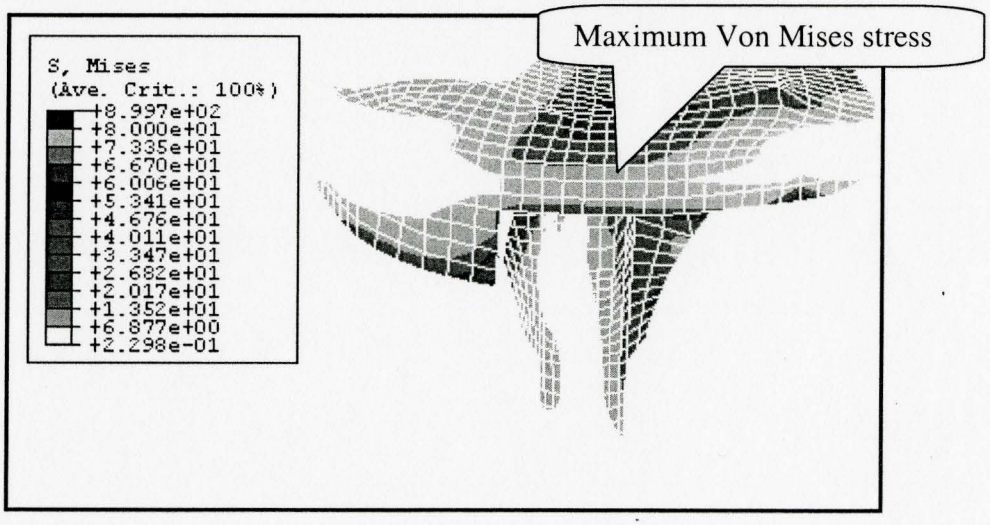

Figure D.6 Von Mises stress contour of the implant (**tray-block, central loading**)

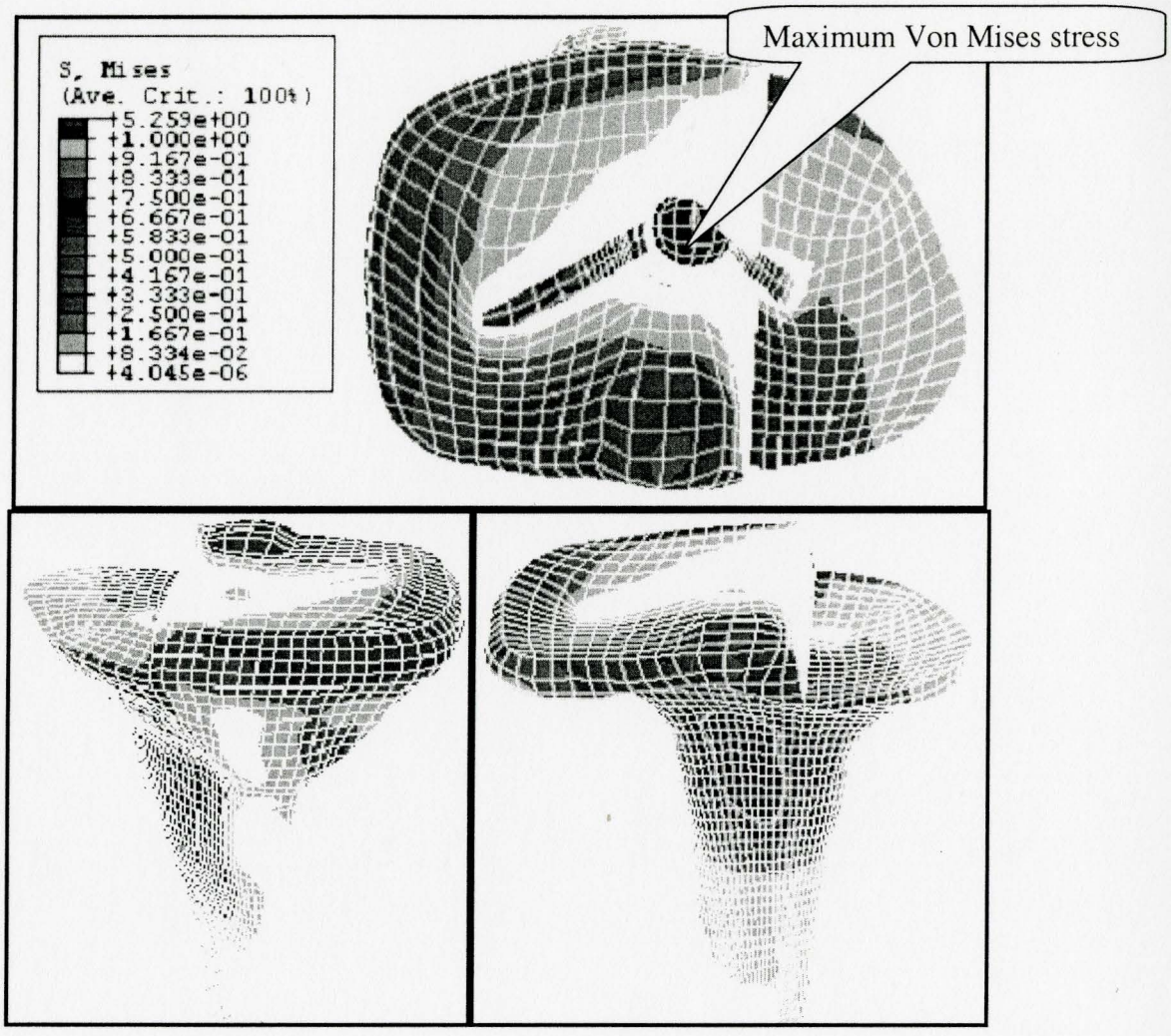

Figure D.7 Von Mises stress contour of the cancellous bone (**tray-block, central loading**)

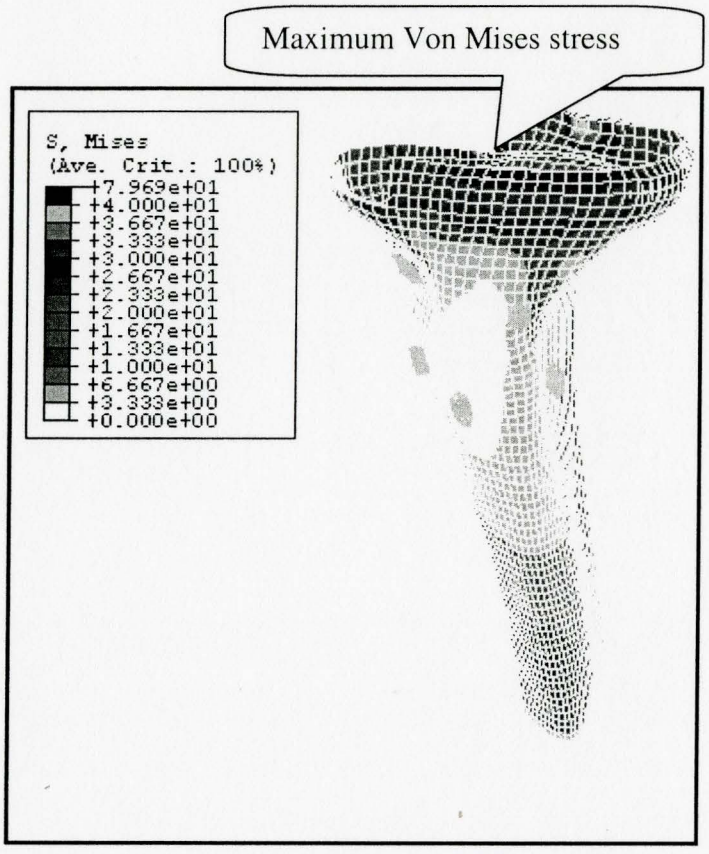

Figure D.8 Von Mises stress contour of the cortical bone (**tray-block, central loading**)

D.3 Configuration of tray-block-stem

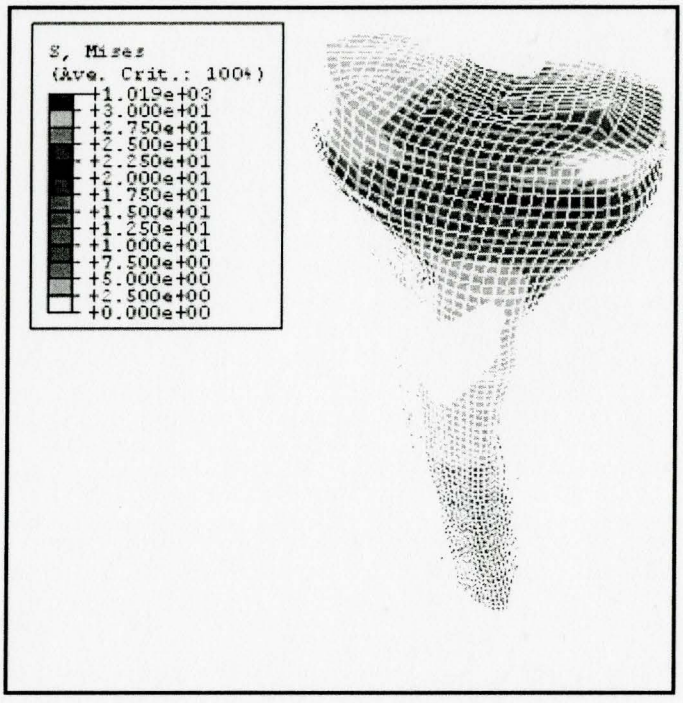

Figure D.9 Von Mises stress contour of the whole model (**tray-block-stem, central loading**)

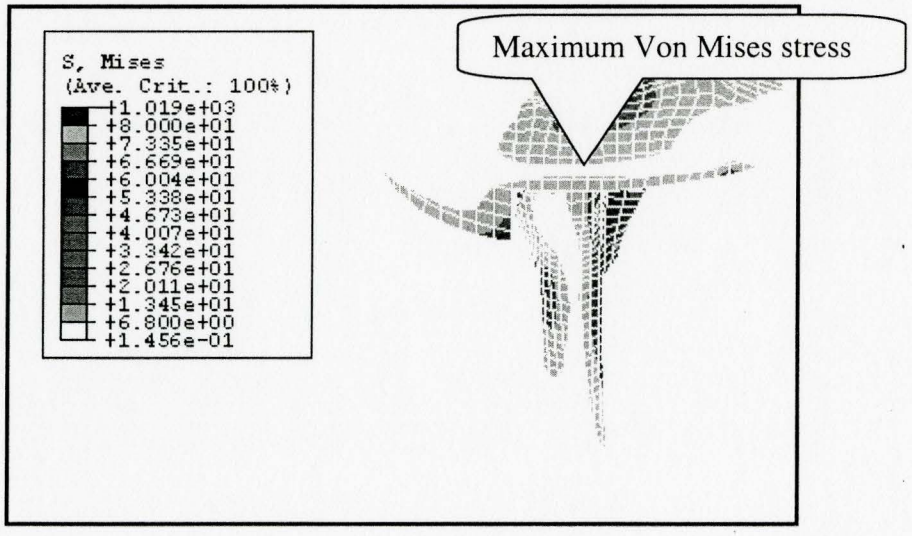

Figure D.10 Von Mises stress contour of the implant (**tray-block-stem, central loading**)

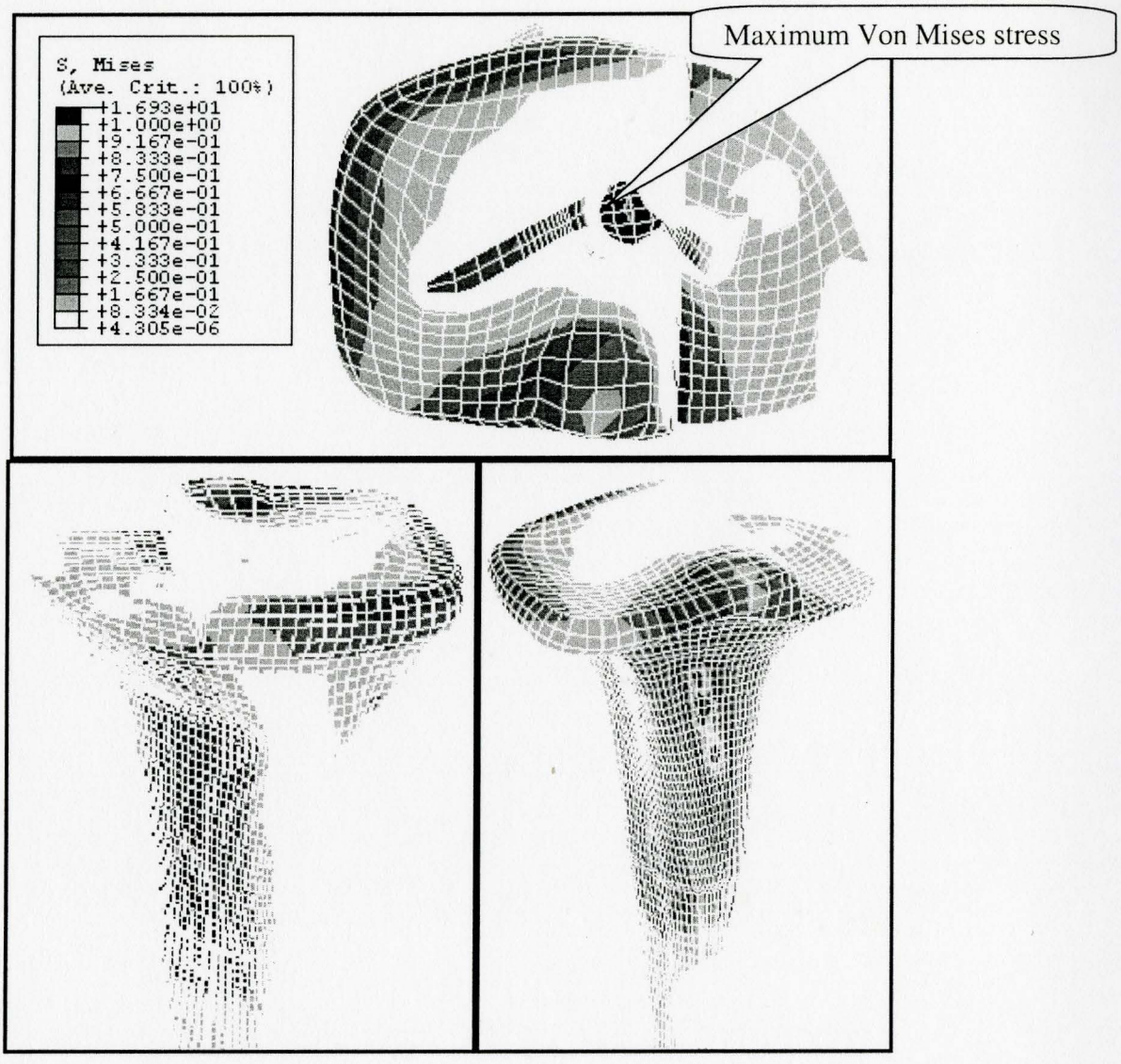

Figure D.11 Von Mises stress contour of the cancellous bone (**tray-block-stem, central loading**)

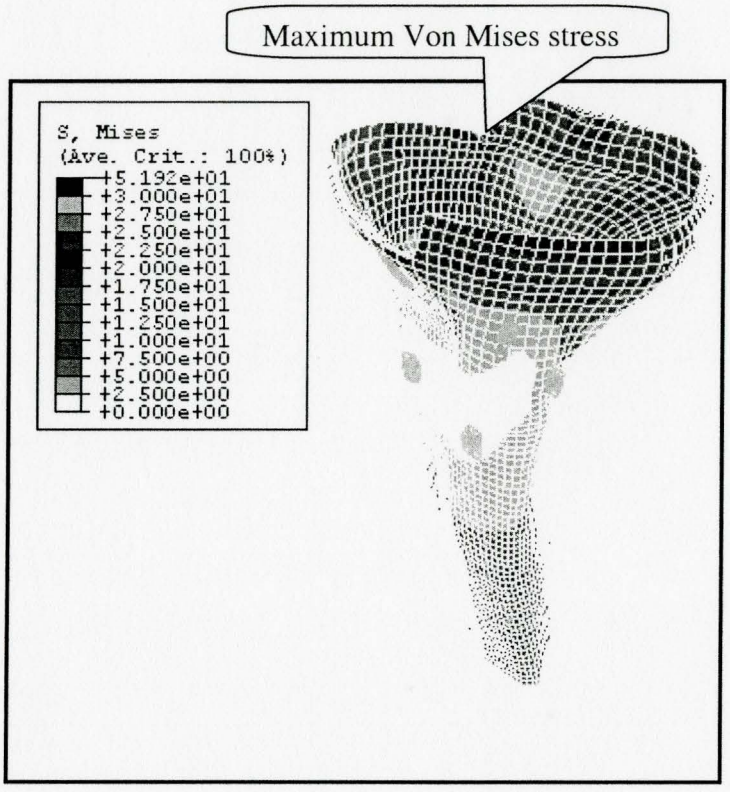

Figure D.12 Von Mises stress contour of the cortical bone (**tray-block-stem, central loading**)

Appendix E

Von Mises Stress Contours (medial loading)

E.1 Configuration of tray only

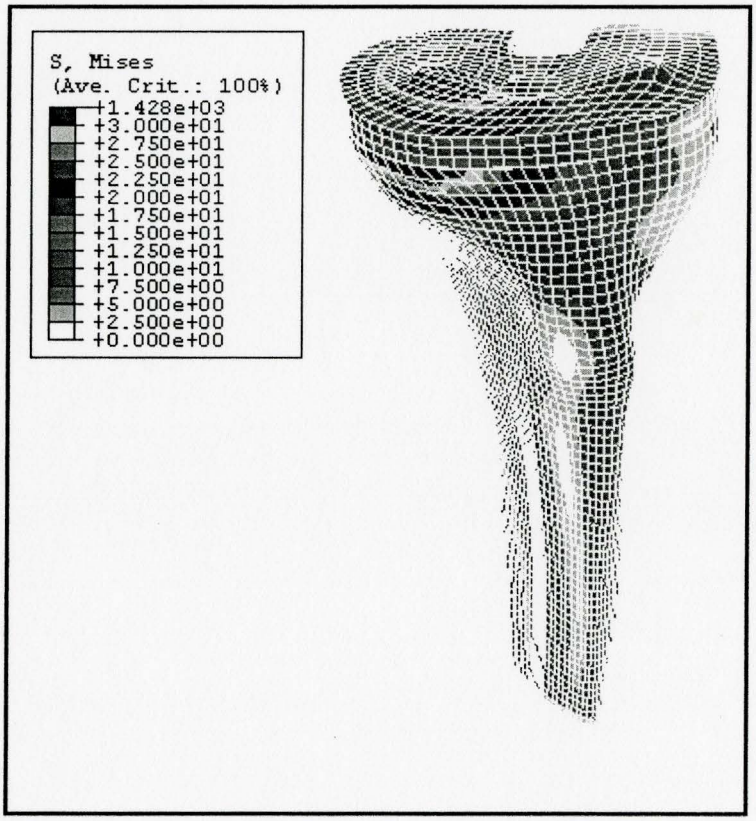

Figure E.1 Von Mises stress contour of the whole model (**tray only, medial loading**)

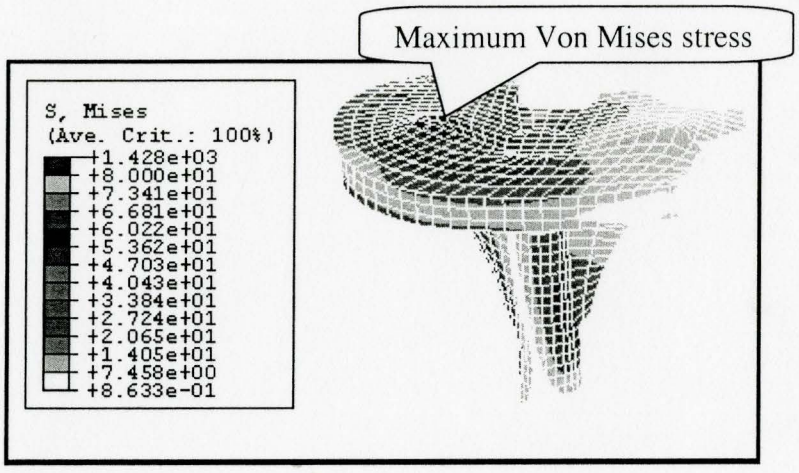

Figure E.2 Von Mises stress contour of the implant (**tray only, medial loading**)

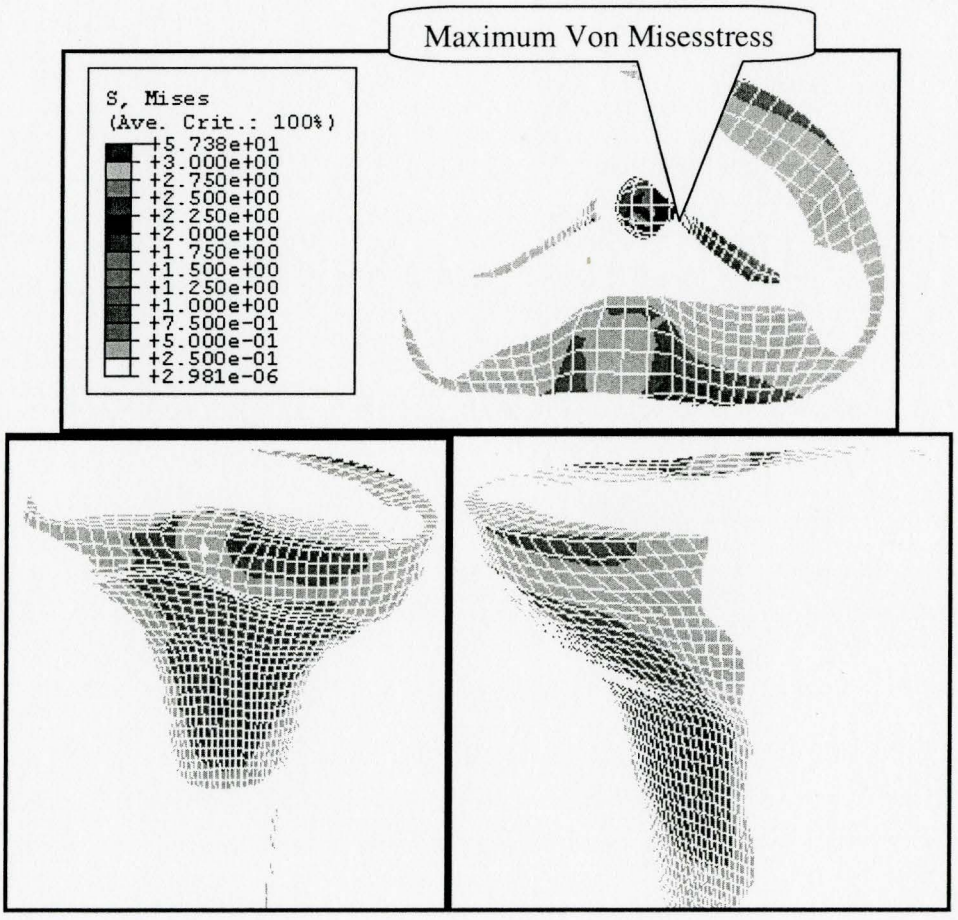

Figure E.3 Von Mises stress contour of the cancellous bone (**tray only, medial loading**)

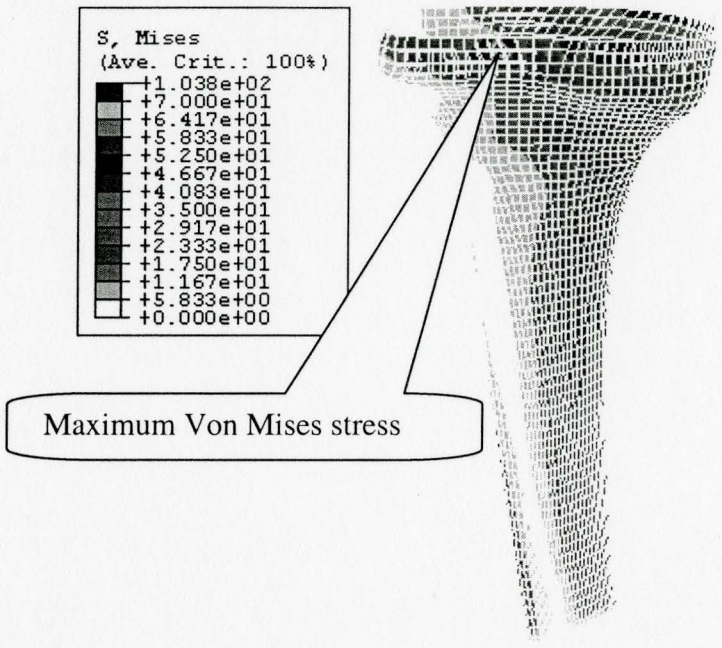

Figure E.4 Von Mises stress contour of the cortical bone (**tray only, medial loading**)

E.2 Configuration of tray-block

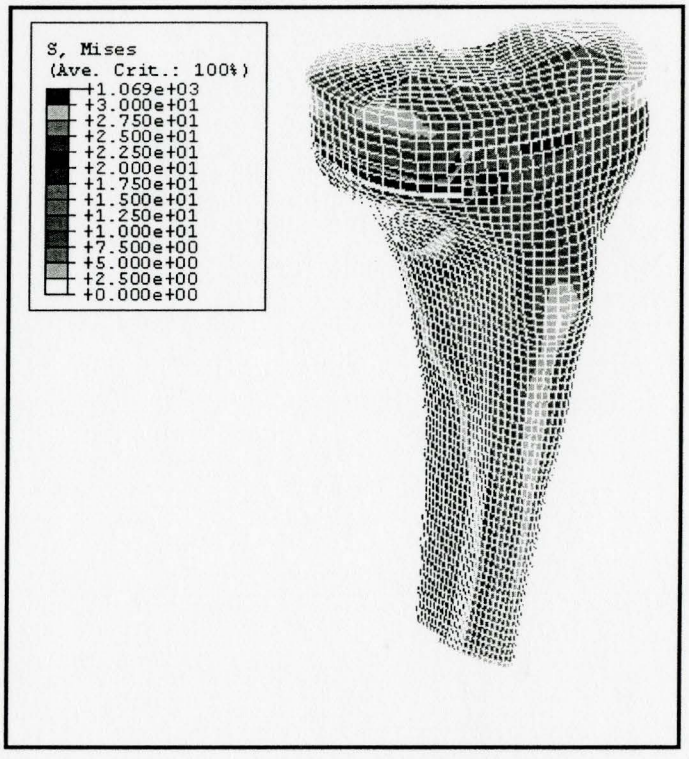

Figure E.5 Von Mises stress contour of the whole model (**tray-block, medial loading**)

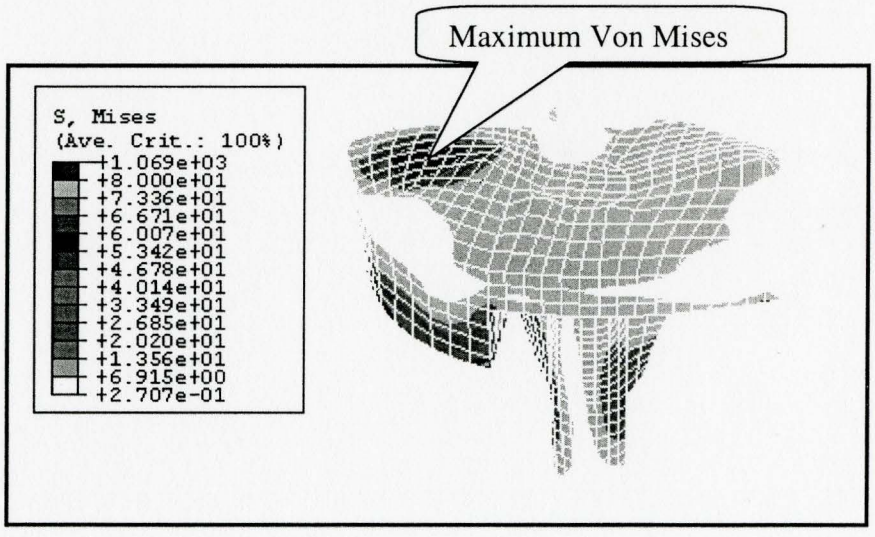

Figure E.6 Von Mises stress contour of the implant (**tray-block, medial loading**)

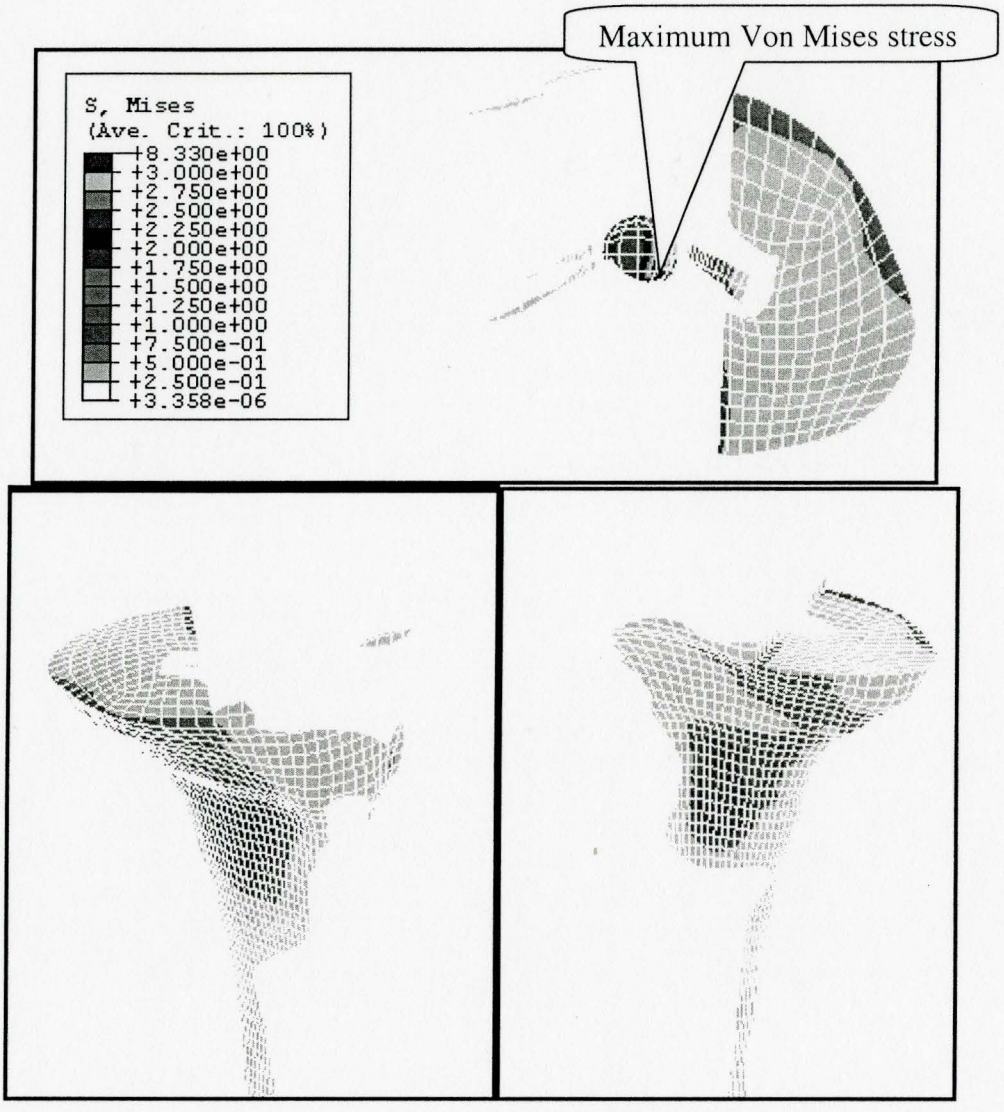

Figure E.7 Von Mises stress contour of the cancellous bone (**tray-block, medial loading**)

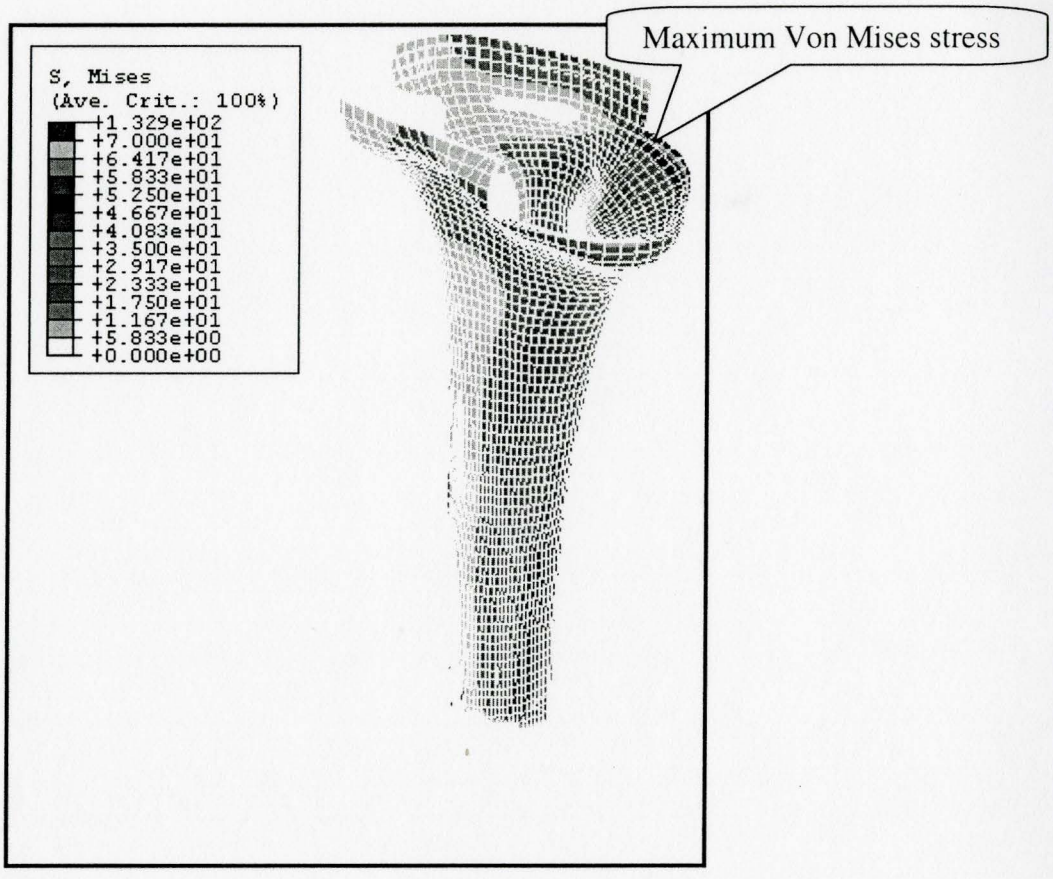

Figure E.8 Von Mises stress contour of the cortical bone (**tray-block, medial loading**)

E.3 Configuration of tray-block-stem

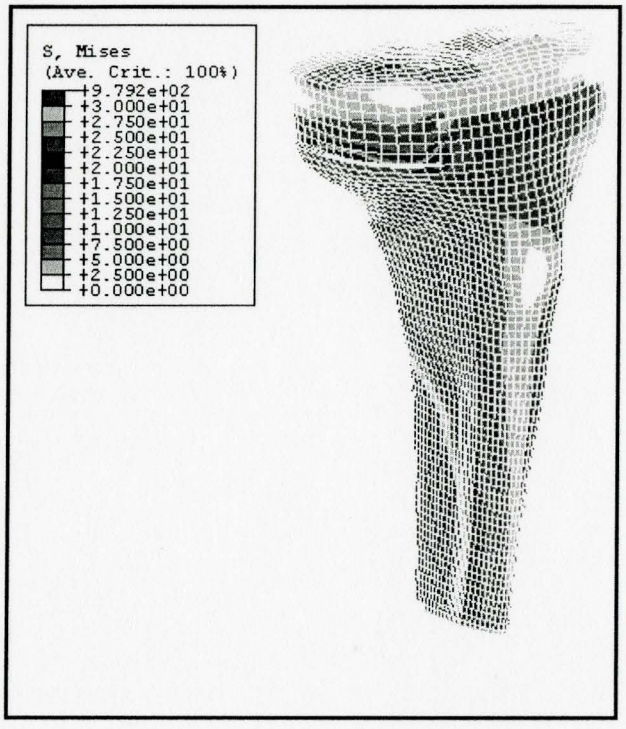

Figure E.9 Von Mises stress contour of the whole model (**tray-block-stem, medial loading**)

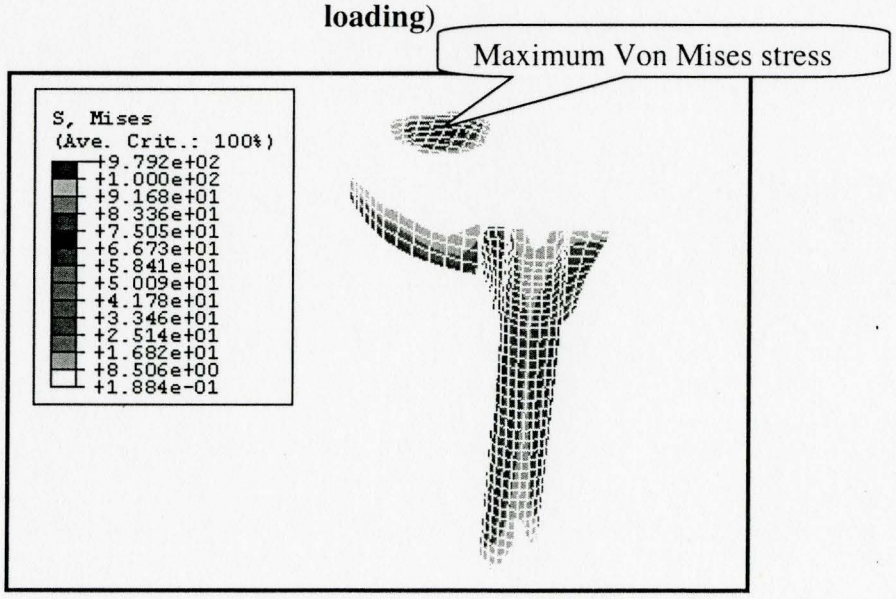

Figure E.10 Von Mises stress contour of the implant (**tray-block-stem, medial loading**)

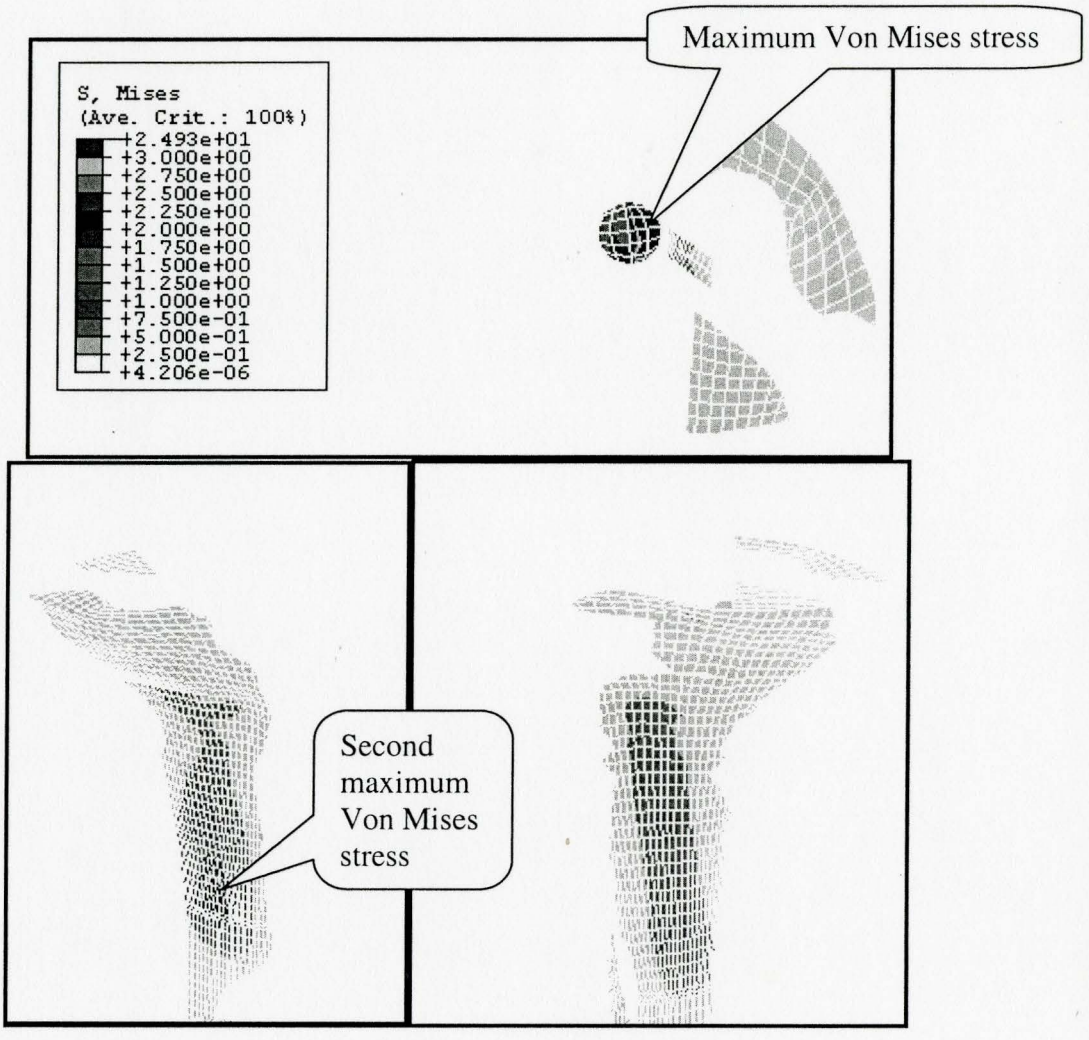

Figure E.11 Von Mises stress contour of the cancellous bone (**tray-block-stem, medial loading**)

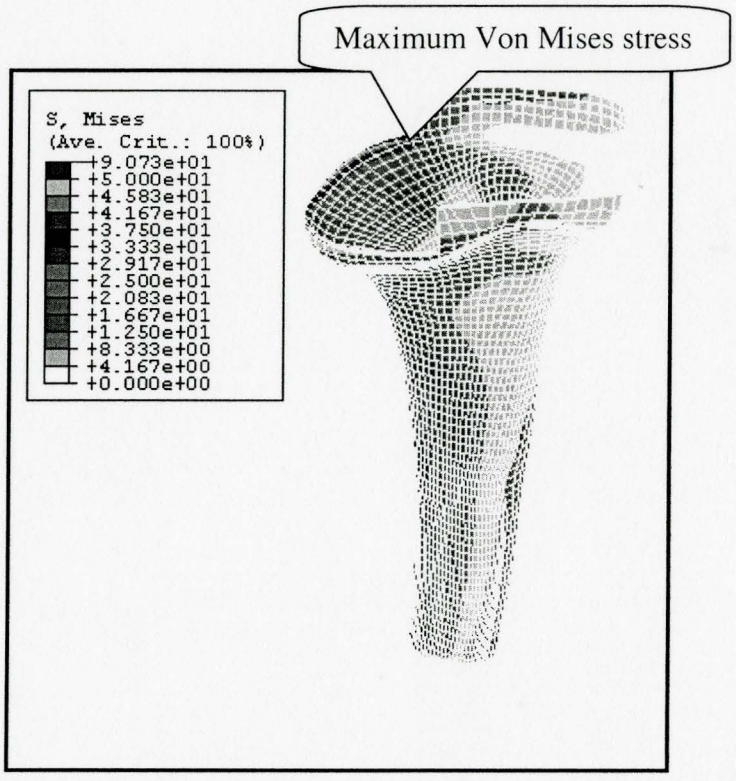

Figure E.12 Von Mises stress contour of the cortical bone (**tray-block-stem, medial loading**)

Appendix F

Von Mises Stress Contours (lateral loading)

F.1 Configuration of tray only

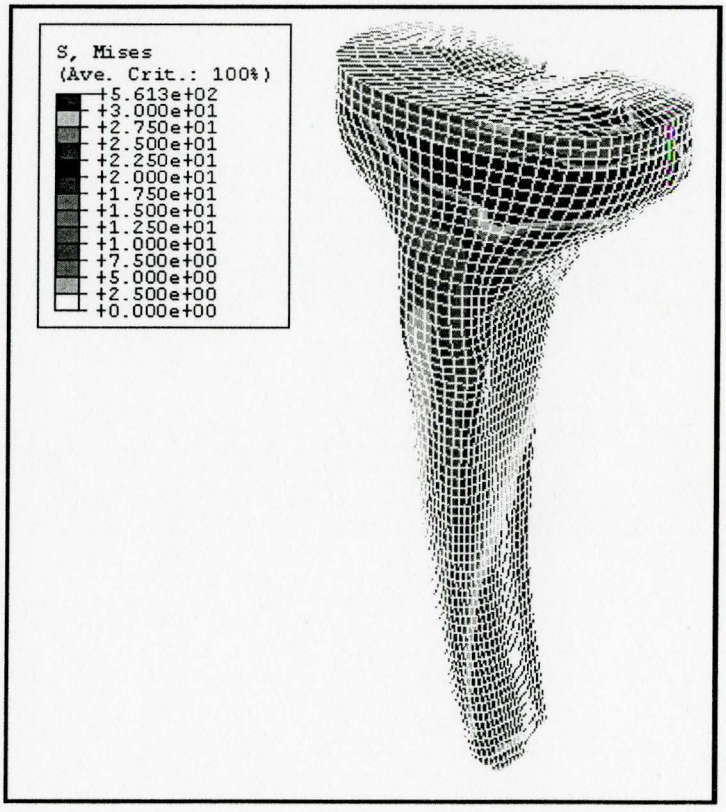

Figure F.1 Von Mises stress contour of the whole model (**tray only, lateral loading**)

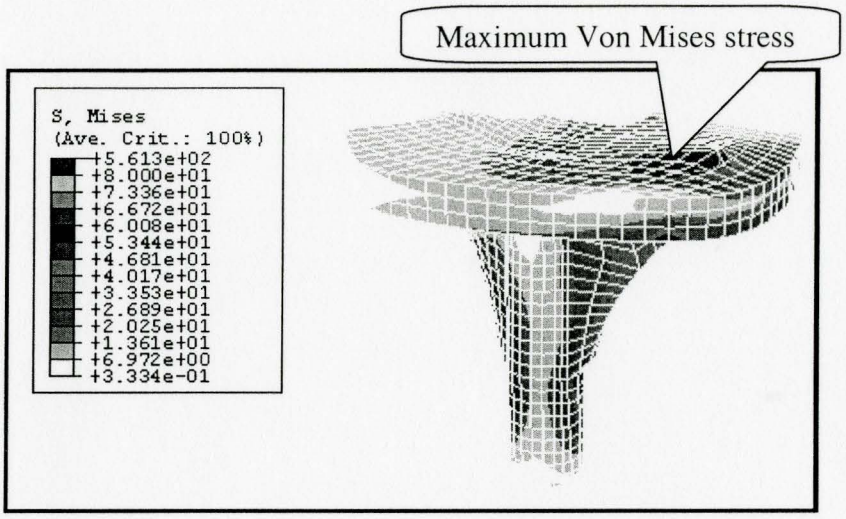

Figure F.2 Von Mises stress contour of the implant (**tray only, lateral loading**)

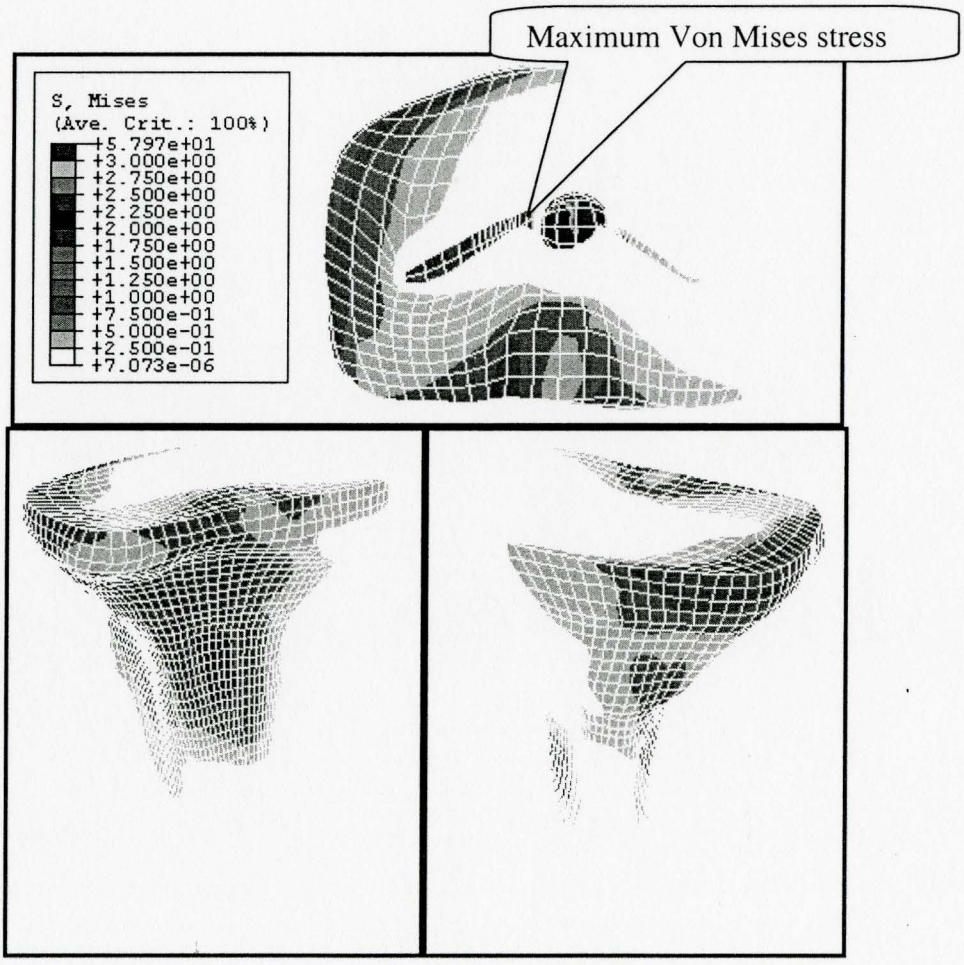

Figure F.3 Von Mises stress contour of the cancellous bone (**tray only, lateral loading**)

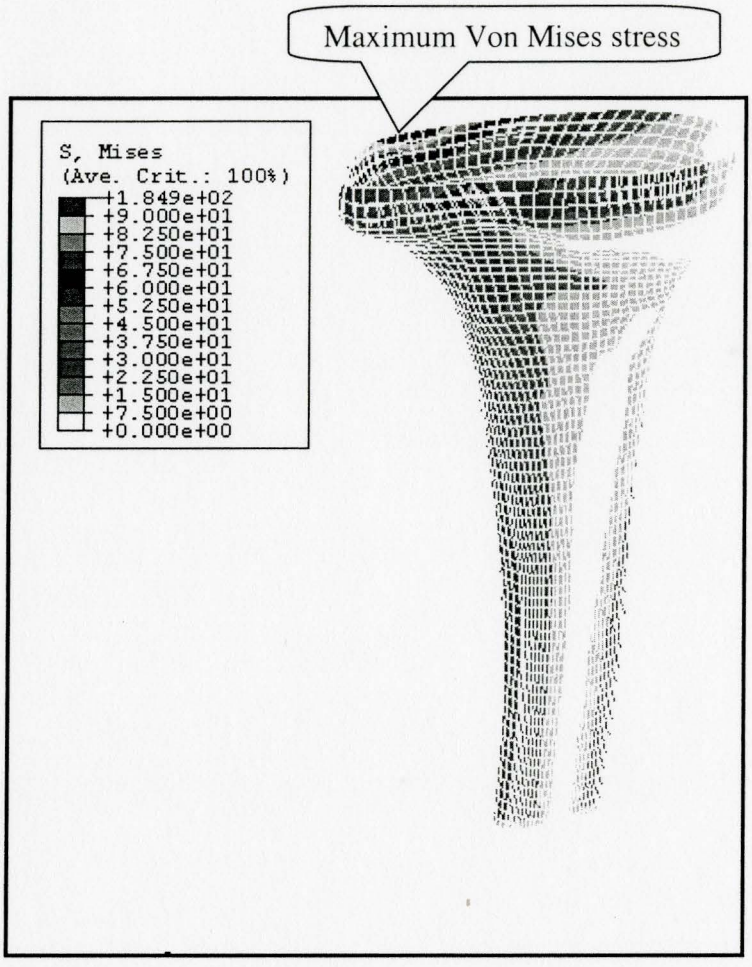

Figure F.4 Von Mises stress contour of the cortical bone (**tray only, lateral loading**)

F.2 Configuration of tray-block

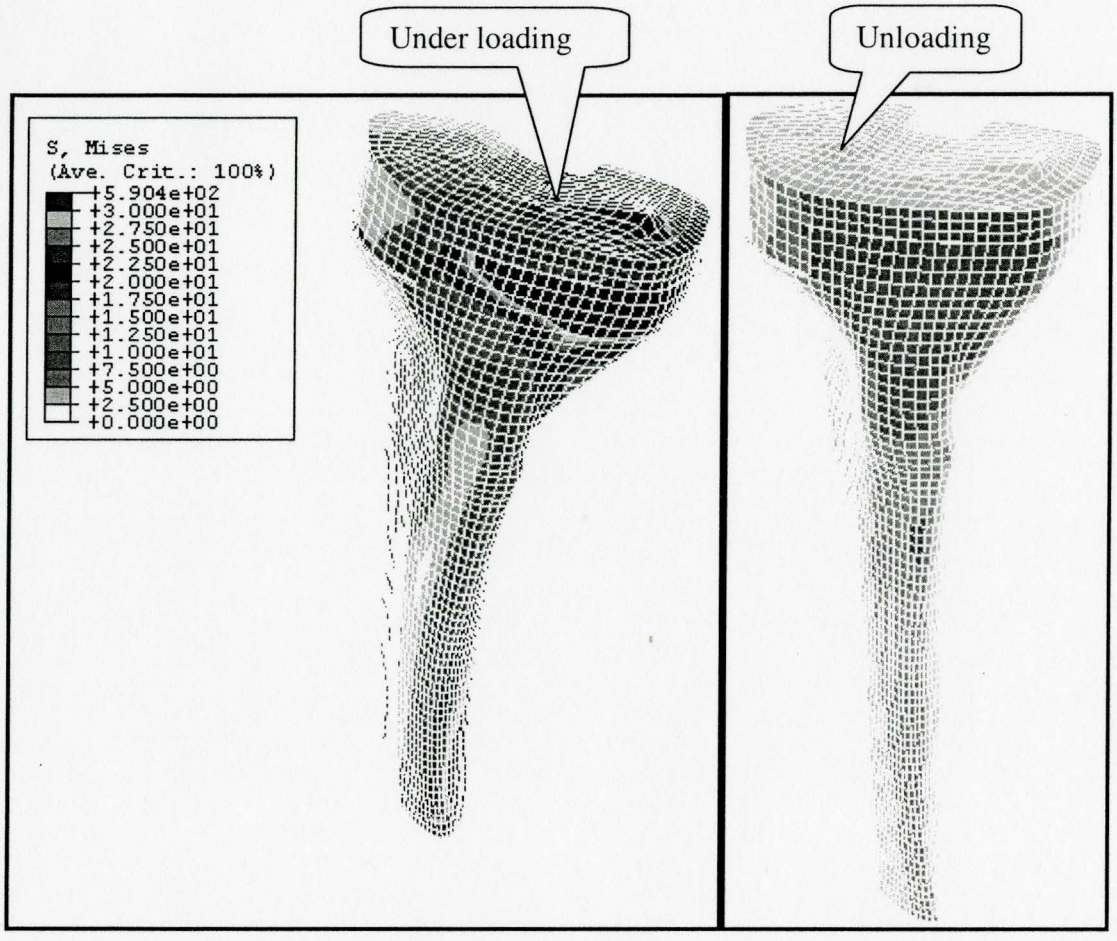

Figure F.5 Von Mises stress contour of the whole model (**tray-block, lateral loading**)

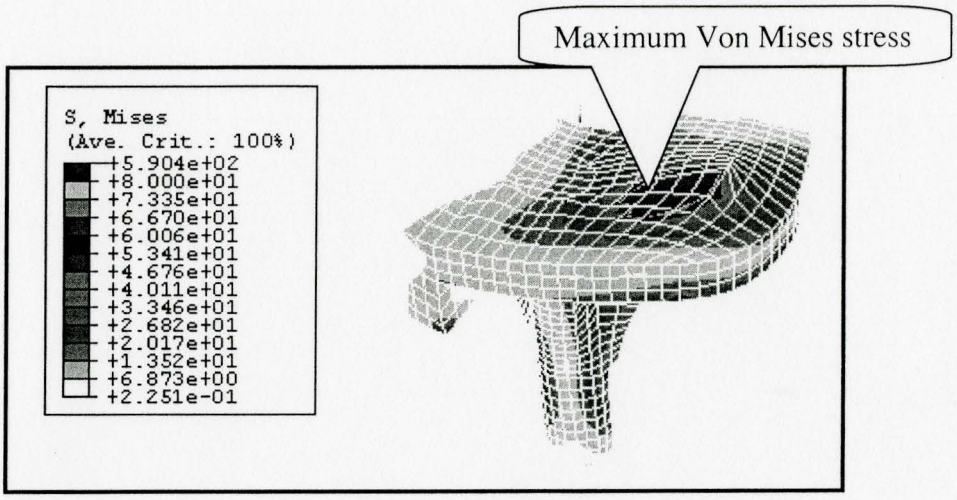

Figure F.6 Von Mises stress contour of the implant (**tray-block, lateral loading**)

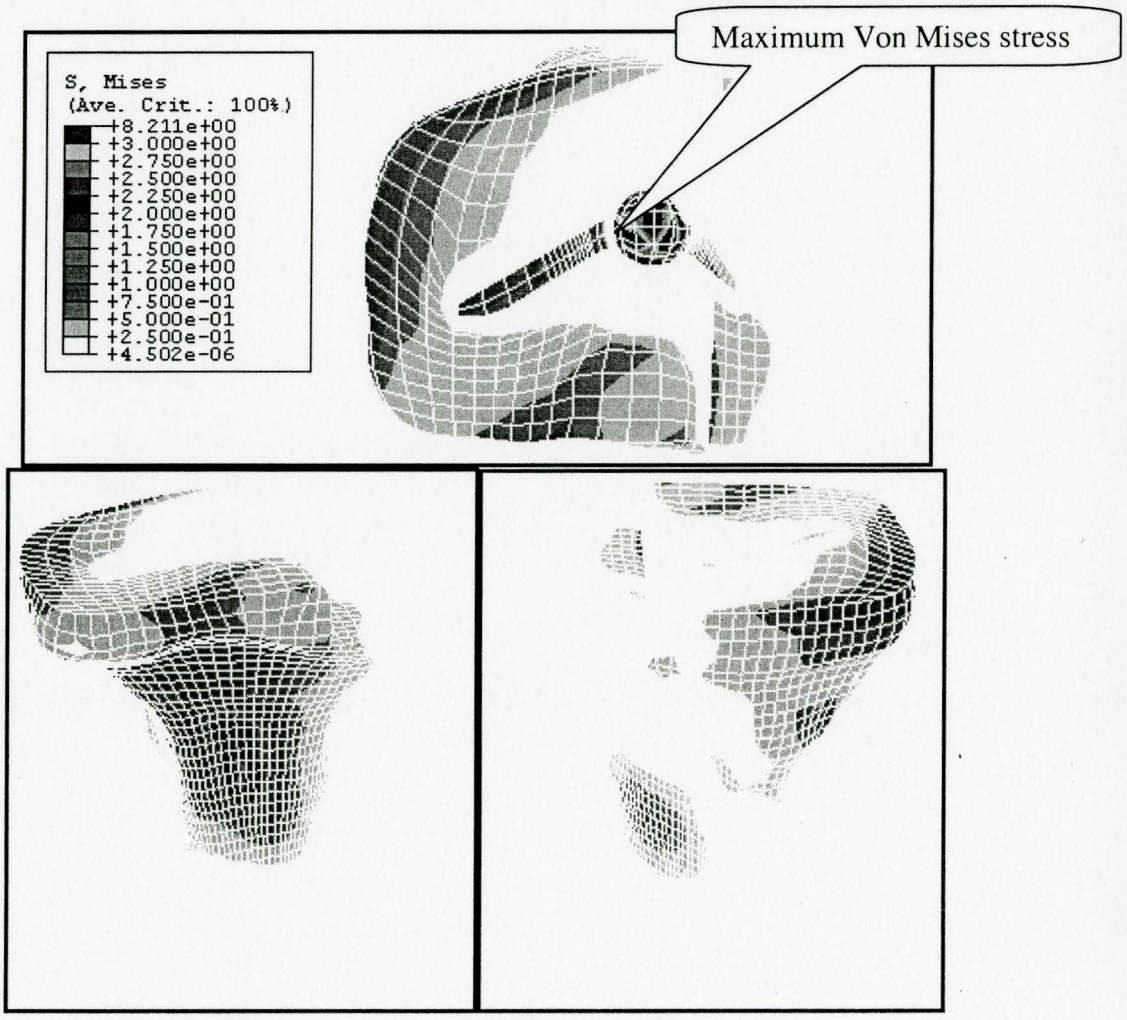

Figure F.7 Von Mises stress contour of the cancellous bone (**tray-block, lateral loading**)

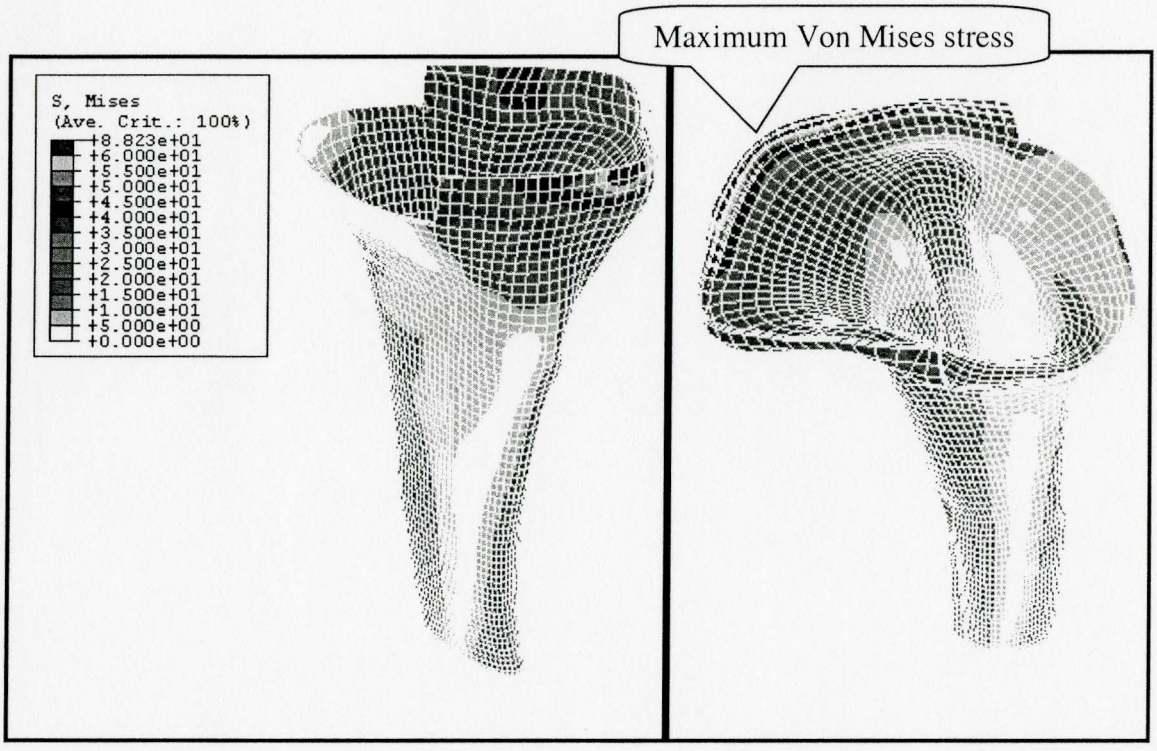

Figure F.8 Von Mises stress contour of the cortical bone (tray-block, lateral loading)

F.3 Configuration of tray-block-stem

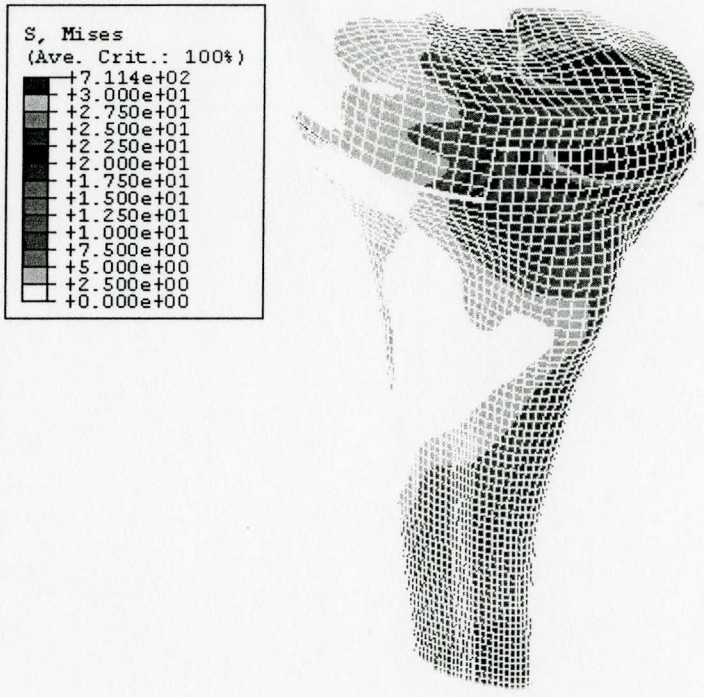

Figure F.9 Von Mises stress contour of the whole model (**tray-block-stem, lateral loading**)

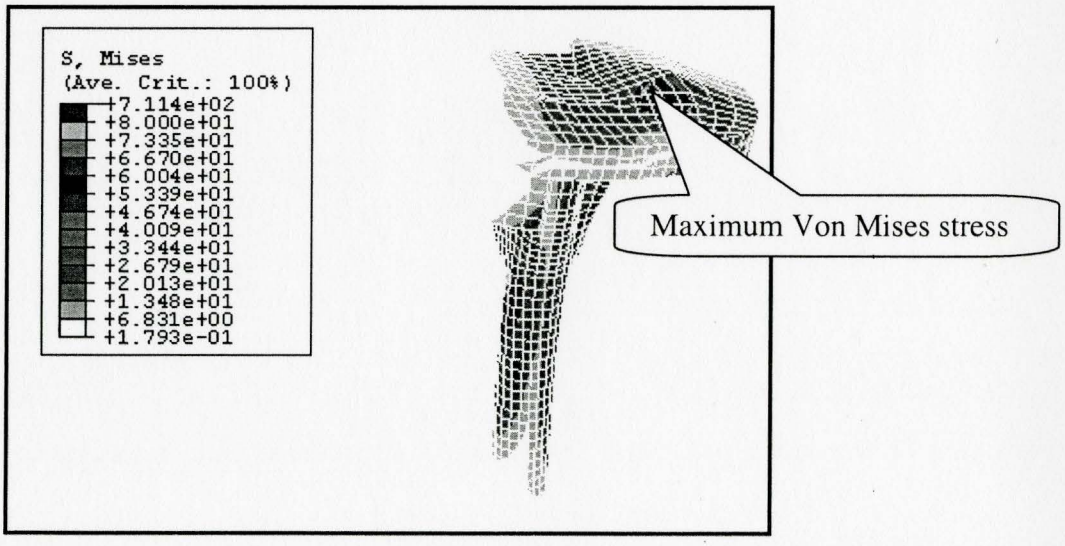

Figure F.10 Von Mises stress contour of the implant (**tray-block-stem, lateral loading**)

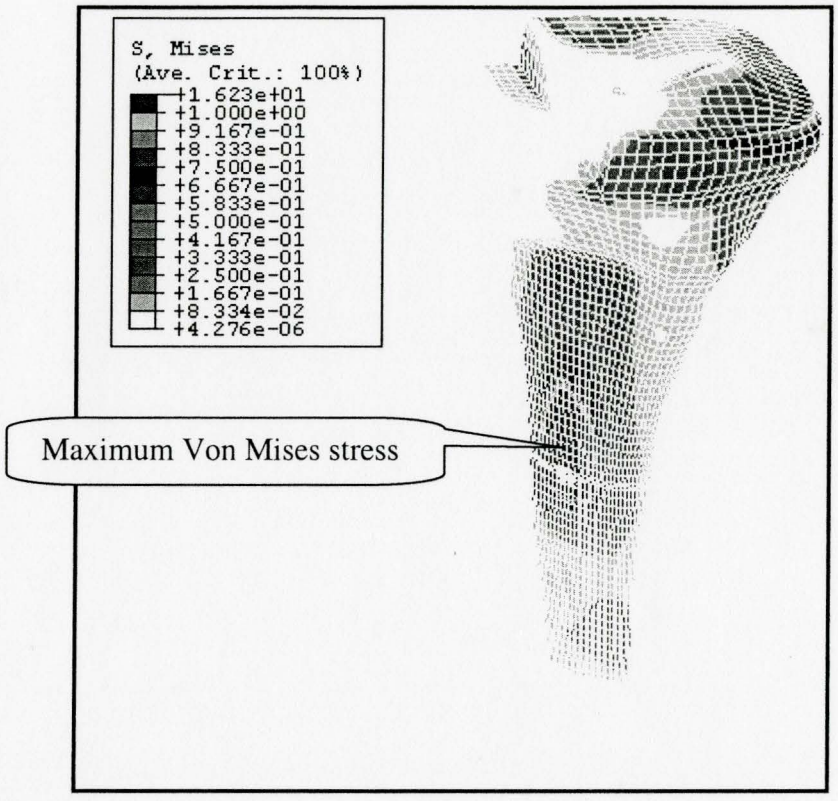

Figure F.11 Von Mises stress contour of the cancellous bone (**tray-block-stem, lateral loading**)

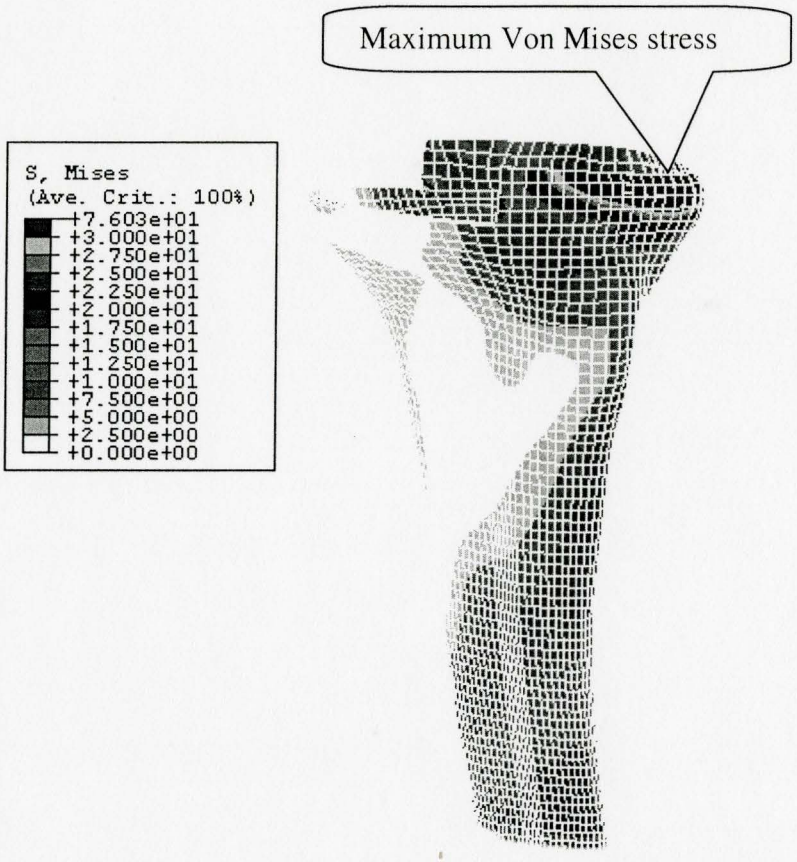

Figure F.12 Von Mises stress contour of the cortical bone (**tray-block-stem, lateral loading**)